Centro Federal de Educação Tecnológica de Minas Gerais
Universidade Federal de São João del-Rei
Graduate Program on Electrical Engineering
Masther's Thesis

Lucas Arantes Lemos Oliveira

State feedback control for discrete-time LPV systems under magnitude and rate saturating actuators.

Belo Horizonte
2021

Lucas Arantes Lemos Oliveira

State feedback control for discrete-time LPV systems under magnitude and rate saturating actuators.

Master's thesis presented to the Graduate Program on Electrical Engineering (Programa de Pós-Graduação em Engenharia Elétrica) of the Federal Center of Technological Education of Minas Gerais (Centro Federal de Educação Tecnológica de Minas Gerais) as a requisite to obtain the title of Master in Electrical Engineering.

Supervisor: Prof. Dr. Valter Júnior de Souza Leite
Co-supervisor: Prof. Dr. Luís Filipe Pereira Silva

Belo Horizonte
2021

(Catalogação - Biblioteca Universitária – Campus Divinópolis – CEFET-MG)

O48s Oliveira, Lucas Arantes Lemos.
State feedback control for discrete-time LPV systems under magnitude and rate saturating actuators. / Lucas Arantes Lemos Oliveira. – Belo Horizonte, 2021.
xiv, 67 f. : *il*.

Texto em inglês.

Orientador: Prof. Dr. Valter Júnior de Souza Leite.
Coorientador: Prof. Dr. Luís Filipe Pereira Silva.

Área de Concentração: Modelagem e Controle de Sistemas.
Linha de Pesquisa: Sistema de Controle.
Dissertação (Mestrado) – Centro Federal de Educação Tecnológica de Minas Gerais/Universidade Federal de São João del-Rei. Programa de Pós-graduação em Engenharia Elétrica.

1. Linear parameter varying (LPV) systems. 2. Magnitude and rate saturating actuators. 3. Discrete-time systems. 4. Regional polyquadratic stabilization. 5. Input-to-State Stability. I. Leite, Valter Júnior de Souza. II. Silva, Luís Filipe Pereira. III. Centro Federal de Educação Tecnológica de Minas Gerais. IV. Universidade Federal de São João del-Rei. V. Título.

CDU: 004.75: 004.414.23

Bibliotecária Responsável Maria Inês Passos Pereira Bueno CRB-6:2805

Lucas Arantes Lemos Oliveira

State feedback control for discrete-time LPV systems under magnitude and rate saturating actuators.

Master's thesis presented to the Graduate Program on Electrical Engineering (Programa de Pós-Graduação em Engenharia Elétrica) of the Federal Center of Technological Education of Minas Gerais (Centro Federal de Educação Tecnológica de Minas Gerais) as a requisite to obtain the title of Master in Electrical Engineering.

Evaluators:

Prof. Dr. Valter Júnior de Souza Leite
CEFET-MG

Prof. Dr. Luís Filipe Pereira Silva
CEFET-MG

Prof. Dr. Erivelton Geraldo Nepomuceno
UFSJ

Prof. Dr. Kevin Guelton
URCA

Belo Horizonte
2021

Centro Federal de Educação Tecnológica de Minas Gerais
Universidade Federal de São João del-Rei
Graduate Program on Electrical Engineering
Masther's Thesis

Master thesis titled "*State feedback control for discrete-time LPV systems under magnitude and rate saturating actuators.*", developed by Lucas Arantes Lemos Oliveira, evaluated by the following professors:

Prof. Dr. Valter Júnior de Souza Leite
CEFET-MG / *Campus* Divinópolis - PPGEL CEFET-MG / UFSJ

Prof. Dr. Luís Filipe Pereira Silva
CEFET-MG / *Campus* Divinópolis

Prof. Dr. Erivelton Geraldo Nepomuceno
Universidade Federal de São João Del-Rei - PPGEL CEFET-MG / UFSJ

Prof. Dr. Kevin Guelton
Université de Reims Champagne-Ardene

Belo Horizonte
2021

To my beloved father (in memoriam), who made me feel what it's like to love someone and taught me to listen to good music.

Acknowledgments

I thank,

my mother, Wanderlene, for being the best friend I could have and always trusting me.

My father, Áureo (in memoriam), who went from this world to a better place during my journey in this work. Thanks for all the love. I can hardly imagine his joy and pride with this.

My sister Lívia for the complicity in difficult times and for always believing in me.

My dear Luiza, for all understanding and support.

To my friends, for always supporting me.

My supervisor Valter Leite, no word here would never be able to describe my gratitude for everything. I will never forget the encouragement, opportunity and confidence he conveyed to me. All my effort to repay such dedication will never be enough.

My old friend and now co-supervisor Luís Filipe, for the countless talks, disposition to clarify doubts and knowledge transmitted.

My project partner Marcus, for the contributions to the results presented in this thesis.

My friends and fellows, Gabriel, Larissa, Álan, and Rômulo, for the daily friendship and for sharing this journey with me.

All teachers from PPGEL and evaluators, for contributing to the improvement of this work. And the CEFET-MG for the financial support.

Thank you all for everything.

I believe that the right cadence and harmony at the right time can awaken any feeling, including happiness in the darkest moments.

Yoñlu

Abstract

In this work, we propose new conditions for the synthesis of parameter-dependent state feedback controllers that guarantee the local asymptotic and input-to-state stability of linear parameter varying (LPV) discrete-time systems with magnitude and rate saturating actuators and subject to energy bounded disturbances. Moreover, the closed-loop system has an ensured exponential stability performance. A nonlinear first-order model models the magnitude and rate saturation of the actuators. Therefore, the saturations of the actuator are represented in terms of dead-zone nonlinearity type, with the application of the generalized sector condition. The design conditions are proposed through a parameter-dependent candidate Lyapunov function in terms of a finite set of linear matrix inequalities (LMIs) and provide regional stabilization in the sense of polyquadratic stability, allowing an estimate of the region of initial conditions yielding trajectories with guaranteed convergence to the origin. Additionally, different convex optimization procedures are formulated according to the control objective. For instance, it is possible to maximize the set of initial admissible conditions, maximize the energy disturbance tolerance, or even minimize the ℓ_2-gain of the admissible perturbations. Finally, numerical examples are presented to demonstrate the efficiency of the proposed methods, and a real-time nonlinear level control illustrates its potentialities for practical applications.

Key-words: Linear parameter varying (LPV) systems. Magnitude and rate saturating actuators. Discrete-time systems. Regional polyquadratic stabilization. Input-to-State Stability.

Contents

List of Figures

List of Tables

List of Acronyms and Notation

LPV	Linear parameter-varying.
LMI	Linear matrix inequality.
PIO	Pilot-induced oscillation.
PTFMSL	Position-type feedback model with speed limitation.
MPC	Model predictive control.
ISS	Input-to-state stable.
HP	Horsepower.
PLC	Programmable logic controller.
m	Meters.
s	Seconds.
SOS	Sum of Squares.
$\mathbb{R}$	set of real numbers.
$\mathbb{R}^n$	the set of vectors of dimensions n with real elements.
$\mathbb{R}^+$	represents the set of non-negative real numbers.
$\mathbb{R}^{n\times m}$	the set of matrices of dimensions $n \times m$ with real elements.
$M \in \mathbb{R}^{n\times m}$	a matrix with dimension $n \times m$ with real entries.
$x \in \mathbb{R}^n$	a vector with n positions and real entries.
$M^\top$	the transpose of matrix M.
$M_{(i)}$	the i-th row of matrix M.
M_{ii}	the diagonal element (i,i) of matrix M.
$M_{(i)}^\top$	stands for $(M_{(i)})^\top$.
$M > 0$	indicates that the matrix M is symmetric positive definite.
$M \geq 0$	indicates that the matrix M is symmetric positive semi-definite.
$\\|\cdot\\|$	the Euclidean norm of a vector or matrix.
$\|\|\cdot\|\|_2$	2-norm of a vector or matrix.
$\star$	represents the symmetric transposed blocks in square matrices.
$\mathbf{I}$	the identity matrix of appropriate dimension.
$\mathbf{0}$	the null matrix of appropriate dimension.
N	represents the number of vertices of the system.
$\mathcal{R}_\mathcal{A}$	represents the region of attraction.
$\mathcal{R}_\mathcal{E}$	represents the estimate of the region of attraction.
$\mathcal{R}_0$	represents the region of initial conditions.
$\mathcal{R}_{\mathcal{E}0}$	represents the estimate of the region of initial conditions.
$\mathcal{L}_2$	denotes the set of energy-limited signals.
$A \subseteq B$	A is a subset of B.
diag$\{A,B\}$	denotes a diagonal block matrix $\left[\begin{smallmatrix} A & 0 \\ 0 & B \end{smallmatrix}\right]$ for A and B matrices.

Chapter 1

Introduction

This work presents new conditions for the design of state feedback linear parameter varying (LPV) controllers for discrete-time systems under magnitude and rate saturating actuators. The regional stabilization is ensured through a parameter-dependent Lyapunov function candidate, and a design convex condition formulated thought a set of linear matrix inequalities (LMIs). The saturating actuators in magnitude and rate are present in many engineering applications, and may cause performance losses and even instability in control systems.

The main problem addressed in this work is the stability and controller design of systems with actuators' saturation in magnitude and rate. Therefore, in this chapter, the main idea is to briefly show the relevance of considering rate saturation on the controller design stage. A literature review concerning with the main topics covered in this work is presented. Lastly, the main objectives of this work and the text organization are listed at the end of this chapter. The ideas presented here and the mathematical tools used will be formally described in detail in the next chapter.

1.1 Problem Formulation

This section presents the relevance of considering the presence of rate saturation in actuators, in addition to magnitude saturation. Some consequences of such limitations are illustrated by an LPV system example, demonstrating the importance of considering the maximum limit of the actuator's rate of change in the controllers' design in closed-loop systems.

1.1.1 Magnitude and rate saturation effects

Magnitude and rate saturations may occur in actuators due to finite power and security reasons. The magnitude limitation may degenerate performance, leads to spurious equilibrium points, and even yields unstable behavior (Tarbouriech *et al.*, 2011, pp. 5). On the other hand, the relevance of addressing rate saturation is well known in several sensitive applications, such as aerospace systems (Tarbouriech *et al.*, 2016). Berg *et al.* (1996) have demonstrated the stability losses due to the phase delay caused by rate-limited actuators. One of the consequences is induced oscillations, for instance, the pilot-induced oscillation (PIO), which has occurred in the YF-22 and JAS 39 fighters aircraft crashes (Klyde *et al.*, 1997) and some commercial transport aircraft (Duda, 1997). This phenomenon can happen because of the delayed actuator response from rate limitations. Consequently, the pilot can apply commands more aggressively since the aircraft does not respond to cockpit controls as expected. Thus, the aircraft responds with an action essentially opposite to the desired command, which can lead to oscillatory movements that even result in the aircraft's instability (Acosta *et al.*, 2014).

To illustrate the effects of magnitude and rate saturation on a system, a controller is firstly designed for an LPV system presenting only magnitude saturation. Then, the same designed controller is used in a system that also has rate limitations.

Assume discrete-time linear parameter varying (LPV) systems given by:

$$x_{k+1} = A(\alpha_k)x_k + B(\alpha_k)\mathtt{sat}\left(u_k\right), \tag{1.1}$$

where $x_k \in \mathbb{R}^n$ is the state vector, $u_k \in \mathbb{R}^{n_u}$ is the control signal vector, the linear parameter-dependent matrices $A(\alpha_k) \in \mathbb{R}^{n\times n}$ and $B(\alpha_k) \in \mathbb{R}^{n\times n_u}$ belong to a polytopic domain given by the convex combination of N known vertices:

$$\begin{bmatrix} A(\alpha_k) & B(\alpha_k) \end{bmatrix} = \sum_{i=1}^{N} \alpha_{k(i)} \begin{bmatrix} A_i & B_i \end{bmatrix}, \tag{1.2}$$

and $\alpha_k \in \mathcal{P}$ is the time-varying vector of parameters belonging to the unitary simplex:

$$\mathcal{P}=\left\{\alpha_k \in \mathbb{R}^N : \sum_{i=1}^{N} \alpha_{k(i)} = 1,\, \alpha_{k(i)} \geq 0,\, i = 1,\ldots,N\right\}, \tag{1.3}$$

which is assumed to be online available (Briat, 2015, pp. 10).

The control signal u_k is limited in magnitude, and $\mathtt{sat}\left(u_k\right)$ is the decentralized saturation function, i.e., the r^{th} actuator's output yields

$$\mathtt{sat}\left(u_k\right)_{(r)} = \mathtt{sign}(u_{k(r)}) \min\left(|u_{k(r)}|,\rho_{(r)}\right), \tag{1.4}$$

for $r = 1,\ldots,n_u$, where $\rho_{(r)}$ is the maximum symmetrical value of the control signal that each actuator r can apply, and the $\mathtt{sign}$ function returns the sign of the control signal.

Example 1.1 (Magnitude saturation) *Consider a discrete-time LPV system with $n = 2$, $N = 2$ and $n_u = 1$ adapted from (Bertolin* et al.*, 2018) given by the matrices*

$$A_1 = 0.45 \begin{bmatrix} -1 & -1 \\ -4 & 0 \end{bmatrix},\ A_2 = 0.45 \begin{bmatrix} 3 & 3 \\ -2 & 1 \end{bmatrix},\ B_1 = B_2 = \begin{bmatrix} 1 \\ 0 \end{bmatrix}, \tag{1.5}$$

with $\rho = 1$. The control law is given by

$$u_k = K(\alpha_k)x_k, \tag{1.6}$$

where $K(\alpha_k) \in \mathbb{R}^{n_u \times n}$, and belong to a polytopic domain given by the convex combination of N known vertices:

$$K(\alpha_k) = \sum_{i=1}^{N} \alpha_{k(i)} K_i. \tag{1.7}$$

According to (Figueiredo, 2020, Corollary 4.1), a state feedback LPV controller gain under (1.6)–(1.7) that stabilizes the system is defined by the gain vectors

$$K_1 = \begin{bmatrix} 0.8839 & 0.2701 \end{bmatrix}, \; K_2 = -\begin{bmatrix} 0.5847 & 0.8768 \end{bmatrix}. \tag{1.8}$$

With a initial condition $x_0 = \begin{bmatrix} -0.2925 & -0.9017 \end{bmatrix}$, Figure 1.1 shows the closed-loop system states trajectories in the phase plan. Notably, the state trajectories converge towards the origin, as expected, despite the magnitude saturating actuator. Therefore, the designed controller guarantees the stability of the closed-loop system for this specific initial condition and actuator's magnitude saturation. See (Figueiredo, 2020) for initial conditions that may diverge in the presence of magnitude saturation. The control signal is shown in the top plot of Figure 1.2, and the bottom plot shows the variation of the parameters α_k.

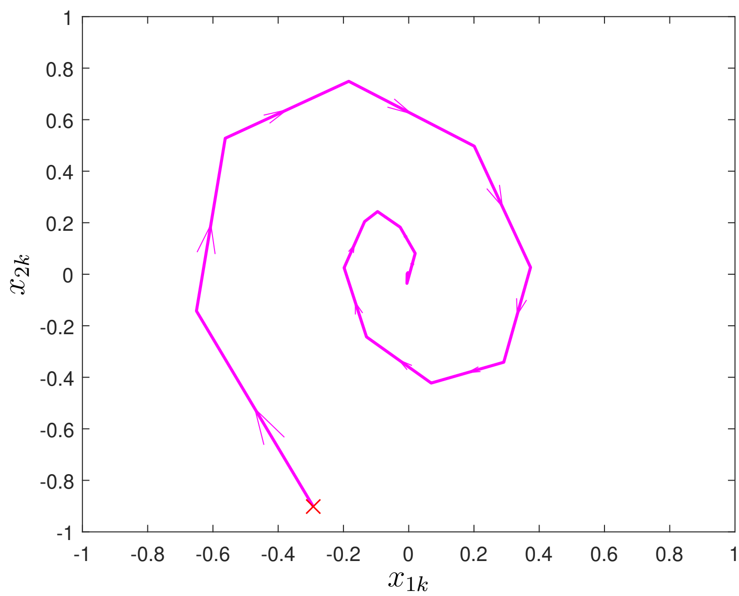

Figure 1.1: State trajectories of closed-loop system with magnitude saturation.

Suppose that additionally to the actuator's magnitude saturation, the actuator's output is subject to rate constraint. In such a case, system (1.1) is rewritten as:

$$x_{k+1} = A(\alpha_k)x_k + B(\alpha_k)\phi_k(u_k), \tag{1.9}$$

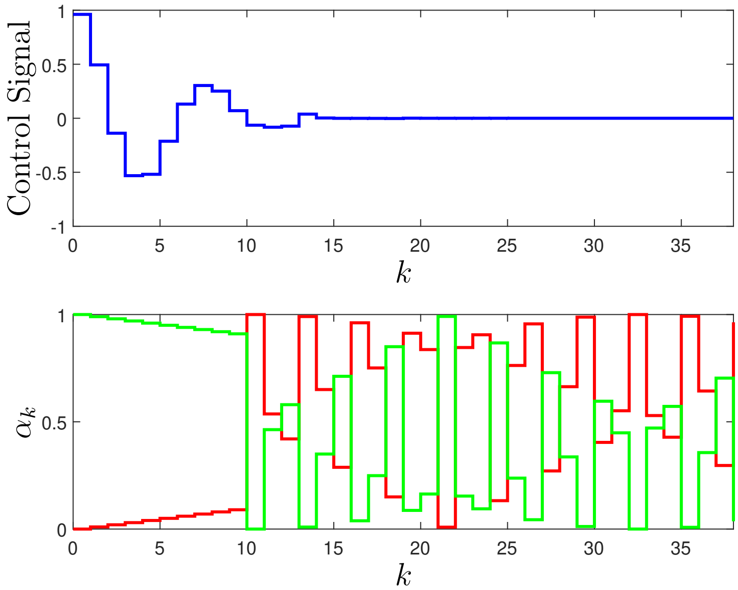

Figure 1.2: Control signal (top) and varying parameters (bottom).

where $\phi_k(u_k) \in \mathbb{R}^{n_u}$ is the actuator's output. Therefore, $\phi_k(u_k)$ must handle both magnitude and rate saturating aspects of the actuator. By using the discrete-time version of the position-type feedback model with speed limitation (PTFMSL) presented in Figure 1.3, whose dynamics is given by:

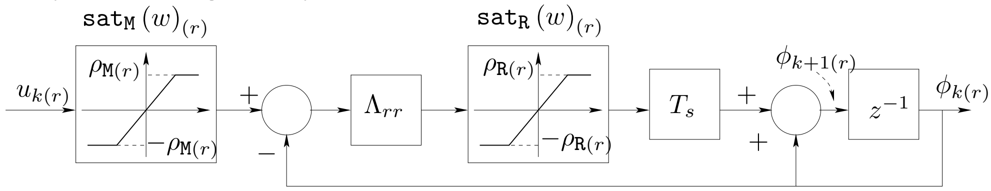

Figure 1.3: Diagram of first-order nonlinear system used to model magnitude and rate saturation.

$$\bar{x}_{k+1(r)} = \bar{x}_{k(r)} + T_s\mathtt{sat}_{\mathtt{R}}\left(\Lambda\mathtt{sat}_{\mathtt{M}}\left(u_k\right) - \Lambda\bar{x}_k\right)_{(r)}, \tag{1.10}$$

$$\phi_k(u_k) = \bar{x}_k, \tag{1.11}$$

for $r = 1, \ldots, n_u$, where $\bar{x}_k \in \mathbb{R}^{n_u}$ is the actuators' state, $\Lambda \in \mathbb{R}^{n_u \times n_u}$ is a diagonal matrix composed by the actuators' poles, T_s is the sampling period of the actuator, and for a signal $w \in \mathbb{R}^{n_u}$ the symmetric saturation functions concerning the magnitude and rate are given by $\mathtt{sat}_{\mathtt{M}}(w)_{(r)} = \mathtt{sign}(w_{(r)})\min(|w_{(r)}|, \rho_{\mathtt{M}(r)})$ and $\mathtt{sat}_{\mathtt{R}}(w)_{(r)} = \mathtt{sign}(w_{(r)})\min(|w_{(r)}|, \rho_{\mathtt{R}(r)})$, respectively, with $\rho_{\mathtt{M}} \in \mathbb{R}^{n_u}$ and $\rho_{\mathtt{R}} \in \mathbb{R}^{n_u}$ denoting the respective symmetrical bounds. As the modulus of Λ_{rr} goes to ∞, the output signal of the proposed model fits better a static rate saturation (Tyan & Bernstein, 1997).

The state feedback control law that may use the state of the actuator to stabilize the system (1.9)-(1.11) is given as follows:

$$u_k = K(\alpha_k)x_k + \bar{K}(\alpha_k)\bar{x}_k = \hat{K}(\alpha_k)z_k, \tag{1.12}$$

where $K(\alpha_k) \in \mathbb{R}^{n_u \times n}$, $\bar{K}(\alpha_k) \in \mathbb{R}^{n_u \times n_u}$, $\hat{K}(\alpha_k) = \begin{bmatrix} K(\alpha_k) & \bar{K}(\alpha_k) \end{bmatrix}$, and $z_k = \begin{bmatrix} x_k^\top & \bar{x}_k^\top \end{bmatrix}^\top \in \mathbb{R}^{n+n_u}$ is an augmented state vector including the plant and actuator states. Observe that, whenever the actuator's states are not available for feedback, $\bar{K}(\alpha_k) = 0$ is required $\forall \alpha_k \in \mathcal{P}$.

Example 1.2 (Magnitude and rate saturation) *Considering the same system (1.5), with $\rho_{\mathtt{M}} = 1$, $\rho_{\mathtt{R}} = 1$, $T_s = 1$, $\Lambda = 10$. The gain vectors are the same used in Example 1.1, Equation (1.8). Since the actuator's state is not used in the feedback, we have $\bar{K}_1 = \bar{K}_2 = 0$, yielding:*

$$\hat{K}_1 = \begin{bmatrix} 0.8839 & 0.2701 & 0 \end{bmatrix}, \; \hat{K}_2 = -\begin{bmatrix} 0.5847 & 0.8768 & 0 \end{bmatrix}.$$

Figure 1.4 shows the closed-loop system states trajectories in (1.1) (magenta line) and (1.9)-(1.11) (blue line) in the phase plan cut at $\bar{x} = 0$, with the same initial condition used in Example 1.1, i.e, $z_0 = \begin{bmatrix} x_0 & \bar{x} \end{bmatrix} = \begin{bmatrix} -0.2925 & -0.9017 & 0 \end{bmatrix}$, and the same variation of parameters α_k given in Figure 1.2. With the addition of rate bounds, the controller cannot guarantee the system's asymptotic stability and presents unstable behavior, one of the consequences of rate saturation.

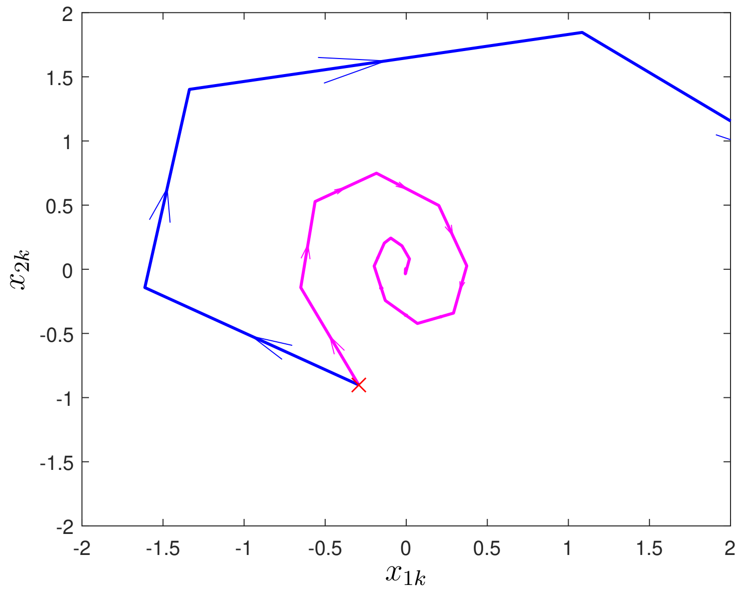

Figure 1.4: State trajectories of the closed-loop system with only magnitude saturation (magenta) and with magnitude and rate saturation (blue).

The actuator's output is shown in Figure 1.5 and it is possible to notice that the controller's efforts are insufficient to take the trajectory to the origin. Therefore, due to the actuator constraints' nonlinearities, global closed-loop stability cannot be ensured in general.

Thus, it is necessary to determine the region of attraction $\mathcal{R}_{\mathcal{A}} \subseteq \mathbb{R}^{n+n_u}$ of all initial conditions such that the corresponding trajectories of the closed-loop system converge to

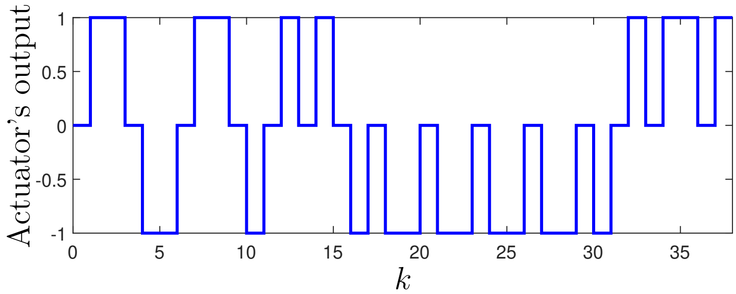

Figure 1.5: Actuator's output subject to magnitude and rate saturation.

the origin. Once $\mathcal{R}_{\mathcal{A}}$ can be non-convex, open, and even unbounded in some directions (Gomes da Silva Jr. & Tarbouriech, 2005), an estimate $\mathcal{R}_{\mathcal{E}} \subseteq \mathcal{R}_{\mathcal{A}}$ is computed as large as possible.

1.2 Literature Review

The stability analysis and controller synthesis of linear parameter varying (LPV) systems have been extensively investigated in control systems. The main reason is that LPV models can accurately represent the dynamics of a broad class of processes, where parameters may change over time (or with the operating conditions). Moreover, LPV models can capture nonlinear dynamics while maintaining a relatively simple mathematical representation in terms of a family of linear models (Rugh & Shamma, 2000). A particular case is the *quasi*-LPV systems, in which the variant parameters are calculated in functions that depend on the system states, unlike *pure* LPV systems, in which the parameters are measured in real-time from exogenous signals (Sename *et al.*, 2013, pp. 5).

A wide range of modeling and control applications utilize the LPV framework due to its ability to describe systems with variable and nonlinear operating conditions. The practical applications vary from advances in medicine to industrial engineering implementations. Tasoujian *et al.* (2020) have used an LPV representation to describe the mean arterial blood pressure response to drug injections for blood pressure control. In (Colmegna *et al.*, 2021) the authors have proposed using a switched LPV controller for automatic glucose control for patients with type 1 diabetes. Morato *et al.* (2019) have presented an LPV model predictive control system for semi-active vehicle suspensions, and in (Vafamand *et al.*, 2019) the authors have addressed the speed control of electric vehicles. Other several automotive applications can be found in (Sename *et al.*, 2013). Yang *et al.* (2020) have applied anti-disturbance control of a switched LPV system in an aircraft engine. A last example of LPV systems application is the case presented in (Quadros *et al.*, 2020), where fault tolerant control is exemplified in a level control system.

The Lyapunov stability theory is an important tool in the stability investigations and controller designs for LPV systems, allowing convex formulations in terms of linear matrix inequalities (LMIs). The advantage of using LMIs is the efficiency of numerical resolutions and the guarantee of optimal solutions (Boyd *et al.*, 1994). The first mention of LPV systems was made by Shamma & Athans (1990) investigating the analysis and synthesis of gain-scheduled controllers. The challenges of using gain-scheduled controllers for LPV systems were addressed by Shamma & Athans (1992), where a restriction to slow parameter variation is pointed to ensure closed-loop stability, and it is suggested the development of the control design methodologies for LPV systems to overcome these limitations. Therefore, several studies about this class of systems emerged, as presented by the surveys (Leith & Leithead, 2000; Rugh & Shamma, 2000) that present the state-of-the-art about gain-scheduling control in the 2000s. Since then, several works addressing the LPV systems framework based on different Lyapunov functions have been published in the literature. In (Geromel *et al.*, 1991), the robust stability and state feedback control are proposed using quadratic Lyapunov functions with a parameter-independent matrix to continuous and discrete-time systems. In such an approach, the controller is constant, i.e., the controller parameters are time-invariant. Therefore, the controller design adopts a robust controller design, ensuring the closed-loop stability of uncertain polytopic systems. In order to find less conservative solutions, some authors have proposed the use of parameter-dependent Lyapunov functions. In (Daafouz & Bernussou, 2001), the authors propose the robust polyquadratic stability of discrete-time systems with arbitrary parameter variation inside a polytope, finding an affine parameter-dependent Lyapunov function. Considering piecewise Lyapunov matrices, Leite & Peres (2004) address the robust stabilization of linear discrete-time systems with uncertain parameters. Some other important contributions to the literature in this context can be found in (Montagner *et al.*, 2006; Oliveira & Peres, 2009; De Caigny *et al.*, 2009) and references therein. Pursuing more relaxed conditions of performance and stability, the development of controllers with varying parameters was suggested. Based on this, De Caigny *et al.* (2012) proposed synthesizing gain-scheduled dynamic output feedback controllers for discrete-time LPV systems assuming that the plant and the controller matrices can have a homogeneous polynomial dependence on the scheduling parameters. In (Sato, 2015), the gain-scheduled state feedback control is designed considering the uncertainty of the scheduling parameters. Recently, the relevance of LPV systems has received attention from a survey of results that have been certified by experiments and high-fidelity simulations (Hoffmann & Werner, 2015) and some special issues (Edwards *et al.*, 2014; Zhang *et al.*, 2020).

Although LPV models are quite general, some nonlinearities often found in physical systems may be handled without using LPV modeling to ensure stability and performance. Saturating actuators are of particular interest due to physical restrictions (such as limited energy available) and security constraints in actuators and processes, leading to bounds on magnitude. Moreover, actuators are also limited in their output signals' rate of change (or speed). Thus, they cannot respond immediately to a sudden change in the control signal. Especially in more energetic designs, if these limitations are not considered in the synthesis stage, the magnitude and rate saturation can cause loss of performance, presence of multiple equilibrium points, limit-cycles, and even instability in closed-loop systems (Tarbouriech *et al.*, 2011, pp. 14). Some examples of saturating elements present in control systems are motors, heaters or coolers, hydraulic valves, and sensors. In practice, usually, any component has a physical limitation, which is mathematically modeled by the nonlinear saturation function.

There are three main approaches to model the presence of magnitude saturation in control systems in the literature. The first one is based on modeling saturation as a dead zone nonlinearity and is called generalized sector condition, proposed by Gomes da Silva Jr. & Tarbouriech (2005). The second approach describes the saturated system in a polytopic model and presents three types of particular models. The so-called polytopic model I was introduced by Molchanov & Pyatnitskii (1989), the polytopic model II was suggested by Hu & Lin (2001) and the model III originally proposed in (Alamo *et al.*, 2006). These denominations are found in (Tarbouriech *et al.*, 2011, pp. 33) where the reader can find more details. The main disadvantage of the polytopic approach is the numerical complexity increasing in optimization procedures, which becomes even more critical in uncertain systems and LPV. The third approach for saturating systems is derived from model predictive control (MPC), in which, from the system's model, the future instants outputs and the control law are calculated through an optimization procedure at every instant (Wang, 2009). Some works about stability analysis and controller synthesis in systems that present magnitude saturation stand out in the literature, such as (Hu & Lin, 2001; Tarbouriech *et al.*, 2011; Zaccarian & Teel, 2011), and therein references. LPV systems under magnitude saturating actuators have found attention in the recent literature. Palmeira *et al.* (2018) address the problem of aperiodic sampled-data control of LPV systems under input saturation. Figueiredo *et al.* (2021) use homogeneous polynomial parameter-dependent functions for synthesizing rational parameter-dependent state feedback gain controllers to stabilize discrete-time LPV systems subject to saturating actuators. de Souza *et al.* (2021) investigate the regional asymptotic stability of discrete-time LPV systems subject to saturating actuators through event-triggered dynamic output-feedback control.

However, in addition to saturation in magnitude, actuators can also have limits on the rate of change. As briefly discussed in 1.1.1, the need to consider the effects of magnitude and rate saturation in controller design is evident. From here, a specific literature review on saturation in magnitude and rate, the main subject of this work, is shown. Searches were made through the *Scopus* and *Google Scholar* platforms, with the keywords: magnitude and rate saturation, nested saturation, rate constraints, among other synonyms. Thus, the most relevant and current works on this subject were found, and the references therein. From this review, we can say that saturating actuators in magnitude and rate can be handled by two main methods (Baiomy & Kikuuwe, 2020). In the first one, a controller is designed embedding the nonlinear actuator model in the designed controller such that the control signal do not violate the magnitude and rate limits of the actuator. This approach has been presented in (Kapila & Haddad, 1998) and (Kapila *et al.*, 1999) for continuous-time systems and in (Pan & Kapila, 2001) for discrete-time systems, using the classic sector condition Tarbouriech *et al.* (2011) to describe the saturation nonlinearity phenomenon. In (Gomes da Silva Jr. *et al.*, 2008), the authors propose a synthesis method for a dynamic cascade controller with saturating integrators and two static anti-windup compensators for discrete-time systems using the generalized sector condition (Gomes da Silva Jr. & Tarbouriech, 2005). They also consider the region of attraction's size, seeking to guarantee the local asymptotic stability of the closed-loop system. In (Bender & Gomes da Silva Jr., 2012), a similar approach is used to ensure the internal and external stability of continuous systems subject to $\mathcal{L}_2$ disturbances. In (Baiomy & Kikuuwe, 2020), sliding mode type controllers are proposed for both continuous and discrete-time systems. Also see (Galeani *et al.*, 2008; Forni *et al.*, 2012), in the context of continuous-time systems, where anti-windup action is designed to handle rate saturation.

In the second method, called *position-type feedback model with speed limitation*, a first-order system with a saturating input signal (describing the magnitude saturation) and the rate saturation modeled as the actuator state's constraint is employed, leading to a particular case of nested saturations (Tarbouriech *et al.*, 2006). In (Tyan & Bernstein, 1997), a dynamic compensator is designed to deal with independent magnitude and rate saturation. A semi-global stabilization is proposed in (Lin, 1997) and a local one in (Gomes da Silva Jr. *et al.*, 2003). More general conditions of systems presenting nested saturations are given in (Bateman & Lin, 2003) (continuous-time) and (Bateman & Lin, 2002; Zhou, 2013) (discrete-time). Besides, the polytopic model of the saturating signals is employed. In the continuous-time systems, nested saturations are addressed in (Tarbouriech *et al.*, 2006) by using the generalized sector condition. More recently, Palmeira *et al.* (2016) addresses the stability analysis of rate-saturating sampled-data control, and Flores (2019) discusses the reference tracking of LPV systems. Both works are based on Tarbouriech *et al.* (2006) and give synthesis conditions considering magnitude and rate saturations. However, none of the aforementioned works concerns with LPV discrete-time systems and thus, cannot be used to stabilize them.

1.3 Goals

The main objective of this work is to develop new conditions for the synthesis of parameter-dependent state feedback controllers that guarantee the asymptotic and input-to-state stability of LPV linear discrete-time systems with saturation in magnitude and rate of change for a set of initial conditions and limited energy input disturbances.

To complement the main objective of this project, some specific goals are also pursued. To allow the controllers to have a certain specified performance, it is proposed to consider an ensured exponential stability performance at the controller design phase. Also, to obtain the largest estimates of regions of attraction in the considered problems, it is necessary to develop convex optimization procedures for different design objectives. Finally, to demonstrate the efficiency of the proposed methodology is expected to apply the synthesis conditions in real systems and numerical examples.

1.4 Text organization

This thesis is divided into five chapters. This chapter contains an introduction to the problem addressed, a literature review about the main topics, the objectives, and the organization of the document. Next, the second chapter presents the main fundamental mathematical tools for developing and understanding the main results of this work. The third chapter presents conditions to design state feedback controllers for discrete-time LPV systems subject to magnitude and rate saturation, and energy bounded disturbances. Then, some optimization procedures are presented, such as minimization of the $\mathcal{L}_2$-gain, maximization of the set of admissible initial states, and maximum tolerance to disturbance. Finally, numerical examples are presented to consolidate the proposed approach. In the fourth chapter, an experimental result of a level control in a nonlinear system is presented, using the conditions proposed in this work. Finally, the last chapter presents the conclusion and proposals for future works.

Chapter 2

Mathematical fundamentals

This chapter presents some fundamental mathematical tools for developing and understanding the main results of this work. For a better reader's understanding of the mathematical developments made in the following chapters, the concepts of discrete-time LPV systems, stability in the Lyapunov sense, input-to-state stability, and actuators saturation are presented.

2.1 Discrete-time LPV systems

Consider the following discrete-time linear parameter varying (LPV) system

$$x_{k+1} = A(\alpha_k)x_k + B(\alpha_k)u_k, \tag{2.1}$$

where $x_k \in \mathbb{R}^n$ is the state vector, $u_k \in \mathbb{R}^{n_u}$ is the control signal vector, the matrices $A(\alpha_k) \in \mathbb{R}^{n\times n}$ and $B(\alpha_k) \in \mathbb{R}^{n\times n_u}$ depend linearly on the time-varying parameter vector α_k. More specifically, these matrices belong to a polytopic domain given by the convex combination of N known vertices:

$$M(\alpha_k) = \sum_{i=1}^{N} \alpha_{k(i)} M_i, \tag{2.2}$$

with M replacing matrices A and B, where $\alpha_k \in \mathcal{P}$ is the time-varying vector of parameters belonging to the unitary simplex:

$$\mathcal{P}=\left\{\alpha_k \in \mathbb{R}^N : \sum_{i=1}^{N} \alpha_{k(i)} = 1, \alpha_{k(i)} \geq 0, i = 1, \ldots, N\right\}, \tag{2.3}$$

which is assumed to be online available (Briat, 2015, pp. 10).

2.2 Stability in the Lyapunov sense

The stability of a system in relation to its equilibrium point can be characterized by its internal energy. If the system's equilibrium point energy tends to zero when the time approaches infinity, then it is said to be asymptotically stable. Throughout the text, when the expression that a system is stable is used, it means that the equilibrium point is stable. Lyapunov's method uses a scalar function representing the amount of energy in the system in relation to its equilibrium point. If this function $V(x_k)$ is always positive, radially unbounded, null only at the equilibrium point, and with strictly negative variations for $V(x_k) \neq 0$ and null for $V(x_k) = 0$, the system trajectories converge towards the origin, i.e., the system is asymptotically stable, and it is called a Lyapunov function (Khalil, 2002, pp. 114). The procedure for certifying the Lyapunov asymptotic stability of a linear discrete-time system is illustrated as follows.

Consider the discrete-time parameter-dependent system given by (2.1) and analyzing the autonomous configuration, i.e., with $u_k = \mathbf{0}$, for an initial condition $x_0 \neq 0$. The stability can be demonstrated using special comparison functions, where the bounds of Lyapunov functions are known as class $\mathcal{K}$ functions. This kind of functions are defined in the range $[0,a) \to [0,\infty)$ and are strictly increasing.

Lemma 2.1 (Adapted from (Khalil, 2002)) *If there exists $V(x_k)$, being this a Lyapunov function, and being κ_1, κ_2, and κ_3 class $\mathcal{K}$ functions, $\forall k > 0$, if the conditions*

$$\kappa_1(\|x_k\|) \leq V(x_k) \leq \kappa_2(\|x_k\|), \tag{2.4}$$

and

$$\Delta V(x_k) \leq -\kappa_3(\|x_k\|), \tag{2.5}$$

are fulfilled for all $x_k \in \mathbb{R}^n$, then system (2.1) is asymptotically stable.

Therefore, it is necessary to define a candidate Lyapunov function that satisfies Lemma 2.1. One of the most used candidate Lyapunov functions is the quadratic function defined as

$$V(x_k) = x_k^\top P x_k, \tag{2.6}$$

where $P \in \mathbb{R}^{n\times n}$ (Boyd *et al.*, 1994). To guarantee the positivity of $V(x_k)$, the matrix P must be symmetric and positive definite ($P = P^\top > \mathbf{0}$), i.e., all eigenvalues of P must be real and greater than zero. For the function $V(x_k)$ to be decreasing, the temporal variation $\Delta V(x_k)$ must be negative along the trajectories of the system.

However, the quadratic function is quite restrictive for time-varying systems such as system (2.1). This happens because the conditions formulated from this function are defined only on the polytope vertices, so the results using this type of function are very conservative. So, an alternative is to use time-varying parameter-dependent functions, making the function more general, decreasing conservatism. Daafouz & Bernussou (2001) proposed the polyquadratic stability using a parameter-dependent Lyapunov function, which are quadratic on the system state and depend in a polytopic way on the uncertain parameter, and it can be described as:

$$V(x_k,\alpha_k) = x_k^\top P(\alpha_k) x_k, \tag{2.7}$$

$$P(\alpha_k) = \sum_{i=1}^{N} \alpha_{k(i)} P_i > \mathbf{0}. \tag{2.8}$$

The following theorem provides a solution through LMIs to the polyquadratic stability problem of system (2.1):

Lemma 2.2 *Consider the discrete-time system given by* (2.1) *and analyzing the autonomous configuration. If there are positive definite symmetric matrices $P_i \in \mathbb{R}^{n\times n}$ such that the LMIs*

$$\begin{bmatrix} P_i & A_i^\top P_j \\ \star & P_j \end{bmatrix} > \mathbf{0}. \tag{2.9}$$

are satisfied, for all i, $j = 1,\ldots,N$, so the system (2.1) *is asymptotically stable.*

Proof: Assuming the feasibility of (2.9), multiply by $\alpha_{k(i)}$, $\alpha_{k+1(j)}$, $\alpha_k \in \mathcal{P}$, sum it up for $i,j = 1,\ldots,N$, then,

$$\begin{bmatrix} P(\alpha_k) & A(\alpha_k)^\top P(\alpha_{k+1}) \\ \star & P(\alpha_{k+1}) \end{bmatrix} > \mathbf{0}.$$

By applying Schur's complement (see Appendix A.1), it is possible to get

$$A(\alpha_k)^\top P(\alpha_{k+1}) A(\alpha_k) - P(\alpha_k) < \mathbf{0}.$$

Pre- and post-multiplying the resulting inequality by $x_k^\top$ and x_k, respectively, and replacing $x_{k+1} = A(\alpha_k)x_k$ on it, results in

$$x_{k+1}^\top P(\alpha_{k+1}) x_{k+1} - x_k^\top P(\alpha_k) x_k < 0,$$

that is equal to,

$$\Delta V(x_k,\alpha_k) < 0.$$

Therefore, the conditions given in (2.9) implies the positivity of the Lyapunov function given in (2.7)–(2.8) and the negativity of the temporal variation $\Delta V(x_k,\alpha_k)$ with class $\mathcal{K}$ functions given by $\beta_1\|x_k\|^2 \leq V(x_k,\alpha_k) \leq \beta_2\|x_k\|^2$, and $\Delta V(x_k,\alpha_k) \leq -\beta_3\|x_k\|^2$, where

$$\beta_1 = \min_{i=1,\ldots,N} \texttt{eig}(P_i),$$
$$\beta_2 = \max_{i=1,\ldots,N} \texttt{eig}(P_i),$$

and there exists a sufficiently small $\beta_3 > 0$, following the Lemma 2.1, it is concluded that the system (2.1) is asymptotically stable. ∎

The system is said to be polyquadratically stable, according to the following definition:

Definition 2.1 (**(Daafouz & Bernussou, 2001)**) *System (2.1) is said polyquadratically stable, if there exists a parameter-dependent quadratic Lyapunov function (2.7)–(2.8) that satisfies Lemma 2.1.*

Therefore, the following level set can be associated with the system:

$$\mathcal{L}_{\mathcal{V}}(c) = \{x_k \in \mathbb{R}^n : V(x_k,\alpha_k) \leq c, \, \forall \alpha_k \in \mathcal{P}\}, \tag{2.10}$$

where $0 < c < \infty$, where if $c = 1$, the set is denoted by $\mathcal{L}_{\mathcal{V}}$. Thus, the level set $\mathcal{L}_{\mathcal{V}}(c)$ can be calculated by the following lemma, adapted from (Jungers & Castelan, 2011, Lemma 4):

Lemma 2.3 *If (2.7)–(2.8) is a Lyapunov function for the system (2.1) then the level set (2.10) can be computed using the finite dimensional condition*

$$\mathcal{L}_{\mathcal{V}}(c) = \bigcap_{\alpha_k \in \mathcal{P}} \mathcal{E}(P(\alpha_k),c) = \bigcap_{i=1}^{N} \mathcal{E}(P_i,c), \tag{2.11}$$

where $\mathcal{E}(P_i,c)$ are ellipsoidal sets defined by

$$\mathcal{E}(P_i,c) = \{x_k \in \mathbb{R}^n : x_k^\top P_i x_k \leq c\}, \tag{2.12}$$

for $i = 1,\ldots,N$.

This proof is presented in the Appendix A.2. The main advantage of this result is that the level set $\mathcal{L}_{\mathcal{V}}(c)$ can be calculated through a finite number of ellipsoidal sets defined by P_i, $i = 1,\ldots,N$, thus, it is not necessary to solve an infinite dimensional problem related to α_k.

When $V(x_k,\alpha_k)$ is a Lyapunov function, then $\Delta V(x_k,\alpha_k) < 0$ means that when the system trajectory crosses the level set $\mathcal{L}_{\mathcal{V}}(c)$, it moves inward and never leaves it again. In such a case, the level set $\mathcal{L}_{\mathcal{V}}(c)$ is a contractive set. Notice that as c decreases, the level set shrinks towards the origin. Therefore, when $\Delta V(x_k,\alpha_k) < 0$ the system trajectory enters $\mathcal{L}_{\mathcal{V}}(c)$ which shrinks towards the origin as time increases, resulting in the convergence of the trajectories towards the origin. In cases where global stability cannot be determined, a region that contains initial conditions of converging trajectories can be estimated with the aid of $\mathcal{L}_{\mathcal{V}}(c)$. The presence of saturation in actuators is one of these cases of interest. Due to its nonlinear behavior, it is relevant to investigate whether there is a neighborhood around the origin where asymptotic stability is guaranteed. Based on this, the definition of region of attraction emerges.

Definition 2.2 (**Tarbouriech *et al.* (2011)**) *The region of attraction $\mathcal{R}_{\mathcal{A}}$ of any system $x_{k+1} = f(x_k)$ is defined as set of all initial conditions x_0 whose respective trajectories converge asymptotically towards the origin. In other words, if $x_0 \in \mathcal{R}_{\mathcal{A}}$ then $x_k \to 0$ when $k \to \infty$.*

Analytically, determining the system's region of attraction $\mathcal{R}_{\mathcal{A}}$ is often a difficult or, in some cases, a impossible task. However, it is possible to determine an estimate of the region of attraction $\mathcal{R}_{\mathcal{E}} \subseteq \mathcal{R}_{\mathcal{A}}$, that is, to determine regions in the state space in which the asymptotic convergence of the system trajectories is guaranteed. In the following chapters, methods of designing controllers and estimating attraction regions $\mathcal{R}_{\mathcal{E}}$ that certify the asymptotic stability of initial conditions are proposed.

2.3 Input-to-State Stability

Consider a discrete-time LPV system subject to external disturbances, such that

$$x_{k+1} = A(\alpha_k)x_k + B(\alpha_k)u_k + B_w(\alpha_k)\omega_k, \tag{2.13}$$

where $x_k \in \mathbb{R}^n$ is the state vector, $u_k \in \mathbb{R}^{n_u}$ is the control signal vector, the linear parameter-dependent matrices $A(\alpha_k) \in \mathbb{R}^{n\times n}$, $B(\alpha_k) \in \mathbb{R}^{n\times n_u}$, and $B_w(\alpha_k) \in \mathbb{R}^{n\times n_w}$ belong to a polytopic domain given by (2.2), with M replaced by A, B, or B_w, and with $\alpha_k \in \mathcal{P}$.

In a control system subject to disturbance signals, state trajectories cannot be expected to converge to the origin as time increases, while disturbances are not null. Therefore, it is necessary to design the controller to reduce the disturbance's influence on the system. In this case, the idea is to guarantee that any trajectories of x_k are bounded for disturbances ω_k also bounded (Sontag, 1999). This work is interested in energy-limited perturbations, i.e., it is considered that the signal ω_k has ℓ_2-norm smaller than a certain quantity δ^{-1}, with $\delta > 0$. Therefore, the vector $\omega_k \in \mathbb{R}^{n_w}$ is composed by quadratically summable perturbation signals, $\omega_k \in \mathcal{W}$ where:

$$\mathcal{W} = \{\omega_k \in \mathbb{R}^{n_w} : \|\omega_k\|_2^2 \leq \delta^{-1}\}, \tag{2.14}$$

with $\|\omega_k\|_2^2 = \sum_{k=0}^{\infty} \omega_k^\top \omega_k$ and $\delta^{-1} \in \mathbb{R}_+$ represents the maximum energy of the disturbance signals.

To ensure that the system (2.13) trajectories are limited, the function

$$\mathcal{J}_k = \Delta V(x_k,\alpha_k) - \omega_k^\top \omega_k,$$

being $V(x_k,\alpha_k) > 0$ a candidate Lyapunov function, then

$$\sum_{i=0}^{k} \mathcal{J}_k = V(x_k,\alpha_k) - V(x_0,\alpha_0) - \sum_{i=0}^{k} \omega_i^\top \omega_i.$$

If $V(x_k,\alpha_k) > 0$ is a Lyapunov function, the following sets can be associated with it:

$$\mathcal{R}_0 = \left\{x_0 \in \mathbb{R}^n : V(x_k,\alpha_k) \leq \beta^{-1}, \forall \alpha_k \in \mathcal{P}\right\},$$

$$\mathcal{R}_{\mathcal{A}} = \left\{ x_k \in \mathbb{R}^n : V(x_k,\alpha_k) \leq \mu^{-1}, \forall \alpha_k \in \mathcal{P} \right\},$$

with $\mu^{-1} = \beta^{-1} + \delta^{-1}$, where $\mathcal{R}_0$ is the set of initial conditions whose trajectories do not leave the region $\mathcal{R}_{\mathcal{A}}$ for any $\omega_k \in \mathcal{W}$. Therefore, if $\mathcal{J}_k < 0$, then $\Delta V(x_k,\alpha_k) < \omega_k^\top \omega_k$, meaning that for non null disturbances signals, the energy function $V(x_k,\alpha_k)$ is allowed to increase by an amount depending on ω_k energy. The system is said input-to-state stable (ISS) when

1. for the system without disturbance, i.e., with $\omega_k = 0$, $\forall k \geq 0$, the set $\mathcal{L}_{\mathcal{V}}(\mu^{-1}) \subseteq \mathcal{R}_{\mathcal{A}}$ is a region of initial conditions that ensures the asymptotic stability of the origin;

2. for $\omega_k \neq 0$ with $\omega_k \in \mathcal{W}$, the trajectories of the closed-loop system do not leave the set $\mathcal{L}_{\mathcal{V}}(\mu^{-1}) \subseteq \mathcal{R}_{\mathcal{A}}$ for every initial state belonging to the set $\mathcal{L}_{\mathcal{V}}(\beta^{-1}) \subseteq \mathcal{R}_0$, with $\beta^{-1} = \mu^{-1} - \delta^{-1}$.

Note that, in case 2, when the maximum allowed disturbance energy (δ^{-1}) tends to infinity, the set $\mathcal{L}_{\mathcal{V}}(\beta^{-1}) \equiv \mathcal{L}_{\mathcal{V}}(\mu^{-1})$.

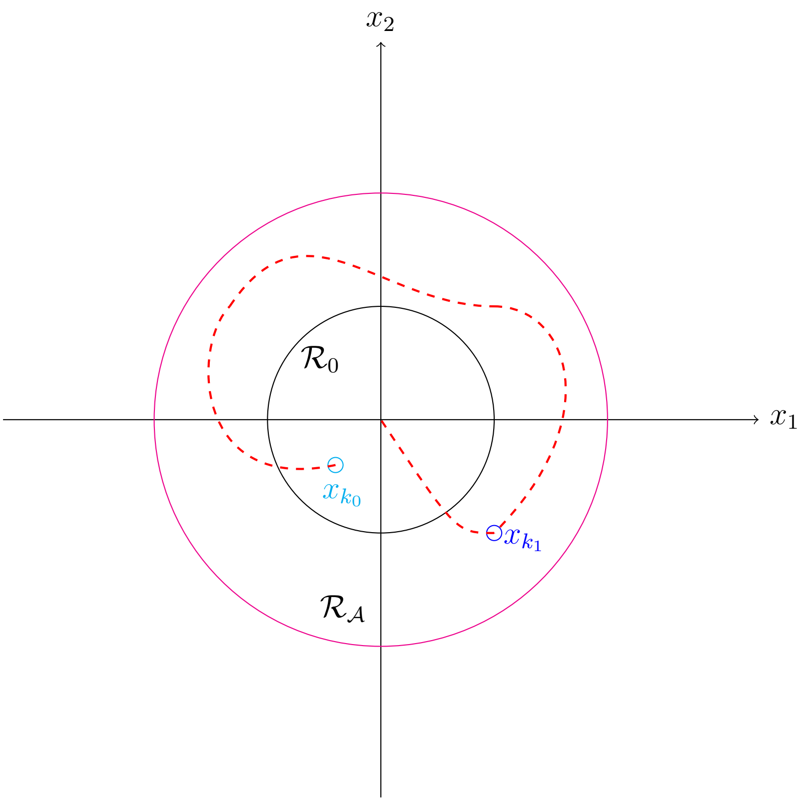

Figure 2.1: An initial condition belonging to $\mathcal{R}_0$ is subject to a disturbance signal that starts to act at the instant k_0. The state trajectory does not leave the region $\mathcal{R}_{\mathcal{A}}$. Thus, when $\omega_k = 0$ for $k \geq k_1$, the state converges asymptotically toward the origin, demonstrating the input-to-state stability.

In Figure 2.1, the input-to-state stability is illustrated. It is assumed that at instant k_0 the disturbance signal ω_k starts to act, and the initial condition belongs to $\mathcal{R}_0$. In this case, the trajectory remains inside the region $\mathcal{R}_{\mathcal{A}}$ for any $\omega_k \in \mathcal{W}$. Considering that the disturbance vanishes in k_1, it is guaranteed that the system trajectories converge asymptotically to the origin when $k \to \infty$.

Therefore, from the input-to-state stability, the control design objective can be seen as projecting a signal u_k in (2.13) to tolerate the highest possible value of disturbance energy δ^{-1} or to maximize the estimate of the region $\mathcal{R}_0$ for a given disturbance energy value.

2.3.1 ℓ_2-gain

Consider a discrete-time LPV system subject to external disturbances, such that

$$\begin{aligned} x_{k+1} &= A(\alpha_k)x_k + B(\alpha_k)u_k + B_w(\alpha_k)\omega_k, \\ y_k &= C(\alpha_k)x_k, \end{aligned} \tag{2.15}$$

where $x_k \in \mathbb{R}^n$ is the state vector, $u_k \in \mathbb{R}^{n_u}$ is the control signal vector, $\omega_k \in \mathbb{R}^{n_w}$ is the vector of supposed quadratically summable perturbation signals belonging to (2.14), $y_k \in \mathbb{R}^{n_y}$ is the measurable output signal, the linear parameter-dependent matrices $A(\alpha_k) \in \mathbb{R}^{n\times n}$, $B(\alpha_k) \in \mathbb{R}^{n\times n_u}$, $B_w(\alpha_k) \in \mathbb{R}^{n\times n_w}$ and $C(\alpha_k) \in \mathbb{R}^{n_y\times n}$ belong to a polytopic domain given by (2.2) with $\alpha_k \in \mathcal{P}$.

Considering

$$\tilde{\mathcal{J}}_k = \Delta V(x_k,\alpha_k) - \omega_k^\top \omega_k + \gamma^{-1} y_k^\top y_k,$$

$\forall k > 0$, being $V(x_k,\alpha_k) > 0$ a candidate Lyapunov function, then

$$\sum_{i=0}^{k} \tilde{\mathcal{J}}_k = V(x_k,\alpha_k) - V(x_0,\alpha_0) - \sum_{i=0}^{k} \omega_i^\top \omega_i + \gamma^{-1} \sum_{i=0}^{k} y_i^\top y_i.$$

So, if $\tilde{\mathcal{J}}_k < 0$, it follows that:

1. for the system without disturbance, i.e., with $\omega_k = 0$, $\forall k \geq 0$, then $\Delta V(x_k,\alpha_k) < -\gamma^{-1} y_k^\top y_k \leq 0$, which guarantees that the set $\mathcal{L}_{\mathcal{V}}(\mu^{-1}) \subseteq \mathcal{R}_{\mathcal{A}}$ is a region of initial conditions that ensures the asymptotic stability of the origin;

2. (a) for $\omega_k \neq 0$ with $\omega_k \in \mathcal{W}$, the trajectories of the closed-loop system do not leave the set $\mathcal{L}_{\mathcal{V}}(\mu^{-1}) \subseteq \mathcal{R}_{\mathcal{A}}$ for every initial state belonging to the set $\mathcal{L}_{\mathcal{V}}(\beta^{-1}) \subseteq \mathcal{R}_0$, with $\beta^{-1} = \mu^{-1} - \delta^{-1}$;

   (b) for $\omega_k \neq 0$ with $\omega_k \in \mathcal{W}$, for $k \to \infty$, $\|y_k\|_2^2 \leq \gamma(\|\omega_k\|_2^2 + V(x_0,\alpha_0))$. Then, if $x_0 = 0$, it follows that $\|y_k\|_2^2 < \gamma\|\omega_k\|_2^2$, i.e., γ is a bound factor for ℓ_2-gain.

See that if there is no concern about the ℓ_2-gain in the problem, it can be treated as the previous case presented in Section 2.3.

In this case, a problem of interest added to the one presented before Section 2.3.1 is to design the control signal u_k to minimize the relation between the signals y_k and ω_k, that is, minimizing the gain ℓ_2.

2.4 Saturating Actuators

In this section, the development to treat the stabilization of systems subject to saturating actuators is shown. First, the mathematical tools considering magnitude saturation are presented. Next, we consider the magnitude and rate saturation.

2.4.1 Magnitude Saturation

Consider the following discrete-time LPV system

$$x_{k+1} = A(\alpha_k)x_k + B(\alpha_k)\texttt{sat}\left(u_k\right), \tag{2.16}$$

where $x_k \in \mathbb{R}^n$ is the state vector, $u_k \in \mathbb{R}^{n_u}$ is the control signal vector, the linear parameter-dependent matrices $A(\alpha_k) \in \mathbb{R}^{n\times n}$ and $B(\alpha_k) \in \mathbb{R}^{n\times n_u}$ belong to polytopic domain given (2.2) with $\alpha_k \in \mathcal{P}$.

The system has input magnitude bounds, given by $\rho_{(r)} \in \mathbb{R}^{n_u}$, where the saturation function is described as

$$\texttt{sat}\left(u_k\right)_{(r)} = \begin{cases} \rho_{(r)}, & \text{if} \quad u_{k(r)} > \rho_{(r)} \\ u_{k(r)}, & \text{if} \quad -\rho_{(r)} \leq u_{k(r)} \leq \rho_{(r)} \\ -\rho_{(r)}, & \text{if} \quad u_{k(r)} < -\rho_{(r)} \end{cases} \tag{2.17}$$

where $\rho_{(r)}$ is the symmetrical magnitude bound for each saturating actuator and $r = 1,\ldots,n_u$.

The control law applied in the system, considering a time-varying parameters dependent controller, is given by

$$u_k = K(\alpha_k)x_k, \tag{2.18}$$

where $K(\alpha_k) \in \mathbb{R}^{n_u\times n}$, and belong to polytopic domain given by (2.2) with $\alpha_k \in \mathcal{P}$. Note that the control signal is limited in magnitude and the closed-loop system can be written substituting (2.18) in (2.16), resulting in

$$x_{k+1} = A(\alpha_k)x_k + B(\alpha_k)\texttt{sat}\left(K(\alpha_k)x_k\right). \tag{2.19}$$

Hence, the control signal available in system (2.19) is shown in Figure 2.2, where the nonlinear behavior of the saturation function can be observed.

Due to the actuator constraints' nonlinearities, in general, global closed-loop stability cannot be ensured. Thus, it is necessary to determine the region of attraction $\mathcal{R}_{\mathcal{A}} \subseteq \mathbb{R}^n$

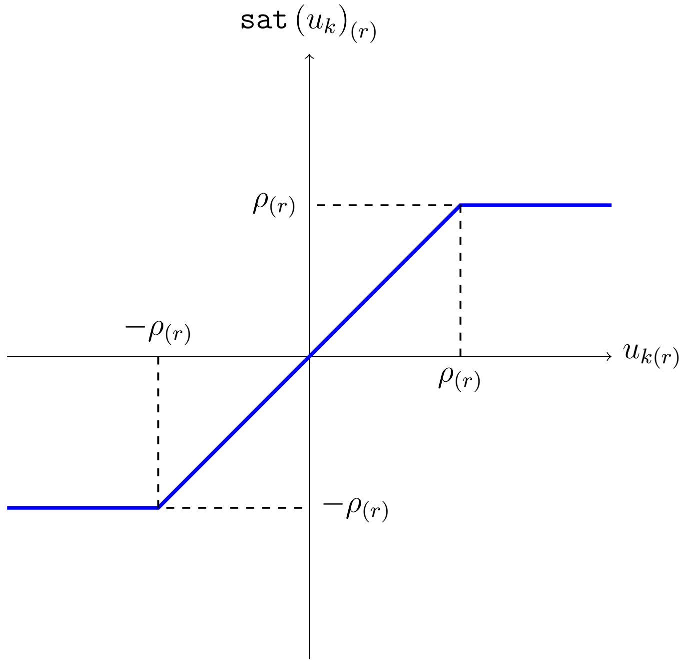

Figure 2.2: Saturation function.

of all initial conditions such that the corresponding trajectories of (2.19) converge to the origin. Because $\mathcal{R}_{\mathcal{A}}$ can be non-convex, open, and even unbounded in some directions (Tarbouriech *et al.*, 2006), an estimate $\mathcal{R}_{\mathcal{E}} \subseteq \mathcal{R}_{\mathcal{A}}$ is calculated as large as possible. In the literature, this estimate is made through several approaches. Among them, the most common are through ellipsoidal (Jungers & Castelan, 2011) and polyhedral (Olaru & Niculescu, 2008) sets. Thus, the controller designed considering the saturation's effect guarantees the local asymptotic stability of the system (2.19).

There are different ways to treat the problem of saturation. A brief overview of some methods is presented in Section 1.2, and more details can be found in Chapter 1 of Tarbouriech *et al.* (2011). In this work, saturation is treated through the generalized sector condition (Gomes da Silva Jr. & Tarbouriech, 2005). In this method, the saturating actuators are modeled as a dead-zone nonlinearity, illustrated in Figure 2.3, defined by

$$\psi(u_k) = \mathtt{sat}\,(u_k) - u_k, \tag{2.20}$$

that is, $\psi(u_k) = \left[\psi_1(u_k), \ldots, \psi_{n_u}(u_k)\right]^\top$, where

$$\psi(u_k)_{(r)} = \begin{cases} u_{k(r)} - \rho_{(r)}, & \text{if} \quad u_{k(r)} > \rho_{(r)} \\ 0, & \text{if} \quad -\rho_{(r)} \leq u_{k(r)} \leq \rho_{(r)} \\ u_{k(r)} + \rho_{(r)}, & \text{if} \quad u_{k(r)} < -\rho_{(r)} \end{cases} \tag{2.21}$$

for all $r = 1, \ldots, n_u$.

The nonlinearity $\psi(u_k)$ belongs locally to the sector as long as

$$-\rho^{\lambda}_{(r)} = \frac{-\rho_{(r)}}{1-\lambda_{(r)}} \leq u_{k(r)} \leq \frac{\rho_{(r)}}{1-\lambda_{(r)}} = \rho^{\lambda}_{(r)}, \tag{2.22}$$

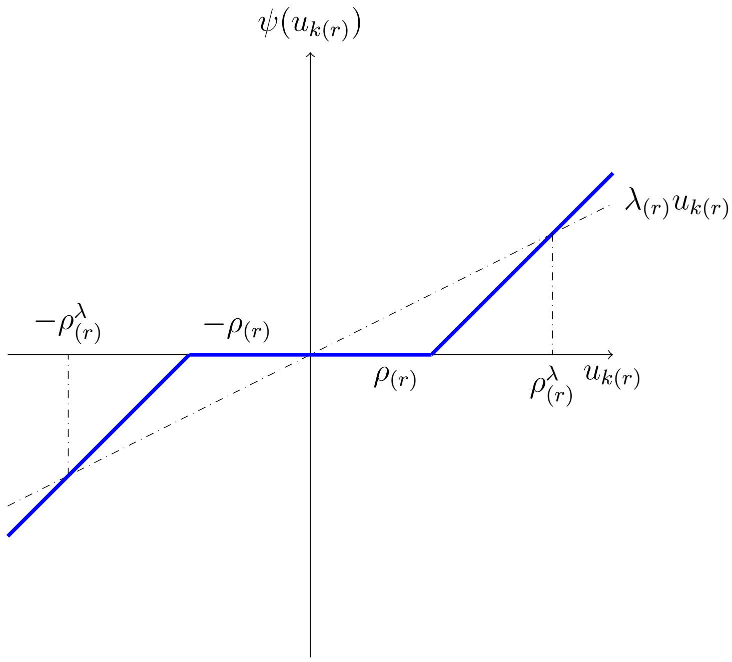

Figure 2.3: Dead-zone function.

where $0 \leq \lambda_{(r)} \leq 1$.

Replacing the dead-zone function (2.20) in (2.19), the closed-loop system can be written as

$$x_{k+1} = \Big(A(\alpha_k) + B(\alpha_k)K(\alpha_k)\Big)x_k + B(\alpha_k)\psi\Big(K(\alpha_k)x_k\Big). \tag{2.23}$$

Therefore, the system can be seen as a Lur'e type system, which is characterized by having a linear part and a memoryless nonlinearity satisfying a sector condition in its dynamics (Tarbouriech *et al.*, 2011, pp. 40). Then, the stability of the system with saturation can be assured using the generalized sector condition.

Consider the signal $u_k - v_k$ where the auxiliary signal $v_k = Gx_k$ is used as a degree of freedom in the controller design. Therefore, the set $\mathbb{S}(\rho)$ is defined such that $u_k - v_k$ belong to:

$$\mathbb{S}(\rho) = \Big\{u_k \in \mathbb{R}^{n_u}, v_k \in \mathbb{R}^{n_u} : \big|u_{k(r)} - v_{k(r)}\big| \leq \rho_{(r)}\Big\}, \tag{2.24}$$

for all $r = ,1 \ldots, n_u$. Then, the following lemma presented by Gomes da Silva Jr. & Tarbouriech (2005) can be stated:

Lemma 2.4 (Generalized sector condition) *Consider the function $\psi(u_k)$ defined in (2.20). If $x_k \in \mathbb{S}(\rho)$, then the relation*

$$\psi(u_k)^{\top}T\left[\psi(u_k) + v_k\right] \leq 0 \tag{2.25}$$

is verified for any positive definite diagonal matrix $T \in \mathbb{R}^{n_u \times n_u}$.

Note that, for the system (2.23) stabilization, the gain matrix $K(\alpha_k)$ is parameter-dependent. Then, the extra degree of freedom signal $v_k = G(\alpha_k)x_k$ can be considered with a similar structure to the control signal u_k, depending linearly on α_k.

2.4.2 Magnitude and Rate Saturation

In addition to magnitude saturation, the signal rate of change saturation is a nonlinearity that can be critical, and its effects need to be considered in many applications, as exemplified in Chapter 1. In this work, the actuator with magnitude and rate saturation is modeled as a first-order system with saturations in the input signal (representing the magnitude limitation) and the actuator state (describing the rate limitation). This topology is known as *position-feedback-type model with speed limitation*, and its main advantage is to treat both types of saturation as magnitude limitations. It should also be considered that saturations are nested, with the magnitude and rate saturation problem being a particular case of nested saturation problems, as discussed in (Tarbouriech *et al.*, 2006).

Therefore, consider the following discrete-time LPV system:

$$x_{k+1} = A(\alpha_k)x_k + B(\alpha_k)\phi_k(u_k), \tag{2.26}$$

where the linear parameter-dependent matrices $A(\alpha_k) \in \mathbb{R}^{n\times n}$ and $B(\alpha_k) \in \mathbb{R}^{n\times n_u}$ belong to the polytopic domain given (2.2) with $\alpha_k \in \mathcal{P}$, and each actuator saturating in magnitude and rate is modeled as a discrete-time version of the *position-type feedback model with speed limitation* presented in Figure 1.3, which is reproduced in Figure 2.4 for the reader's convenience. The output is given by $\phi_k(\cdot) : \mathbb{R}^{n_u} \to \mathbb{R}^{n_u}$, whose dynamics is given

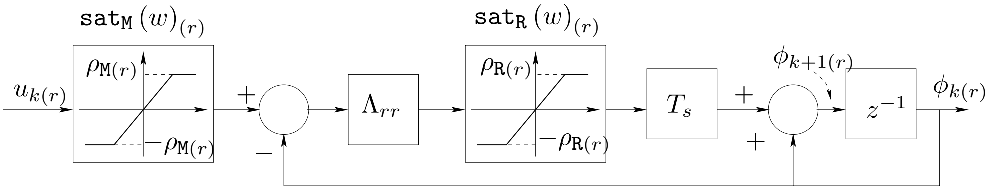

Figure 2.4: Diagram of first-order nonlinear system used to model magnitude and rate saturation.

by:

$$\bar{x}_{k+1(r)} = \bar{x}_{k(r)} + T_s\mathtt{sat}_\mathtt{R}\left(\Lambda\mathtt{sat}_\mathtt{M}\left(u_k\right) - \Lambda\bar{x}_k\right)_{(r)}, \tag{2.27}$$

$$\phi_k(u_k) = \bar{x}_k, \tag{2.28}$$

for $r = 1,\ldots,n_u$, where $\bar{x}_k \in \mathbb{R}^{n_u}$ is the actuators' state, $\Lambda \in \mathbb{R}^{n_u\times n_u}$ is a diagonal matrix composed by the actuators' poles, T_s is the sampling period of the actuator, and the symmetric saturation functions concerning the magnitude and rate are described as

(2.17) indicated respectively by $\mathtt{sat}_{\mathtt{M}}$ and $\mathtt{sat}_{\mathtt{R}}$, with $\rho_{\mathtt{M}} \in \mathbb{R}^{n_u}$ and $\rho_{\mathtt{R}} \in \mathbb{R}^{n_u}$ denoting the respective symmetrical bounds.

The control law applied in the system, considering a time-varying parameters dependent controller is given by

$$u_k = K(\alpha_k)x_k + \bar{K}(\alpha_k)\bar{x}_k = \hat{K}(\alpha_k)z_k, \tag{2.29}$$

where $K(\alpha_k) \in \mathbb{R}^{n_u \times n}$, $\bar{K}(\alpha_k) \in \mathbb{R}^{n_u \times n_u}$, $\hat{K}(\alpha_k) = \begin{bmatrix} K(\alpha_k) & \bar{K}(\alpha_k) \end{bmatrix}$, and $z_k = \begin{bmatrix} x_k^\top & \bar{x}_k^\top \end{bmatrix}^\top \in \mathbb{R}^{n+n_u}$ is an augmented state vector including the plant and actuator states. Observe that, whenever the actuator's states are not available for feedback, $\bar{K}(\alpha_k) = 0$ is required $\forall \alpha_k \in \mathcal{P}$. Therefore, the resulting closed-loop system is given by:

$$x_{k+1} = A(\alpha_k)x_k + B(\alpha_k)\phi_k\big(\hat{K}(\alpha_k)z_k\big). \tag{2.30}$$

Since the modeling of the actuators allows both saturations to be treated as magnitude saturation, it is possible to use the generalized sector condition to guarantee the system's stability. The dead-zone functions are defined as

$$\psi_1(z_k) = \psi_{\mathtt{M}k} = \mathtt{sat}_{\mathtt{M}}\left(\hat{K}(\alpha_k)z_k\right) - \hat{K}(\alpha_k)z_k, \tag{2.31}$$

$$\begin{aligned}\psi_2(z_k,\psi_{\mathtt{M}k}) = \psi_{\mathtt{R}k} = \mathtt{sat}_{\mathtt{R}}&\left(\Lambda\mathtt{sat}_{\mathtt{M}}\left(\hat{K}(\alpha_k)z_k\right) - \Lambda\bar{x}_k\right)\\ &- \left(\Lambda\mathtt{sat}_{\mathtt{M}}\left(\hat{K}(\alpha_k)z_k\right) - \Lambda\bar{x}_k\right).\end{aligned} \tag{2.32}$$

Note that (2.31) can be replaced in (2.32), resulting in

$$\psi_{\mathtt{R}k} = \mathtt{sat}_{\mathtt{R}}\left(\big(\hat{\Lambda} + \Lambda\hat{K}(\alpha_k)\big)z_k + \Lambda\psi_{\mathtt{M}k}\right) - \left(\big(\hat{\Lambda} + \Lambda\hat{K}(\alpha_k)\big)z_k + \Lambda\psi_{\mathtt{M}k}\right).$$

where $\hat{\Lambda} = \begin{bmatrix} \mathbf{0} & -\Lambda \end{bmatrix}$.

Therefore, the following polyhedral sets are defined with the aid of parameter-dependent matrices $G_{\mathtt{M}}(\alpha_k)$, $G_{\mathtt{R}_1}(\alpha_k)$, $G_{\mathtt{R}_2}(\alpha_k) \in \mathbb{R}^{n_u \times (n+n_u)}$:

$$\mathbb{S}_{\mathtt{M}}(\rho_{\mathtt{M}}) = \left\{ z_k \in \mathbb{R}^{n+n_u} : \left| \left(\big(\hat{K}(\alpha_k) - G_{\mathtt{M}}(\alpha_k)\big)z_k\right)_{(r)} \right| \leq \rho_{\mathtt{M}(r)} \right\}, \tag{2.33}$$

and

$$\mathbb{S}_{\mathtt{R}}(\rho_{\mathtt{R}}) = \left\{ z_k \in \mathbb{R}^{n+n_u}, \psi_{\mathtt{M}k} \in \mathbb{R}^{n_u} : \left| \left(\left(\begin{bmatrix} \hat{\Lambda} + \Lambda\hat{K}(\alpha_k) & \Lambda \end{bmatrix} - G_{\mathtt{R}}(\alpha_k) \right) \begin{bmatrix} z_k \\ \psi_{\mathtt{M}k} \end{bmatrix} \right)_{(r)} \right| \leq \rho_{\mathtt{R}(r)} \right\}, \tag{2.34}$$

for all $r = 1, \ldots, n_u$ with $G_{\mathtt{R}}(\alpha_k) = \begin{bmatrix} G_{\mathtt{R}_1}(\alpha_k) & G_{\mathtt{R}_2}(\alpha_k) \end{bmatrix}$.

Applying Lemma 2.4, in the dead-zone functions given in (2.31) and (2.32), if $z_k \in \mathbb{S}_{\mathtt{M}}(\rho_{\mathtt{M}})$, z_k and $\psi_{\mathtt{M}k}$ belong to $\mathbb{S}_{\mathtt{R}}(\rho_{\mathtt{R}})$, then the following inequalities are satisfied:

$$\psi_{\mathtt{M}k}^\top T_{\mathtt{M}}(\psi_{\mathtt{M}k} + G_{\mathtt{M}}(\alpha_k)z_k) \leq 0, \tag{2.35}$$

$$\psi_{\mathtt{R}k}^\top T_{\mathtt{R}}(\psi_{\mathtt{R}k} + G_{\mathtt{R}}(\alpha_k) \begin{bmatrix} z_k^\top & \psi_{\mathtt{M}k}^\top \end{bmatrix}^\top) \leq 0, \tag{2.36}$$

where $T_{\mathtt{M}}$ and $T_{\mathtt{R}}$ are diagonal positive definite matrices belonging to $\mathbb{R}^{n_u \times n_u}$.

2.5 Final Considerations

In this chapter, the main theoretical concepts and essential mathematical tools necessary for the development and understanding of this work were addressed, such as LPV system definitions; stability in the sense of Lyapunov, more specifically using parameter-dependent functions; input-to-state stability and ℓ_2-gain estimation; and stabilization of systems with saturating actuators.

Chapter 3

ISS under magnitude and rate saturating actuators

This chapter presents new convex conditions to design state-feedback LPV controllers for discrete-time systems subject to magnitude and rate saturating actuators and energy bounded disturbances. The input-to-state stability conditions are used to design controllers ensuring the minimization of the ℓ_2-gain between the disturbance input and the controlled output. Furthermore, optimization procedures to maximize the estimate of the region of attraction and the tolerance to disturbance are formulated. The efficacy of the proposed methods is illustrated with numerical examples.

3.1 Problem Formulation

Consider the discrete-time system with time-varying parameters, subject to magnitude and rate saturations, and energy-limited disturbances, described by:

$$\begin{aligned} x_{k+1} &= A(\alpha_k)x_k + B(\alpha_k)\phi_k(u_k) + B_w(\alpha_k)\omega_k, \\ y_k &= C(\alpha_k)x_k, \end{aligned} \tag{3.1}$$

where $x_k \in \mathbb{R}^n$ is the state vector, $u_k \in \mathbb{R}^{n_u}$ is the control signal vector, $y_k \in \mathbb{R}^{n_y}$ is the measurable output signal, $\omega_k \in \mathbb{R}^{n_w}$ is an ℓ_2 signal, i.e., ω_k is a quadratically summable perturbation signal belonging to

$$\mathcal{W} = \{\omega_k \in \mathbb{R}^{n_w} : \|\omega_k\|_2^2 \leq \delta^{-1}\}, \tag{3.2}$$

with $\|\omega_k\|_2 = \sqrt{\sum_{k=0}^{\infty} \omega_k^\top \omega_k}$ and $\delta^{-1} \in \mathbb{R}_+$ represents the maximum energy of the disturbance signals. The linear parameter-dependent matrices $A(\alpha_k) \in \mathbb{R}^{n\times n}$, $B(\alpha_k) \in \mathbb{R}^{n\times n_u}$, $B_w(\alpha_k) \in \mathbb{R}^{n\times n_w}$ and $C(\alpha_k) \in \mathbb{R}^{n_y\times n}$ belong to a polytopic domain given by the convex combination of N known vertices:

$$M(\alpha_k) = \sum_{i=1}^{N} \alpha_{k(i)} M_i, \tag{3.3}$$

with M replacing matrices A, B, B_w and C where $\alpha_k \in \mathcal{P}$ is the time-varying vector of parameters, which is assumed to be online available (Briat, 2015, pp. 10) and belongs to the unit simplex:

$$\mathcal{P}=\left\{\alpha_k \in \mathbb{R}^N : \sum_{i=1}^{N} \alpha_{k(i)} = 1, \alpha_{k(i)} \geq 0, i = 1, \ldots, N\right\}. \tag{3.4}$$

The discrete-time version of the PTFMSL presented in Figure 1.3, which is reproduced in Figure 3.1 for the reader's convenience, is employed for each actuator, where the output is given by $\phi_k(\cdot) : \mathbb{R}^{n_u} \to \mathbb{R}^{n_u}$, whose dynamics is given by

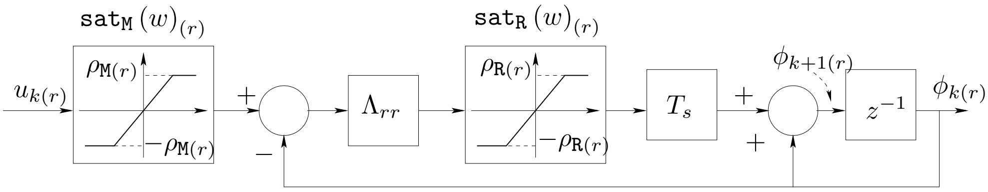

Figure 3.1: Diagram of first-order nonlinear system used to model magnitude and rate saturation.

$$\bar{x}_{k+1(i)} = \bar{x}_{k(i)} + T_s \mathtt{sat}_{\mathtt{R}}\left(\Lambda \mathtt{sat}_{\mathtt{M}}(u_k) - \Lambda \bar{x}_k\right)_{(i)}, \tag{3.5}$$

$$\phi_k(u_k) = \bar{x}_k, \tag{3.6}$$

for $i = 1, \ldots, n_u$, where $\bar{x}_k \in \mathbb{R}^{n_u}$ is the actuators' state, $\Lambda \in \mathbb{R}^{n_u \times n_u}$ is a diagonal matrix composed by the actuators' poles, T_s is the sampling period of the actuator, and for a signal $w \in \mathbb{R}^{n_u}$ the symmetric saturation functions concerning the rate and magnitude are given by

$$\mathtt{sat}_{\mathtt{R}}(w)_{(i)} = \mathtt{sign}(w_{(i)}) \min(|w_{(i)}|, \rho_{\mathtt{R}(i)}), \tag{3.7}$$

and

$$\mathtt{sat}_{\mathtt{M}}(w)_{(i)} = \mathtt{sign}(w_{(i)}) \min(|w_{(i)}|, \rho_{\mathtt{M}(i)}), \tag{3.8}$$

respectively, with $\rho_{\mathtt{R}} \in \mathbb{R}^{n_u}$ and $\rho_{\mathtt{M}} \in \mathbb{R}^{n_u}$ denoting the respective symmetrical bounds.

Considering a state feedback parameter-dependent control law that may use the state of the actuator to stabilize system (3.1)–(3.6), given as

$$u_k = K(\alpha_k)x_k + \bar{K}(\alpha_k)\bar{x}_k = \hat{K}(\alpha_k)z_k, \tag{3.9}$$

where $K(\alpha_k) \in \mathbb{R}^{n_u \times n}$, $\bar{K}(\alpha_k) \in \mathbb{R}^{n_u \times n_u}$,

$$\hat{K}(\alpha_k) = \begin{bmatrix} K(\alpha_k) & \bar{K}(\alpha_k) \end{bmatrix},$$

and

$$z_k = \begin{bmatrix} x_k^\top & \bar{x}_k^\top \end{bmatrix}^\top \in \mathbb{R}^{n+n_u}$$

is an augmented state vector including the plant and actuator states.

Therefore, the resulting closed-loop system (3.1)–(3.9), is given by:

$$\begin{aligned} x_{k+1} &= A(\alpha_k)x_k + B(\alpha_k)\phi_k\left(\hat{K}\left(\alpha_k\right)z_k\right) + B_w(\alpha_k)\omega_k, \\ y_k &= C(\alpha_k)x_k. \end{aligned} \tag{3.10}$$

Since the actuators are saturating, the resulting closed-loop system (3.10) is nonlinear. Therefore, generally, global stability cannot be achieved for the cases where $A(\alpha_k)$ is not exponentially stable. Hence, it is necessary to determine the set of initial conditions $\mathcal{R}_\mathcal{A} \subseteq \mathbb{R}^{n+n_u}$ that result in trajectories that converge asymptotically to the origin, being called the region of attraction. In particular, considering the energy of $\omega_k \in \mathcal{W}$ with $\delta > 0$, the set of initial conditions $\mathcal{R}_0 \subseteq \mathcal{R}_\mathcal{A}$ must be determined to ensure that the closed-loop trajectories do not leave the set $\mathcal{R}_\mathcal{A}$. To guarantee regional stability in the presence of energy-limited exogenous signals, the following definition (Sontag, 2008) is considered:

Definition 3.1 *Consider a positive scalar δ and any sequence $\omega_k \in \mathcal{W}$. The resulting closed-loop system is said to be input-to-state stable (ISS) if for any initial state belonging to $\mathcal{R}_0$ the resulting state trajectories remain bounded in $\mathcal{R}_\mathcal{A}$ for all $k \geq 0$. Moreover, if the disturbance is vanishing, then the state trajectories converge towards the origin.*

Due to the difficulties in determining the region of attraction, such as non-convexity and eventually not being limited in certain directions (see (Tarbouriech *et al.*, 2011, pp. 14)), we search for an estimate $\mathcal{R}_\mathcal{E} \subseteq \mathcal{R}_\mathcal{A}$ and $\mathcal{R}_{\mathcal{E}0} \subseteq \mathcal{R}_0$ as large as possible. Thus, one of the problems investigated in this work is described as follows:

Problem 3.1 *Given the discrete-time LPV system represented by (3.1)–(3.4), the actuator dynamics in (3.5)–(3.6), and the control law (3.9), determine parameter-dependent state feedback gains $K(\alpha_k)$ and $\bar{K}(\alpha_k)$ and estimates $\mathcal{R}_{\mathcal{E}0} \subseteq \mathcal{R}_0$ and $\mathcal{R}_\mathcal{E} \subseteq \mathcal{R}_\mathcal{A}$ such that the resulting closed-loop system is ISS for all $\omega_k \in \mathcal{W}$ and $\alpha_k \in \mathcal{P}$. In addition, the designed controller must ensure a certain upper limit of the ℓ_2-gain, denoted by γ, between the disturbance signal ω_k and the regulated output y_k, such that*

$$\|y_k\|_2 = \sqrt{\gamma}(\|\omega_k\|_2 + \mathfrak{b}), \tag{3.11}$$

where the bias term $\mathfrak{b}$ due to the non-null initial conditions.

It is important to mention that based on Problem 3.1, some optimization procedures, concerning the maximization of the region of attraction $\mathcal{R}_\mathcal{A}$ or the region $\mathcal{R}_0$, the maximization of the disturbance tolerance, or even the minimization of the ℓ_2-gain, can be developed and will be presented later.

3.2 Auxiliary Results

Using the dead-zone functions to handle the actuators' nonlinearities as described in Section 2.4.2, repeated here for convenience

$$\psi_{\mathtt{M}k} = \mathtt{sat}_{\mathtt{M}}\left(u_k\right) - u_k, \tag{3.12}$$

$$\psi_{\mathtt{R}k} = \mathtt{sat}_{\mathtt{R}}\left(\Lambda \mathtt{sat}_{\mathtt{M}}\left(u_k\right) - \Lambda \bar{x}_k\right) - \left(\Lambda \mathtt{sat}_{\mathtt{M}}\left(u_k\right) - \Lambda \bar{x}_k\right), \tag{3.13}$$

and using the control law (3.9), $\psi_{\mathtt{R}k}$ can be rewritten as

$$\psi_{\mathtt{R}k} = \mathtt{sat}_{\mathtt{R}}\left(\left(\hat{\Lambda} + \Lambda \hat{K}(\alpha_k)\right) z_k + \Lambda \psi_{\mathtt{M}k}\right) - \left(\left(\hat{\Lambda} + \Lambda \hat{K}(\alpha_k)\right) z_k + \Lambda \psi_{\mathtt{M}k}\right), \tag{3.14}$$

where $\hat{\Lambda} = \begin{bmatrix} \mathbf{0} & -\Lambda \end{bmatrix}$. By taking (3.5)–(3.6), and (3.10), the resulting dynamics of the augmented closed-loop system can be rewritten as:

$$\begin{aligned} z_{k+1} &= \left(\hat{A}\left(\alpha_k\right) + \bar{B}\hat{K}\left(\alpha_k\right)\right) z_k + \begin{bmatrix} \bar{B} & \hat{B} \end{bmatrix} \begin{bmatrix} \psi_{\mathtt{M}k} \\ \psi_{\mathtt{R}k} \end{bmatrix} + \hat{B}_w(\alpha_k)\omega_k, \\ y_k &= \hat{C}(\alpha_k) z_k \end{aligned} \tag{3.15}$$

with

$$\begin{gathered} \hat{A}(\alpha_k) = \begin{bmatrix} A(\alpha_k) & B(\alpha_k) \\ \mathbf{0} & \mathbf{I} - T_s\Lambda \end{bmatrix}, \ \bar{B} = \begin{bmatrix} \mathbf{0} \\ T_s\Lambda \end{bmatrix}, \ \hat{B} = \begin{bmatrix} \mathbf{0} \\ T_s\mathbf{I} \end{bmatrix}, \\ \hat{B}_w(\alpha_k) = \begin{bmatrix} B_w(\alpha_k) \\ \mathbf{0} \end{bmatrix}, \ \hat{C}(\alpha_k) = \begin{bmatrix} C(\alpha_k) \\ \mathbf{0} \end{bmatrix}^\top. \end{gathered} \tag{3.16}$$

Observe that (3.15) is expressed as a Lur'e type system (see section 2.4.1).

From Lemma 2.4 used to handle the nested saturation function, it yields to the following polyhedral sets defined with the aid of parameter-dependent matrices $G_{\mathtt{M}}(\alpha_k)$, $G_{\mathtt{R}_1}(\alpha_k)$, $G_{\mathtt{R}_2}(\alpha_k) \in \mathbb{R}^{n_u \times (n+n_u)}$:

$$\mathbb{S}_{\mathtt{M}}(\rho_{\mathtt{M}}) = \left\{ z_k \in \mathbb{R}^{n+n_u} : \left| \left(\left(\hat{K}(\alpha_k) - G_{\mathtt{M}}(\alpha_k) \right) z_k \right)_{(r)} \right| \leq \rho_{\mathtt{M}(r)} \right\}, \tag{3.17}$$

and

$$\mathbb{S}_{\mathtt{R}}(\rho_{\mathtt{R}}) = \left\{ z_k \in \mathbb{R}^{n+n_u}, \psi_{\mathtt{M}k} \in \mathbb{R}^{n_u} : \left| \left(\left(\begin{bmatrix} \hat{\Lambda} + \Lambda \hat{K}(\alpha_k) & \Lambda \end{bmatrix} - G_{\mathtt{R}}(\alpha_k) \right) \begin{bmatrix} z_k \\ \psi_{\mathtt{M}k} \end{bmatrix} \right)_{(r)} \right| \leq \rho_{\mathtt{R}(r)} \right\}, \tag{3.18}$$

for $r = 1, \ldots, n_u$, with $G_{\mathtt{R}}(\alpha_k) = \begin{bmatrix} G_{\mathtt{R}_1}(\alpha_k) & G_{\mathtt{R}_2}(\alpha_k) \end{bmatrix}$. Therefore, $\mathbb{S}_{\mathtt{M}}(\rho_{\mathtt{M}})$ is the set of z_k where the modulus of the signal $\left(\hat{K}(\alpha_k) - G_{\mathtt{M}}(\alpha_k)\right) z_k$ has a maximum value of $\rho_{\mathtt{M}}$. Similarly, $\mathbb{S}_{\mathtt{R}}(\rho_{\mathtt{R}})$ is the set of z_k and $\psi_{\mathtt{M}k}$ regarding to the bound $\rho_{\mathtt{R}}$. Then, if $z_k \in \mathbb{S}_{\mathtt{M}}(\rho_{\mathtt{M}})$, z_k and $\psi_{\mathtt{M}k}$ belong to $\mathbb{S}_{\mathtt{R}}(\rho_{\mathtt{R}})$, as stated in Lemma 2.4, the following inequalities are verified:

$$\psi_{\mathtt{M}k}^\top T_{\mathtt{M}}(\psi_{\mathtt{M}k} + G_{\mathtt{M}}(\alpha_k) z_k) \leq 0, \tag{3.19}$$

$$\psi_{\mathtt{R}k}^{\top} T_{\mathtt{R}}(\psi_{\mathtt{R}k} + G_{\mathtt{R}}(\alpha_k) \begin{bmatrix} z_k^{\top} & \psi_{\mathtt{M}k}^{\top} \end{bmatrix}^{\top}) \leq 0, \tag{3.20}$$

where $T_{\mathtt{M}}$ and $T_{\mathtt{R}}$ are positive definite diagonal matrices belonging to $\mathbb{R}^{n_u \times n_u}$.

From (3.15), the input-to-state stability can be investigated by using the Lyapunov theory, with the following parameter-dependent candidate Lyapunov function $V(\cdot,\cdot)$: $\mathbb{R}^{n+n_u} \times \mathcal{P} \to \mathbb{R}^{+}$:

$$V(z_k,\alpha_k) = z_k^{\top} P(\alpha_k) z_k, \tag{3.21}$$

with

$$P(\alpha_k) = \sum_{i=1}^{N} \alpha_{k(i)} P_i > \mathbf{0}. \tag{3.22}$$

If (3.21)–(3.22) fulfills the following conditions for $z_k \in \mathcal{R}_{\mathcal{E}} \subseteq \mathbb{R}^{n+n_u}$ and class $\mathcal{K}$ functions $\beta_1 \|z_k\|^2$, $\beta_2 \|z_k\|^2$, and $\beta_3 \|z_k\|^2$, $\beta_i > 0$, $i \in \{1,2,3\}$:

$$\begin{gathered} \beta_1 \|z_k\|^2 \leq V(z_k,\alpha_k) \leq \beta_2 \|z_k\|^2, \\ \Delta V(z_k,\alpha_k) = V(z_{k+1},\alpha_{k+1}) - V(z_k,\alpha_k) \leq -\beta_3 \|z_k\|^2, \end{gathered} \tag{3.23}$$

for all allowed sequences of $\alpha_k \in \mathcal{P}$, then it ensures the regional stability of the closed-loop system, and the following level set can be associated:

$$\mathcal{L}_{\mathcal{V}}(\mu^{-1}) = \left\{ z_k \in \mathbb{R}^{n+n_u} : V(z_k,\alpha_k) \leq \mu^{-1}, \forall \alpha_k \in \mathcal{P} \right\}, \tag{3.24}$$

with $0 < \mu < \infty$. Therefore, the level set is calculated using the Lemma 2.3 as

$$\mathcal{L}_{\mathcal{V}}(\mu^{-1}) = \bigcap_{\alpha_k \in \mathcal{P}} \mathcal{E}(P(\alpha_k),\mu^{-1}) = \bigcap_{i=1}^{N} \mathcal{E}(P_i,\mu^{-1}), \tag{3.25}$$

where $\mathcal{E}(P_i,\mu^{-1})$ are ellipsoidal sets defined by

$$\mathcal{E}(P_i,\mu^{-1}) = \{ z_k \in \mathbb{R}^{n+n_u} : z_k^{\top} P_i z_k \leq \mu^{-1} \}, \tag{3.26}$$

for $i = 1,\ldots,N$. By this way, the level sets can be calculated through finite dimensions conditions, providing the estimates of the region of attraction and the region of suitable initial conditions of system (3.15), called respectively by $\mathcal{R}_{\mathcal{E}} \subseteq \mathcal{R}_{\mathcal{A}}$ and $\mathcal{R}_{\mathcal{E}0} \subseteq \mathcal{R}_0$.

3.3 Main Results

This section presents a condition proposed in this work that provides a solution to Problem 3.1, as shown in the following theorem:

Theorem 3.1 *Consider the LPV discrete-time system under magnitude and rate saturating actuators given by* (3.1)-(3.6)*, and the saturation limits $\rho_{\mathtt{M}}$ and $\rho_{\mathtt{R}}$ for the actuators' magnitude and rate, respectively. Suppose that there exist symmetric and positive definite matrices $\tilde{P}_i \in \mathbb{R}^{(n+n_u)\times(n+n_u)}$, diagonal matrices $L_{\mathtt{M}}$, $L_{\mathtt{R}} \in \mathbb{R}^{n_u \times n_u}$, matrices Z_i, $X_{\mathtt{M}i}$,*

$X_{\mathtt{R}_1 i} \in \mathbb{R}^{n_u \times (n+n_u)}$, $X_{\mathtt{R}_2 i} \in \mathbb{R}^{n_u \times n_u}$, $\tilde{H} \in \mathbb{R}^{(n+n_u)\times(n+n_u)}$, for i, $j = 1,\ldots,N$, positive scalars μ, δ and a positive scalar $\eta < 1$ such that, with matrices $\hat{A}_i$, $\bar{B}$, $\hat{B}$, $\hat{B}_{wi}$, and $\hat{C}_i$ computed as in (3.16), the following LMIs

$$\begin{bmatrix} -(1-\eta)\tilde{P}_i & -\tilde{H}^\top \hat{A}_i^\top - Z_i^\top \bar{B}^\top & -X_{\mathtt{M}i}^\top & -X_{\mathtt{R}_1 i}^\top & \mathbf{0} & \tilde{H}^\top \hat{C}_i^\top \\ \star & \tilde{P}_j + \tilde{H} + \tilde{H}^\top & -\bar{B}L_{\mathtt{M}} & -\hat{B}L_{\mathtt{R}} & -\hat{B}_{wi} & \mathbf{0} \\ \star & \star & -2L_{\mathtt{M}} & -X_{\mathtt{R}_2 i}^\top & \mathbf{0} & \mathbf{0} \\ \star & \star & \star & -2L_{\mathtt{R}} & \mathbf{0} & \mathbf{0} \\ \star & \star & \star & \star & -\mathbf{I} & \mathbf{0} \\ \star & \star & \star & \star & \star & -\gamma\mathbf{I} \end{bmatrix} < \mathbf{0}, \tag{3.27}$$

$$\begin{bmatrix} -\tilde{P}_i & Z_{i(r)}^\top - X_{\mathtt{M}i(r)}^\top \\ \star & -\mu\rho_{\mathtt{M}(r)}^2 \end{bmatrix} \leq \mathbf{0}, \tag{3.28}$$

$$\begin{bmatrix} -\tilde{P}_i & X_{\mathtt{M}i}^\top & \tilde{H}^\top \hat{\Lambda}_{(r)}^\top + (\Lambda Z_i)_{(r)}^\top - X_{\mathtt{R}_1 i(r)}^\top \\ \star & -2L_{\mathtt{M}} & L_{\mathtt{M}}\Lambda_{(r)}^\top - X_{\mathtt{R}_2 i(r)}^\top \\ \star & \star & -\mu\rho_{\mathtt{R}(r)}^2 \end{bmatrix} \leq \mathbf{0}, \tag{3.29}$$

and

$$\delta - \mu \geq 0 \tag{3.30}$$

are feasible for $\forall r = 1,\ldots,n_u$. Then, the control gain matrices

$$\hat{K}_i = Z_i \tilde{H}^{-1},$$

where $\hat{K}_i = \begin{bmatrix} K_i & \bar{K}_i \end{bmatrix}$, yield the control law (3.9) that

1. *for $\omega_k \neq 0$ with $\omega_k \in \mathcal{W}$, the trajectories of the closed-loop system do not leave the set $\mathcal{R}_{\mathcal{E}} = \mathcal{L}_{\mathcal{V}}(\mu^{-1}) \subseteq \mathcal{R}_{\mathcal{A}}$ for every initial state belonging to the set $\mathcal{R}_{\mathcal{E}0} = \mathcal{L}_{\mathcal{V}}(\beta^{-1}) \subseteq \mathcal{R}_0$, with $\beta^{-1} = \mu^{-1} - \delta^{-1}$ for all $k \geq 0$ and $\alpha_k \in \mathcal{P}$;*

2. *$\|y_k\|_2^2 \leq \gamma(\|\omega_k\|_2^2 + V(z_0,\alpha_0))$ for $k \to \infty$;*

3. *for $\omega_k = 0$, the set $\mathcal{R}_{\mathcal{E}} = \mathcal{L}_{\mathcal{V}}(\mu^{-1}) \subseteq \mathcal{R}_{\mathcal{A}}$ is a region of asymptotic stability for the system (3.15) for all $k \geq 0$.*

Also, the control law (3.9) ensures a certain performance level to the closed-loop system measured by the Lyapunov function's decay rate as $\|z_k\| \leq \sqrt{\frac{\beta_2}{\beta_1}}\left(\sqrt{1-\eta}\right)^k \|z_0\|$, with $\beta_1 = \min_{i=1,\ldots,N} \mathtt{eig}(\tilde{H}^{-\top}\tilde{P}_i\tilde{H}^{-1})$, $\beta_2 = \max_{i=1,\ldots,N} \mathtt{eig}(\tilde{H}^{-\top}\tilde{P}_i\tilde{H}^{-1})$, and a small enough $\beta_3 > 0$, for all initial conditions belonging to the estimated region of attraction $\mathcal{R}_{\mathcal{E}}$.

Proof: The proof is divided into two steps: In the first one, the local input-to-state stability and the ℓ_2-gain for the closed-loop system are proved. In the second, it is shown that with initial conditions in $\mathcal{L}_{\mathcal{V}}(\mu^{-1})$, the sets $\mathbb{S}_{\mathtt{M}}(\rho_{\mathtt{M}})$ and $\mathbb{S}_{\mathtt{R}}(\rho_{\mathtt{R}})$ are verified, ensuring the generalized sector condition.

Step 1: Admitting the feasibility of (3.27), then $L_{\mathtt{M}}$ and $L_{\mathtt{R}}$ are nonsingular. Also, from the positivity of $\tilde{P}_i$ and block (2,2), then $\tilde{H}$ is regular. Perform the replacements: $\tilde{P}_i = \tilde{H}^\top P_i \tilde{H}$, $\tilde{P}_j = \tilde{H}^\top P_j \tilde{H}$, $Z_i = \hat{K}_i \tilde{H}$, $L_{\mathtt{M}} = T_{\mathtt{M}}^{-1}$, $L_{\mathtt{R}} = T_{\mathtt{R}}^{-1}$, $X_{\mathtt{M}i} = G_{\mathtt{M}i}\tilde{H}$, $X_{\mathtt{R}_1 i} = G_{\mathtt{R}_1 i}\tilde{H}$, and $X_{\mathtt{R}_2 i} = G_{\mathtt{R}_2 i} L_{\mathtt{M}}$, resulting in

$$\begin{bmatrix} -(1-\eta)\tilde{H}^\top P_i \tilde{H} & -\tilde{H}^\top \hat{A}_i^\top - \tilde{H}^\top \hat{K}_i^\top \bar{B}^\top & -\tilde{H}^\top G_{\mathtt{M}i}^\top & -\tilde{H}^\top G_{\mathtt{R}_1 i}^\top & \mathbf{0} & \tilde{H}^\top \hat{C}_i^\top \\ \star & \tilde{H}^\top P_j \tilde{H} + \tilde{H} + \tilde{H}^\top & -\bar{B}T_{\mathtt{M}}^{-1} & -\hat{B}T_{\mathtt{R}}^{-1} & -\hat{B}_{wi} & \mathbf{0} \\ \star & \star & -2T_{\mathtt{M}}^{-1} & -T_{\mathtt{M}}^{-1} G_{\mathtt{R}_2 i}^\top & \mathbf{0} & \mathbf{0} \\ \star & \star & \star & -2T_{\mathtt{R}}^{-1} & \mathbf{0} & \mathbf{0} \\ \star & \star & \star & \star & -\mathbf{I} & \mathbf{0} \\ \star & \star & \star & \star & \star & -\gamma\mathbf{I} \end{bmatrix} < \mathbf{0}. \tag{3.31}$$

Pre- and post-multiplying (3.31) by diag$\{H, H, T_{\mathtt{M}}, T_{\mathtt{R}}, \mathbf{I}, \mathbf{I}\}$, where $H = \tilde{H}^{-\top}$, and its transpose, yields

$$\begin{bmatrix} -(1-\eta)P_i & -\hat{A}_i^\top H^\top - \hat{K}_i^\top \bar{B}^\top H^\top & -G_{\mathtt{M}i}^\top T_{\mathtt{M}}^\top & -G_{\mathtt{R}_1 i}^\top T_{\mathtt{R}}^\top & \mathbf{0} & \hat{C}^\top \\ \star & P_j + H + H^\top & -H\bar{B} & -H\hat{B} & -H\hat{B}_w & \mathbf{0} \\ \star & \star & -2T_{\mathtt{M}} & -G_{\mathtt{R}_2 i}^\top T_{\mathtt{R}}^\top & \mathbf{0} & \mathbf{0} \\ \star & \star & \star & -2T_{\mathtt{R}} & \mathbf{0} & \mathbf{0} \\ \star & \star & \star & \star & -\mathbf{I} & \mathbf{0} \\ \star & \star & \star & \star & \star & -\gamma\mathbf{I} \end{bmatrix} < \mathbf{0}. \tag{3.32}$$

Next, multiplying (3.32) by $\alpha_{k(i)}$, $\alpha_{k+1(j)}$, $\alpha_k \in \mathcal{P}$, and summing it for $i,j = 1,\ldots,N$, results in

$$\begin{bmatrix} -(1-\eta)P(\alpha_k) & \Pi_1 & -G_{\mathtt{M}}(\alpha_k)^\top T_{\mathtt{M}}^\top & -G_{\mathtt{R}_1}(\alpha_k)^\top T_{\mathtt{R}}^\top & \mathbf{0} & \hat{C}(\alpha_k)^\top \\ \star & P(\alpha_{k+1}) + H + H^\top & -H\bar{B} & -H\hat{B} & -H\hat{B}_w(\alpha_k) & \mathbf{0} \\ \star & \star & -2T_{\mathtt{M}} & -G_{\mathtt{R}_2}(\alpha_k)^\top T_{\mathtt{R}}^\top & \mathbf{0} & \mathbf{0} \\ \star & \star & \star & -2T_{\mathtt{R}} & \mathbf{0} & \mathbf{0} \\ \star & \star & \star & \star & -\mathbf{I} & \mathbf{0} \\ \star & \star & \star & \star & \star & -\gamma\mathbf{I} \end{bmatrix} < \mathbf{0}, \tag{3.33}$$

with $\Pi_1 = -\hat{A}(\alpha_k)^\top H^\top - \hat{K}(\alpha_k)^\top \bar{B}^\top H^\top$. By applying the Schur's complement in (3.33) it is possible to get

$$\begin{bmatrix} -(1-\eta)\Pi_2 & \Pi_1 & -G_{\mathtt{M}}(\alpha_k)^\top T_{\mathtt{M}}^\top & -G_{\mathtt{R}_1}(\alpha_k)^\top T_{\mathtt{R}}^\top & \mathbf{0} \\ \star & P(\alpha_{k+1}) + H + H^\top & -H\bar{B} & -H\hat{B} & -H\hat{B}_w(\alpha_k) \\ \star & \star & -2T_{\mathtt{M}} & -G_{\mathtt{R}_2}(\alpha_k)^\top T_{\mathtt{R}}^\top & \mathbf{0} \\ \star & \star & \star & -2T_{\mathtt{R}} & \mathbf{0} \\ \star & \star & \star & \star & -\mathbf{I} \end{bmatrix} < \mathbf{0}, \tag{3.34}$$

with $\Pi_2 = P(\alpha_k) + \hat{C}(\alpha_k)^\top \gamma^{-1} \hat{C}(\alpha_k)$.

Pre- and post-multiplying (3.34) by $\xi = \begin{bmatrix} z_k^\top & z_{k+1}^\top & \psi_{\mathtt{M}}^\top & \psi_{\mathtt{R}}^\top & \omega_k^\top \end{bmatrix}^\top$ and its transpose, respectively, considering $\Delta V(z_k,\alpha_k) = z_{k+1}^\top P(\alpha_{k+1})z_{k+1} - z_k^\top P(\alpha_k)z_k$, and replacing $\hat{C}(\alpha_k)z_k$ for y_k, thus

$$\Delta V(z_k,\alpha_k) + \eta V(z_k,\alpha_k) - 2\psi_{\mathtt{M}k}^\top T_{\mathtt{M}}\psi_{\mathtt{M}k} - 2\psi_{\mathtt{M}k}^\top T_{\mathtt{M}} G_{\mathtt{M}}(\alpha_k)z_k - 2\psi_{\mathtt{R}k}^\top T_{\mathtt{R}}\psi_{\mathtt{R}k} - 2\psi_{\mathtt{R}k}^\top T_{\mathtt{R}} G_{\mathtt{R}_1}(\alpha_k)z_k \\ - 2\psi_{\mathtt{R}k}^\top T_{\mathtt{R}} G_{\mathtt{R}_2}(\alpha_k)\psi_{\mathtt{M}k} - \omega_k^\top\omega_k + \gamma^{-1}y_k^\top y_k < 0. \quad (3.35)$$

Therefore, if (3.27) is verified and z_k belongs to both $\mathbb{S}_{\mathtt{M}}(\rho_{\mathtt{M}})$ and $\mathbb{S}_{\mathtt{R}}(\rho_{\mathtt{R}})$, conditions (3.19) and (3.20) are satisfied, then (3.35) yields $\beta_1 = \min_{i=1,\ldots,N} \mathtt{eig}(\tilde{H}^{-\top}\tilde{P}_i\tilde{H}^{-1})$, $\beta_2 = \max_{i=1,\ldots,N} \mathtt{eig}(\tilde{H}^{-\top}\tilde{P}_i\tilde{H}^{-1})$, which with a small enough $\beta_3 > 0$ and (3.23) ensures that $V(z_k,\alpha_k)$ is radially unbounded and that $\Delta V(z_k,\alpha_k) < -\eta V(z_k,\alpha_k) \leq 0$ is verified. Also, the trajectories of the closed-loop system (3.15) under the control law (3.9) are bounded for any disturbance satisfying (3.2), and, in addition, there is an upper bound for the ℓ_2-gain between the disturbance and the regulated output. Moreover, it ensures that

$$V(z_k,\alpha_k) \leq (1-\eta)^k V(z_0,\alpha_0),$$

and

$$\beta_1\|z_k\|^2 \leq \beta_2(1-\eta)^k\|z_0\|^2.$$

Then,

$$\|z_k\| \leq \sqrt{\frac{\beta_2}{\beta_1}}\left(\sqrt{1-\eta}\right)^k\|z_0\|$$

can be written, ensuring the regional exponential convergence to the origin. This proof step can also be obtained by using Finsler's Lemma.

Step 2: It remains to demonstrate that the generalized sector conditions (3.19)-(3.20) are in fact verified. The condition (3.28) ensures the inclusion of the contractive level set given by the Lyapunov function in $\mathbb{S}_{\mathtt{M}}(\rho_{\mathtt{M}})$. Assuming the feasibility of (3.28), and doing the variables' change $\tilde{P}_i = \tilde{H}^\top P_i\tilde{H}$, $Z_i = \hat{K}_i\tilde{H}$, and $X_{\mathtt{M}i} = G_{\mathtt{M}i}\tilde{H}$, yields

$$\begin{bmatrix} -\tilde{H}^\top P_i\tilde{H} & \tilde{H}^\top\hat{K}_{i(r)}^\top - \tilde{H}^\top G_{\mathtt{M}i(r)}^\top \\ \star & -\mu\rho_{\mathtt{M}(r)}^2 \end{bmatrix} \leq \mathbf{0}. \quad (3.36)$$

Moreover, pre- and post-multiplying (3.36) by $\operatorname{diag}\{\tilde{H}^{-\top},1\}$ and its transpose, respectively, resulting in

$$\begin{bmatrix} -P_i & \hat{K}_{i(r)}^\top - G_{\mathtt{M}i(r)}^\top \\ \star & -\mu\rho_{\mathtt{M}(r)}^2 \end{bmatrix} \leq \mathbf{0}. \quad (3.37)$$

From (3.37), multiply it by $\alpha_{k(i)}$ and sum it up for $i = 1,\ldots,N$ to get

$$\begin{bmatrix} -P(\alpha_k) & \hat{K}(\alpha_k)_{(r)}^\top - G_{\mathtt{M}}(\alpha_k)_{(r)}^\top \\ \star & -\mu\rho_{\mathtt{M}(r)}^2 \end{bmatrix} \leq \mathbf{0}. \quad (3.38)$$

By applying the Schur's complement and pre- and post-multiplying by $z_k^\top$ and z_k, it follows that

$$z_k^\top\Theta_{\mathtt{M}}^\top(\mu\rho_{\mathtt{M}(r)}^2)^{-1}\Theta_{\mathtt{M}} z_k - z_k^\top P(\alpha_k)z_k \leq 0, \quad (3.39)$$

where $\Theta_{\mathtt{M}} = \hat{K}(\alpha_k)_{(r)} - G_{\mathtt{M}}(\alpha_k)_{(r)}$ and $r = 1,\ldots,n_u$. If z_0 belongs to $\mathcal{L}_{\mathcal{V}}(\mu^{-1})$, it follows that $z_k^\top P(\alpha_k) z_k \leq V(z_0) \leq \mu^{-1}$, leading to $\rho_{\mathtt{M}(r)}^{-2} |\Theta_{\mathtt{M}} z_k|^2 \leq \mu z_k^\top P(\alpha_k) z_k \leq \mu V(z_0) \leq 1$. Thus, $|\Theta_{\mathtt{M}} z_k|^2 \leq \rho_{\mathtt{M}(r)}^2$, satisfying $\mathbb{S}_{\mathtt{M}}(\rho_{\mathtt{M}})$ given in (3.17).

Lastly, the feasibility of (3.29) ensures the inclusion of the contractive level set given by the Lyapunov function in $\mathbb{S}_{\mathtt{M}}(\rho_{\mathtt{M}}) \cap \mathbb{S}_{\mathtt{R}}(\rho_{\mathtt{R}})$. Then, replacing following variables $\tilde{P}_i = \tilde{H}^\top P_i \tilde{H}$, $Z_i = \hat{K}_i \tilde{H}$, $X_{\mathtt{M}i} = G_{\mathtt{M}i}\tilde{H}$, $X_{\mathtt{R}_1 i} = G_{\mathtt{R}_1 i}\tilde{H}$, $X_{\mathtt{R}_2 i} = G_{\mathtt{R}_2 i} T_{\mathtt{M}}^{-1}$ and $L_{\mathtt{M}} = T_{\mathtt{M}}^{-1}$ in (3.29), leads to

$$\begin{bmatrix} -\tilde{H}^\top P_i \tilde{H} & \tilde{H}^\top G_{\mathtt{M}i}^\top & \tilde{H}^\top \hat{\Lambda}_{(r)}^\top + (\Lambda \hat{K}_i \tilde{H})_{(r)}^\top - \tilde{H}^\top G_{\mathtt{R}_1 i(r)}^\top \\ \star & -2T_{\mathtt{M}}^{-1} & T_{\mathtt{M}}^{-1} \Lambda_{(r)}^\top - T_{\mathtt{M}}^{-\top} G_{\mathtt{R}_2 i(r)}^\top \\ \star & \star & -\mu \rho_{\mathtt{R}(r)}^2 \end{bmatrix} \leq \mathbf{0}. \tag{3.40}$$

Next, pre- and post-multiplying (3.40) by $\operatorname{diag}\{\tilde{H}^{-\top}, T_{\mathtt{M}}, 1\}$ and its transpose, respectively, yields

$$\begin{bmatrix} -P_i & G_{\mathtt{M}i}^\top T_{\mathtt{M}} & \hat{\Lambda}_{(r)}^\top + (\Lambda \hat{K}_i)_{(r)}^\top - G_{\mathtt{R}_1 i(r)}^\top \\ \star & -2T_{\mathtt{M}} & \Lambda_{(r)}^\top - G_{\mathtt{R}_2 i(r)}^\top \\ \star & \star & -\mu \rho_{\mathtt{R}(r)}^2 \end{bmatrix} \leq \mathbf{0}. \tag{3.41}$$

Multiply (3.41) by $\alpha_{k(i)}$, and sum it up for $i = 1,\ldots,N$, then

$$\begin{bmatrix} -P(\alpha_k) & G_{\mathtt{M}}(\alpha_k)^\top T_{\mathtt{M}} & \hat{\Lambda}_{(r)}^\top + (\Lambda \hat{K}(\alpha_k))_{(r)}^\top - G_{\mathtt{R}_1}(\alpha_k)_{(r)}^\top \\ \star & -2T_{\mathtt{M}} & \Lambda_{(r)}^\top - G_{\mathtt{R}_2}(\alpha_k)_{(r)}^\top \\ \star & \star & -\mu \rho_{\mathtt{R}(r)}^2 \end{bmatrix} \leq \mathbf{0}. \tag{3.42}$$

By applying the Schur's complement and pre- and post-multiplying by $\zeta^\top = [z_k^\top \;\; \psi_{\mathtt{M}k}^\top]$ and its transpose, respectively, it follows that

$$\zeta^\top \Big(\begin{bmatrix} \Theta_{\mathtt{R}_1(r)}^\top \\ \Theta_{\mathtt{R}_2(r)}^\top \end{bmatrix} (\mu \rho_{\mathtt{R}(r)}^2)^{-1} \begin{bmatrix} \Theta_{\mathtt{R}_1(r)} & \Theta_{\mathtt{R}_2(r)} \end{bmatrix} - \begin{bmatrix} P(\alpha_k) & \mathbf{0} \\ \mathbf{0} & \mathbf{0} \end{bmatrix} \Big) \zeta \leq 0,$$

where $\Theta_{\mathtt{R}_1(r)} = \hat{\Lambda}_{(r)} + \Lambda \hat{K}(\alpha_k)_{(r)} - G_{\mathtt{R}_1}(\alpha_k)_{(r)}$ and $\Theta_{\mathtt{R}_2(r)} = \Lambda_{(r)} - G_{\mathtt{R}_2}(\alpha_k)_{(r)}$ for $r = 1,\ldots,n_u$. Similar to the analysis above mentioned for equation (3.28), it can be concluded that $|\Theta_{\mathtt{R}_1} z_k + \Theta_{\mathtt{R}_2} \psi_{\mathtt{M}k}|^2 \leq \rho_{\mathtt{R}(r)}^2$ if z_0 belongs to $\mathcal{R}_{\mathcal{E}} \equiv \mathcal{L}_{\mathcal{V}}(\mu^{-1})$, thus, z_0 belongs to both sets $\mathbb{S}_{\mathtt{M}}(\rho_{\mathtt{M}})$ and $\mathbb{S}_{\mathtt{R}}(\rho_{\mathtt{R}})$, given in (3.17) and (3.18), respectively, which ensures the generalized sector condition. Therefore, the convergence to the origin of any trajectory of the closed-loop system (3.15) starting at $\mathcal{L}_{\mathcal{V}}(\mu^{-1})$ for $\omega_k = \mathbf{0}$ is verified, which concludes the proof.

■

Assume that system (3.15) is not subject to any external disturbance signal, i.e., $\omega_k = \mathbf{0}$ for all $k \geq 0$. Then, the following corollary can be stated as a particularity of Theorem 3.1.

Corollary 3.1 *Consider the LPV discrete-time system under magnitude and rate saturating actuators given by (3.15), and the saturation limits $\rho_{\mathtt{M}}$ and $\rho_{\mathtt{R}}$ for the actuators' magnitude and rate, respectively. Suppose that there exist symmetric and positive definite matrices $\tilde{P}_i \in \mathbb{R}^{(n+n_u)\times(n+n_u)}$, diagonal matrices $L_{\mathtt{M}}$, $L_{\mathtt{R}} \in \mathbb{R}^{n_u \times n_u}$, matrices Z_i, $X_{\mathtt{M}i}$,*

$X_{\mathtt{R}_1 i} \in \mathbb{R}^{n_u \times (n+n_u)}$, $X_{\mathtt{R}_2 i} \in \mathbb{R}^{n_u \times n_u}$, $\tilde{H} \in \mathbb{R}^{(n+n_u)\times(n+n_u)}$, for i, $j = 1,\ldots,N$, and positive scalars μ and $\eta < 1$ such that, with matrices $\hat{A}_i$, $\bar{B}$, $\hat{B}$, computed as in (3.16), the following LMIs

$$\begin{bmatrix} -(1-\eta)\tilde{P}_i & -\tilde{H}^\top \hat{A}_i^\top - Z_i^\top \bar{B}^\top & -X_{\mathtt{M}i}^\top & -X_{\mathtt{R}_1 i}^\top \\ \star & \tilde{P}_j + \tilde{H} + \tilde{H}^\top & -\bar{B}L_{\mathtt{M}} & -\hat{B}L_{\mathtt{R}} \\ \star & \star & -2L_{\mathtt{M}} & -X_{\mathtt{R}_2 i}^\top \\ \star & \star & \star & -2L_{\mathtt{R}} \end{bmatrix} < \mathbf{0}, \tag{3.43}$$

(3.28), and (3.29) are feasible for $\forall r = 1,\ldots,n_u$. Then, the control gain matrices

$$\hat{K}_i = Z_i \tilde{H}^{-1},$$

where $\hat{K}_i = \begin{bmatrix} K_i & \bar{K}_i \end{bmatrix}$, yield the control law (3.9) that ensures that the closed-loop system is asymptotically stable for all initial conditions belonging to $\mathcal{R}_{\mathcal{E}} = \mathcal{L}_{\mathcal{V}}(\mu^{-1}) \subseteq \mathcal{R}_{\mathcal{A}}$.

Using the regional polyquadratic stabilization conditions, it is also possible to find a robust gain to ensure the stability of the system (3.1)–(3.6), as shown in the following corollary.

Corollary 3.2 *If Theorem 3.1 or the Corollary 3.1 are satisfied with $Z_i = Z$, $X_{\mathtt{M}i} = X_{\mathtt{M}}$, $X_{\mathtt{R}_1 i} = X_{\mathtt{R}_1}$, and $X_{\mathtt{R}_2 i} = X_{\mathtt{R}_2}$, then the control law $u_k = Kx_k + \bar{K}\bar{x}_k = \hat{K}z_k$ regionally exponentially polyquadratically stabilizes the discrete-time system described in (3.1)–(3.6) with $\hat{K} = Z\tilde{H}^{-1}$.*

The proof of both corollaries follows the same steps as the proof of Theorem 3.1, doing the necessary changes.

Note that for Theorem 3.1, Corollary 3.1 and Corollary 3.2 it is possible to use a quadratic candidate Lyapunov function that is time-varying parameter independent, i.e., $V(z_k) = z_k^\top P z_k$ for the stabilization of system (3.1)–(3.6).

3.3.1 Optimization Procedures

The conditions to controllers synthesis and estimate the region of attraction presented in Section 3.3 can be investigated through different optimization procedures. By convex optimization procedures, it is possible to design controllers that pursue to maximize the attraction region, maximize disturbance tolerance, or minimize the ℓ_2-gain. Some of the possibilities of this work interest are presented in the sequence.

Maximization of the estimation of the region of attraction ($\mathcal{R}_{\mathcal{E}}$): Considering that no disturbance is present, i.e., $w_k = 0$ for all $k \geq 0$, then the control design objective can be maximizing the size of the estimated region of attraction, $\mathcal{R}_{\mathcal{E}}$. So, with a positive definite matrix $Y \in \mathbb{R}^n$, an ellipsoidal set contained in $\mathcal{L}_{\mathcal{V}}(\mu^{-1})$ is defined as

$$\mathcal{E}(Y,1) = \{x_k \in \mathbb{R}^n; x_k^\top Y x_k \leq 1\} \subseteq \mathcal{L}_{\mathcal{V}}(\mu^{-1}), \tag{3.44}$$

leading to $UP_iU^\top - Y \leq \mathbf{0}$, $i = 1,\ldots,N$, where $U = \begin{bmatrix}\mathbf{I}_n & \mathbf{0}_{n\times n_u}\end{bmatrix}$. Therefore, (3.44) can be rewritten as

$$\begin{bmatrix} -Y & \mathbf{I} \\ \mathbf{I} & U(\tilde{P}_i + \tilde{H} + \tilde{H}^\top)U^\top \end{bmatrix} \leq \mathbf{0}. \tag{3.45}$$

Hence, it is possible to (indirectly) maximize the size of $\mathcal{R}_\mathcal{E}$ through the following convex optimization procedure:

$$\mathcal{T}_1 : \begin{cases} \min & \texttt{trace}(Y) \\ \text{subject to:} & \text{LMIs (3.28), (3.29), (3.43), (3.45) and } \mu - 1 \leq 0 \\ & i,j = 1,\ldots,N. \end{cases} \tag{3.46}$$

Maximization of the disturbance tolerance: The interest, in this case, is to determine the control gain vectors that maximize the set of admissible perturbations $\omega_k \in \mathcal{W}$ for a set of allowable initial states $\mathcal{R}_0$. A particular case of this optimization is for when the system is in equilibrium, i.e., $z_0 = \mathbf{0}$, which results in $\delta^{-1} = \mu^{-1}$. Therefore, the following convex optimization procedure maximizes the admissible disturbance energy:

$$\mathcal{T}_2 : \begin{cases} \min & \mu \\ \text{subject to:} & \text{LMIs (3.27)–(3.30)} \\ & i,j = 1,\ldots,N. \end{cases} \tag{3.47}$$

Minimization of the ℓ_2-gain: This optimization procedure investigates determining the control gains that minimizes the ℓ_2-gain between the disturbance signal α_k and the output y_k, for a given disturbance energy limit, δ^{-1}. Particularly, when the system is in equilibrium, i.e., $z_0 = \mathbf{0}$, $\delta^{-1} = \mu^{-1}$. Thus, the following convex optimization procedure minimizes the ℓ_2-gain:

$$\mathcal{T}_3 : \begin{cases} \min & \gamma \\ \text{subject to:} & \text{LMIs (3.27)–(3.30)} \\ & i,j = 1,\ldots,N. \end{cases} \tag{3.48}$$

3.4 Numerical Examples

In this section, numerical examples are presented to illustrate the effectiveness of the conditions proposed for the controllers' synthesis.

3.4.1 Example 1

In this experiment, the objective is to compare the region of attraction obtained by designing the state feedback gain between the robust controller and the parameter-dependent controller. Furthermore, the influence of the use of quadratic and polyquadratic candidate

Lyapunov functions is investigated in the size of the region of attraction. Consider the LPV system (3.1) with the matrices adapted from (De Souza *et al.*, 2019), as

$$\begin{aligned} A_1 &= \begin{bmatrix} -0.48 & 0.71 \\ 0.66 & 1.23 \end{bmatrix}, \; A_2 = \begin{bmatrix} -0.52 & 0.69 \\ 0.54 & 1.17 \end{bmatrix}, \; B_1 = \begin{bmatrix} 0.01 \\ 1.03 \end{bmatrix}, \\ B_2 &= \begin{bmatrix} -0.01 \\ 0.97 \end{bmatrix}, \; B_{w1} = \begin{bmatrix} 0.11 \\ 0.13 \end{bmatrix}, \; B_{w2} = \begin{bmatrix} -0.01 \\ 0.07 \end{bmatrix}, \end{aligned} \tag{3.49}$$

with $\Lambda = 10$, the symmetric limits of magnitude and rate saturation given by $\rho_{\mathtt{M}} = 10$ and $\rho_{\mathtt{R}} = 1$, respectively, and $T_s = 1$. Considering $\eta = 0$, and the system without disturbances, the stabilization of the system with the control law (3.9) using the is investigated in four cases:

1. Using the parameter-dependent gains, and a polyquadratic candidate Lyapunov function using the Corollary 3.1;

2. Using the parameter-dependent gains, and a quadratic candidate Lyapunov function using the Corollary 3.1;

3. Using the robust gain, i.e., $\hat{K}(\alpha_k) = \hat{K}$, for all $k \geq 0$, with a polyquadratic candidate Lyapunov function using the Corollary 3.2;

4. Using the robust gain, with a quadratic candidate Lyapunov function using the Corollary 3.2.

Solving the optimization procedure $\mathcal{T}_1$ with those four situations, the Figure 3.2 shows the cut of the estimates $\mathcal{R}_{\mathcal{E}}$ at $\bar{x}_0 = 0$. Using the LPV controller with a polyquadratic candidate Lyapunov function (case 1), the optimization yields to the bigger estimated $\mathcal{R}_{\mathcal{E}}$, once it is defined by the intersection of the ellipsoids $\mathcal{E}(P_1)$ and $\mathcal{E}(P_2)$ (solid and dashed black lines, respectively), resulting in a larger region. Note that, in this example, the robust controller with a polyquadratic candidate Lyapunov function allows an estimate of the region of attraction as large as the one obtained with the robust controller with a quadratic Lyapunov function.

Considering case 1, the optimization procedure $\mathcal{T}_1$ yields to designed control gain vectors

$$\hat{K}_1 = \begin{bmatrix} -0.0332 & -0.0954 & 0.7895 \end{bmatrix}, \text{ and } \hat{K}_2 = \begin{bmatrix} -0.0261 & -0.0938 & 0.7894 \end{bmatrix}. \tag{3.50}$$

The matrices of the polyquadratic Lyapunov function obtained are

$$P_1 = \begin{bmatrix} 0.0236 & 0.0698 & 0.1513 \\ 0.0698 & 0.2096 & 0.4537 \\ 0.1513 & 0.4537 & 0.9923 \end{bmatrix},$$

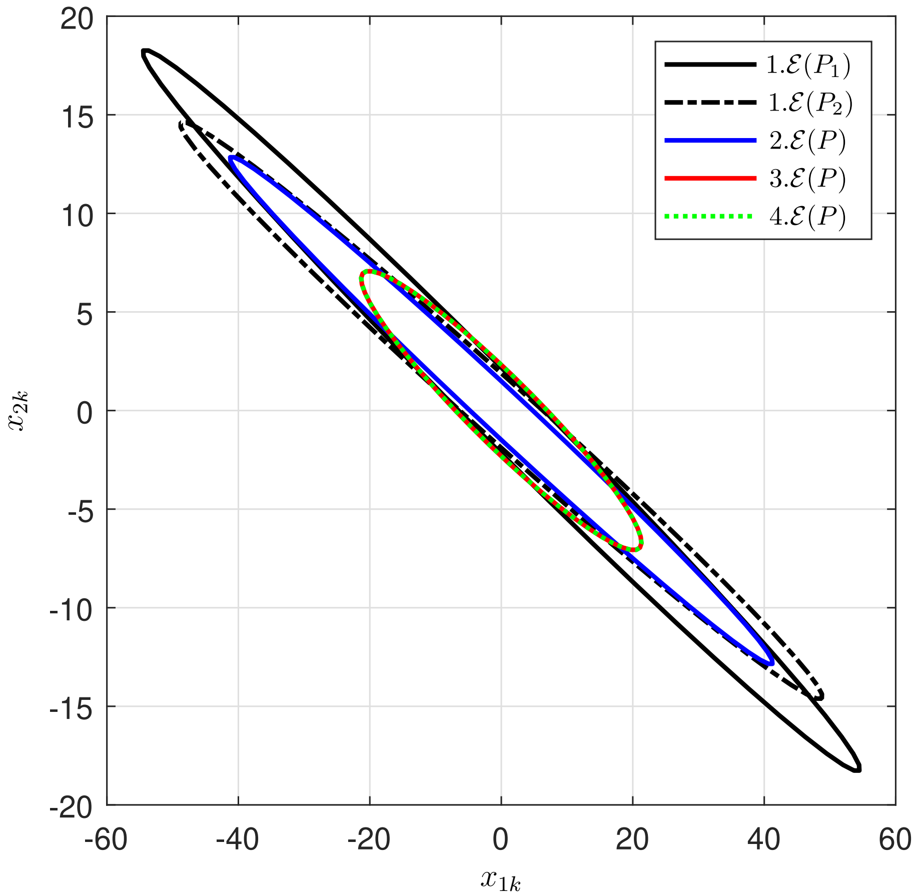

Figure 3.2: Estimated regions of attraction for different approaches of controllers and candidate Lyapunov functions. LPV controller (Corollary 3.1) with polyquadratic stabilization (case 1), LPV controller (Corollary 3.1) with quadratic stabilization (case 2), robust controller (Corollary 3.2) with polyquadratic stabilization (case 3) and robust controller (Corollary 3.2) with quadratic stabilization (case 4).

and

$$P_2 = \begin{bmatrix} 0.0250 & 0.0828 & 0.1784 \\ 0.0828 & 0.2788 & 0.5995 \\ 0.1784 & 0.5995 & 1.2991 \end{bmatrix}.$$

Note that the controller terms ($\bar{K}$) for the actuator state ($\bar{x}$) in (3.50) are positive and considerably larger than the plant controller terms. Thus, with slight variations in the actuator state, it acts more aggressively, aiming to address the saturation problem in the rate of change.

Based on the projected gains and the estimated region of attraction found, Figure 3.3 presents some trajectory projections of states in the $\bar{x} = 0$ plan for the system (3.10). As cited above, $\mathcal{R}_{\mathcal{E}}$ is defined by the intersection of the ellipsoids $\mathcal{E}(P_1)$ and $\mathcal{E}(P_2)$ (solid and dashed black lines, respectively). Two initial conditions (blue points) are selected on the edge of the intersection region, and the corresponding trajectories (in blue) converge towards the origin, as expected. The red lines trajectories of the initial conditions not belonging to the set (marked with a red $\times$) show unstable behaviors. Although the

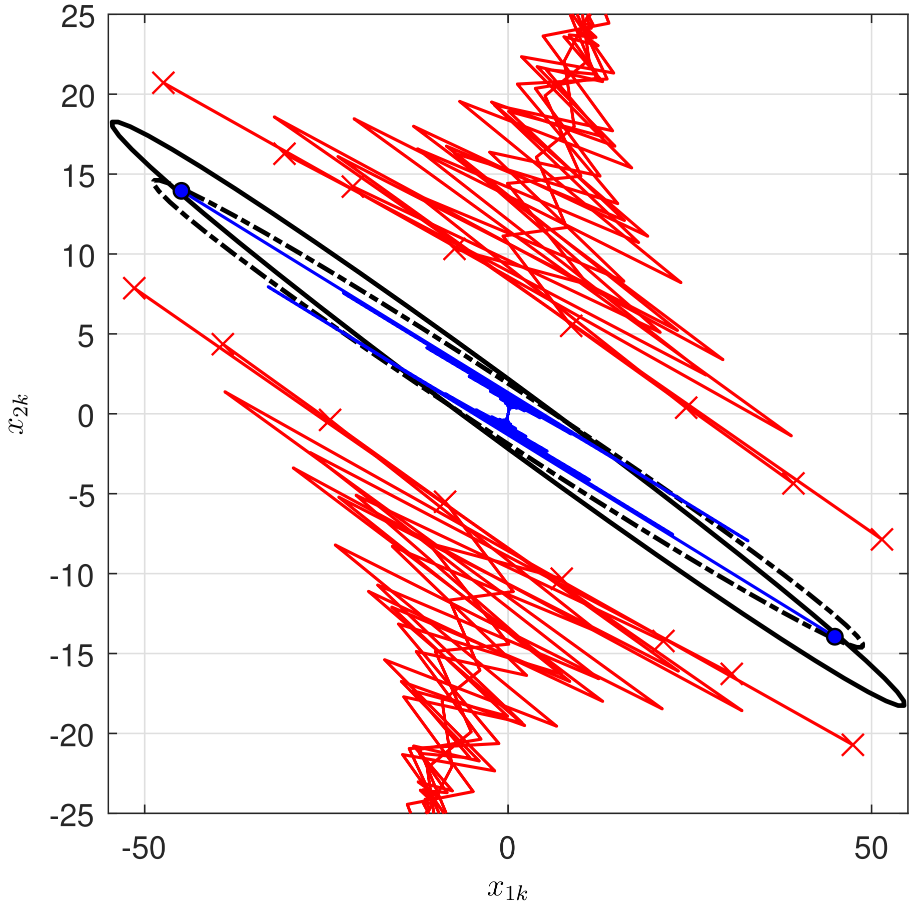

Figure 3.3: Estimate of the region of attraction (intersection of solid and dashed black ellipsoids) and projections state trajectories. The red lines trajectories concern to initial conditions that do not belong to the estimated region of attraction, and therefore, they diverge. On the other hand, the blue lines trajectories with initial conditions close to the set's border, converge to the origin, demonstrating asymptotic stability.

stable trajectories leave the cut of the region, to illustrate that they do not leave $\mathcal{R}_{\mathcal{E}}$, the reader can observe the behavior of $V(z_k,\alpha_k)$ in Figure 3.4 which is always less than 1 and monotonically decreasing.

For one of the selected stable initial conditions, $z_0 = \begin{bmatrix}44.9426 & -13.9497 & 0\end{bmatrix}$, the actuator's output signal ($\bar{x}$) over time is shown in the top plot of Figure 3.5. Note that, as the bottom plot shows, the rate variation limit ($\rho_{\mathrm{R}} = 1$) is achieved in the initial samples. However, the system can still converge to the origin once the chosen initial condition belongs to the region of attraction. Despite the occurrence of rate saturation in the actuator, it does not reach the magnitude saturation limits.

Then, choosing an initial condition from outside the estimated region of attraction, $z_0 = \begin{bmatrix}-51.4268 & 7.8599 & 0\end{bmatrix}$, the actuator output is presented in Figure 3.6 (red line). The presences of magnitude and rate saturation in the signal's behavior are notable. However, by increasing the rate saturation bound to $\rho_{\mathrm{R}} = 10$, allowing the system to have higher dynamic freedom, it can converge to the origin (black line). Thus, it is clear that the

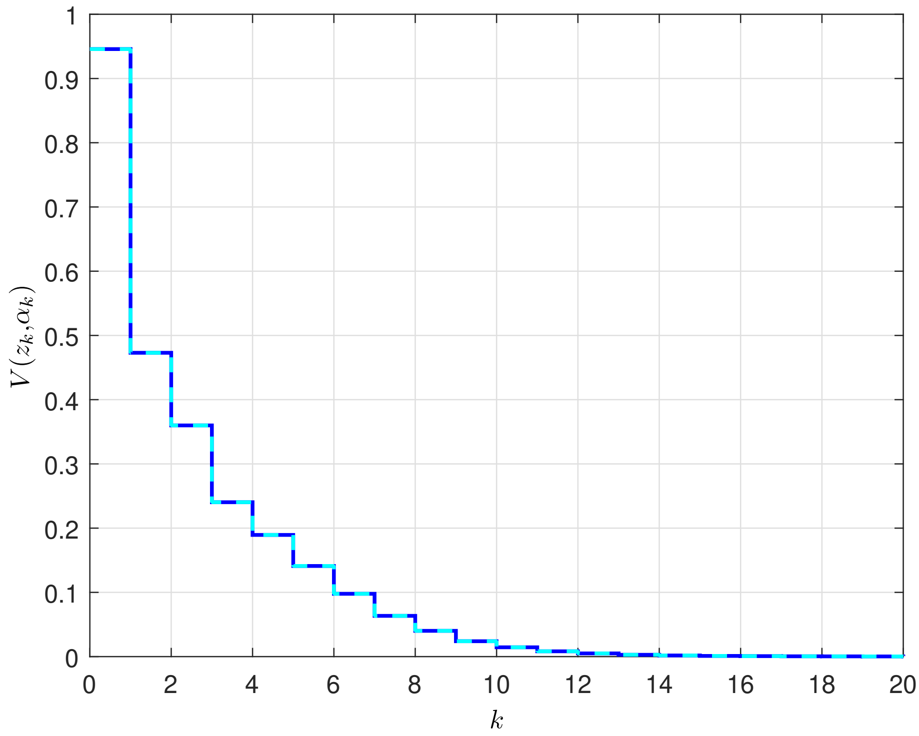

Figure 3.4: Time-behavior of the Lyapunov function for the trajectories with initial state belonging to $\mathcal{E}(P_1) \cap \mathcal{E}(P_2)$ illustrating that no trajectory leaves such region.

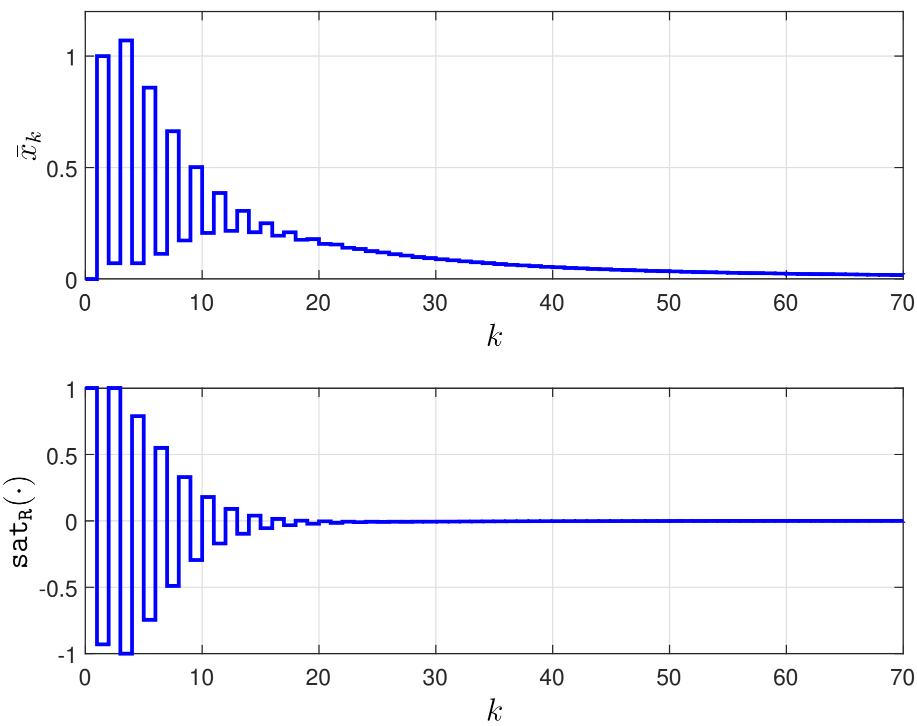

Figure 3.5: Actuator's output (top) and rate saturation (bottom).

dynamic restriction imposed by rate saturation led the system to instability.

As this is an LPV system, its dynamics change as a function of the variant parameter α_k. Figure 3.7 shows the values of α_k used in the simulations.

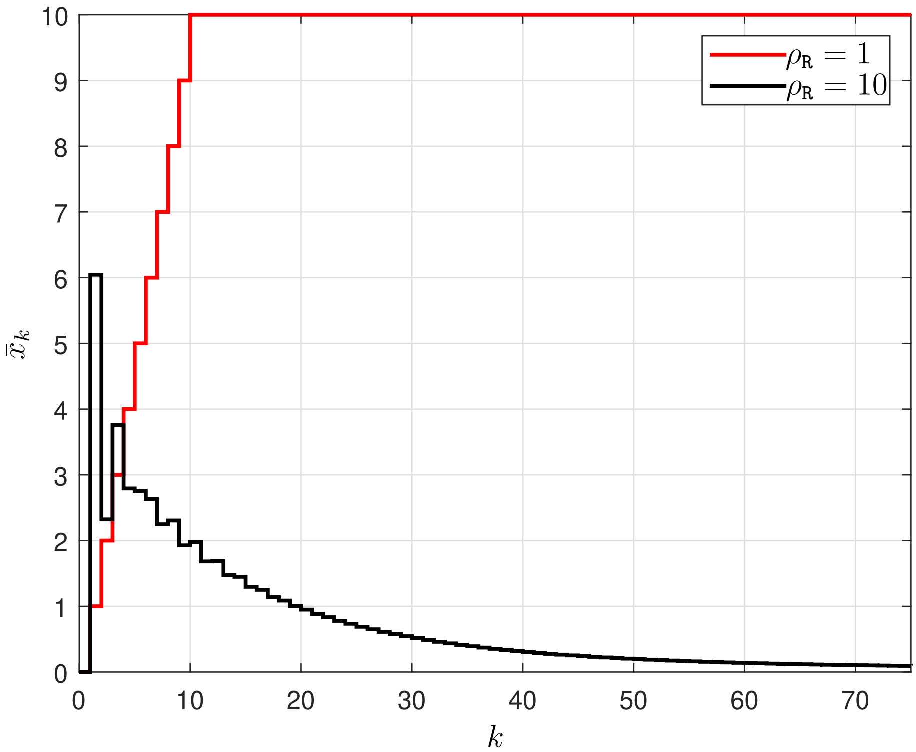

Figure 3.6: Actuator's outputs during the simulations with $\rho_{\mathtt{R}} = 1$ resulting in a unstable behavior (red line) and with $\rho_{\mathtt{R}} = 10$ (black line) with asymptotic stability.

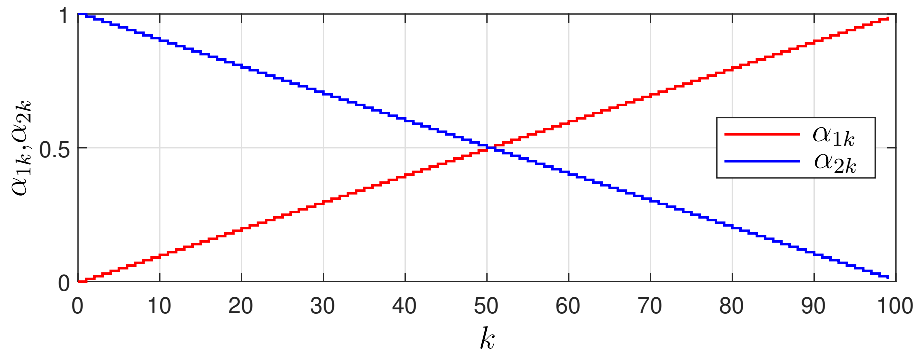

Figure 3.7: Time-varying parameters during the simulations.

3.4.2 Example 2

This example is presented to demonstrate the disturbance tolerance maximization technique applied in LPV systems with saturating actuators. Furthermore, a simulation of the states is performed, indicating that the maximum allowed perturbation does not take the states out of the contractive region. Consider the following scalar LPV system (3.1), with the matrices adapted from (de Souza *et al.*, 2019) as

$$A = 2(1+\rho),\ B = 1(1+\rho),\ B_w = 0.1(1+\rho),\ C = 0.1(1+\rho),$$

where the uncertain parameter $|\rho| \leq 0.1$, the actuator parameter $\Lambda = 15$, the symmetric limits of magnitude and rate saturation given by $\rho_{\mathtt{M}} = 0.7$ and $\rho_{\mathtt{R}} = 0.3$, respectively, and $T_s = 1$.

Assuming a null initial condition, i.e., $z_k = \mathbf{0}$, and applying optimization procedure $\mathcal{T}_2$, given in (3.47), is obtained the value of $\mu = 0.82836$, which leads to $\|\omega_k\|_2^2 \leq \delta^{-1} = \mu^{-1} = 1.2072$, and the gain vectors

$$\hat{K}_1 = \begin{bmatrix} -0.1275 & 0.8738 \end{bmatrix}, \text{ and } \hat{K}_2 = \begin{bmatrix} -0.1999 & 0.8227 \end{bmatrix}.$$

The estimate of the region of attraction $\mathcal{R}_\mathcal{E} \subseteq \mathcal{R}_\mathcal{A}$, defined by the intersection of the ellipsoidal sets $\mathcal{E}(P_1,\mu^{-1}) \cap \mathcal{E}(P_2,\mu^{-1})$, given by the matrices of the polyquadratic Lyapunov function

$$P_1 = \begin{bmatrix} 66.6153 & 55.4132 \\ 55.4132 & 48.5171 \end{bmatrix},$$

and

$$P_2 = \begin{bmatrix} 72.1382 & 59.9968 \\ 59.9968 & 52.3359 \end{bmatrix}.$$

Therefore, considering the system (3.10), the closed-loop response was simulated for the application of an energy disturbance vector with the form $\omega_k = \begin{bmatrix} 1.0987 & \mathbf{0} \end{bmatrix}$, i.e., with the energy bound obtained by the optimization procedure. In Figure 3.8 state trajectory are presented by the blue line, which converge to the equilibrium condition and remain in the resulting $\mathcal{R}_\mathcal{E}$ region, defined by the intersection of the ellipsoids $\mathcal{E}(P_1)$ and $\mathcal{E}(P_2)$ (solid and dashed black lines, respectively). Notably, the trajectory approaches the limiting edge of the region of attraction, which denotes the low conservatism of the proposal. When applying a perturbation vector with energy 55% greater than the energy bound obtained by the optimization procedure, i.e., $\omega_k = \begin{bmatrix} 1.7030 & \mathbf{0} \end{bmatrix}$, yields to the unstable trajectory presented by the magenta line.

Figure 3.9 shows the actuator's output during the simulation for the stable case. It is noticed that the applied disturbance leads the actuator to the limit of the variation rate, keeping the system stable anyway. Note that this is a time-varying system as a function of α_k, so Figure 3.10 shows the variant parameter values throughout the simulation.

3.4.3 Example 3

Consider the precisely known discrete-time pendulum model given by (3.1) investigated by Gomes da Silva Jr. *et al.* (2007), and the matrices adapted as

$$A = \begin{bmatrix} 1.0013 & -0.0500 & -0.0013 \\ -0.0500 & 1.0025 & 0.0500 \\ -0.0013 & 0.0050 & 1.0013 \end{bmatrix}, B = \begin{bmatrix} -0.0021 \\ 0.1251 \\ 5.0021 \end{bmatrix} \times 10^{-2},$$

$$B_w = \begin{bmatrix} -0.0021 \\ 0.1251 \\ 5.0021 \end{bmatrix} \times 10^{-2}, C = \begin{bmatrix} 1 & 0 & 0 \\ 0 & 1 & 0 \end{bmatrix},$$

with the actuator parameter $\Lambda = 20$, the symmetric limits of magnitude and rate saturation given by $\rho_\mathtt{M} = 1.25$ and $\rho_\mathtt{R} = 2$, respectively, and $T_s = 1$. In this example, the

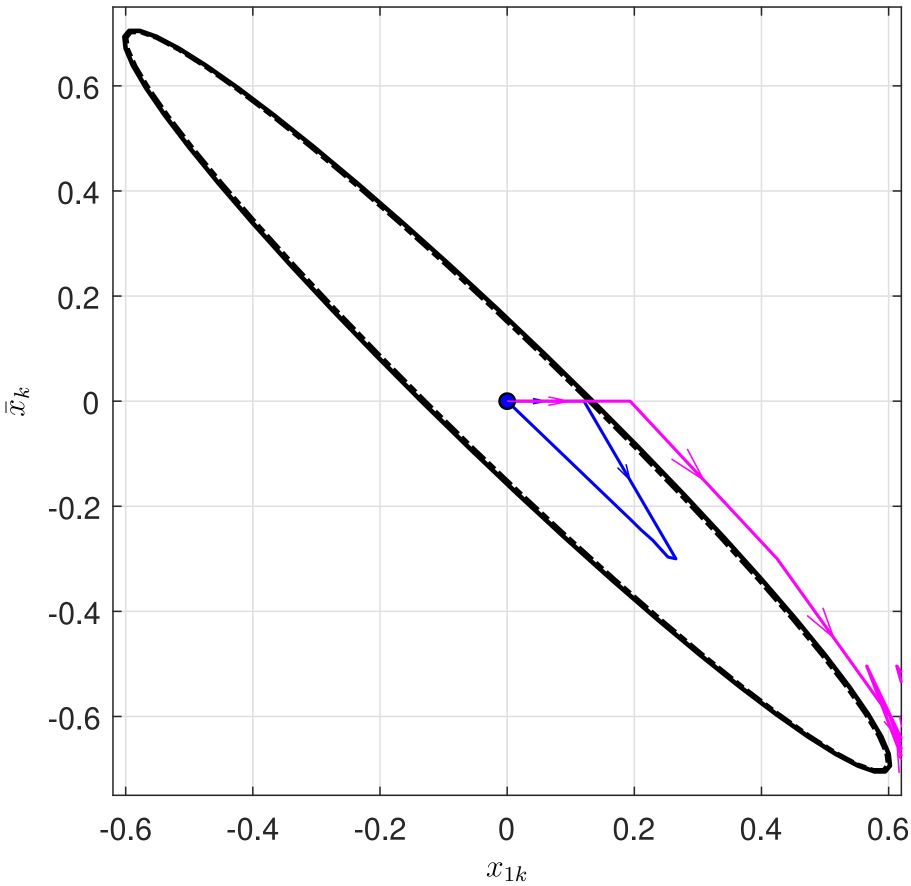

Figure 3.8: Trajectory of the system subject to the maximum admissible disturbance energy (blue line) limited by $\mathcal{R}_{\mathcal{E}}$ and to a disturbance whose energy exceeds the disturbance limit (magenta line).

objective is to analyze the system's disturbance tolerance and rejection and compare the results with a method from the literature. The result presented by Gomes da Silva Jr. *et al.* (2007) deals with discrete-time systems with magnitude and rate saturation through dynamic output feedback controllers. However, this method cannot deal with LPV systems, unlike the one proposed in this work. Another fundamental difference is that the result of Gomes da Silva Jr. *et al.* (2007) is based on considering the saturation in a nonlinear controller (preventing the control signal from violating the saturation limits) and not considering the limitations in an actuator model, which is done here.

First, different values of η are defined, which define a certain performance level for the closed-loop system measured by the Lyapunov function's decay rate, and, through the optimization procedure $\mathcal{T}_2$, the maximum value of allowed disturbance energy (δ^{-1}) for the system is evaluated. Considering null initial conditions, yields to $\delta^{-1} = \mu^{-1}$. Table 3.1 shows the values of μ^{-1} obtained for different values of η using the Theorem 3.1 and the ones presented in (Gomes da Silva Jr. *et al.*, 2007). As expected, the faster the decay rate (smaller $(1-\eta)$), the lower the maximum admitted disturbance energy. Note that the maximum disturbances admitted resulting from this work are bigger than the ones

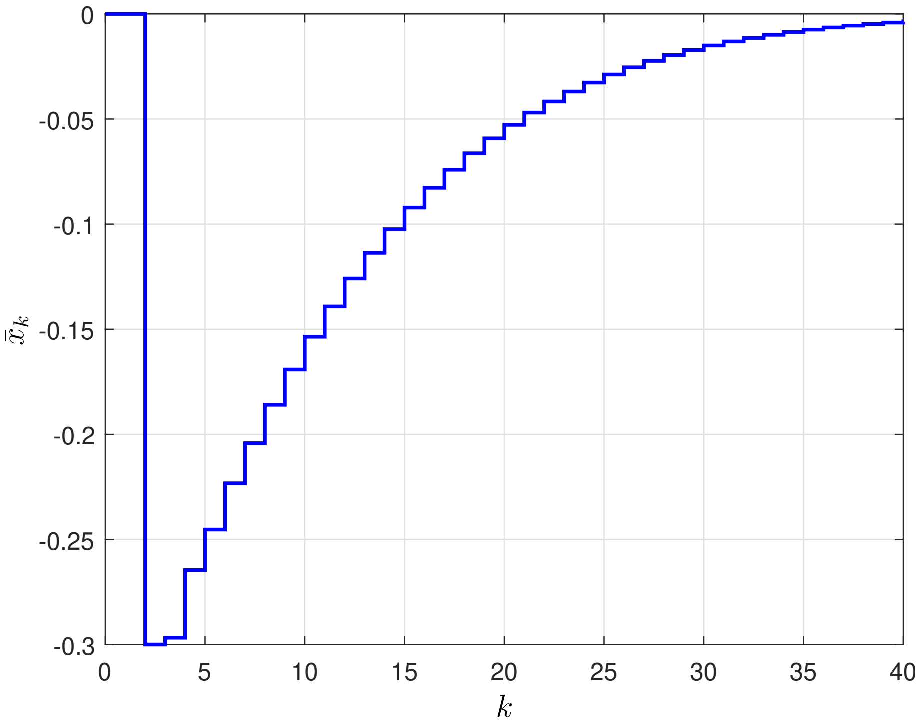

Figure 3.9: Actuator's output reaching the rate variation limit in the presence of the maximum admissible disturbance.

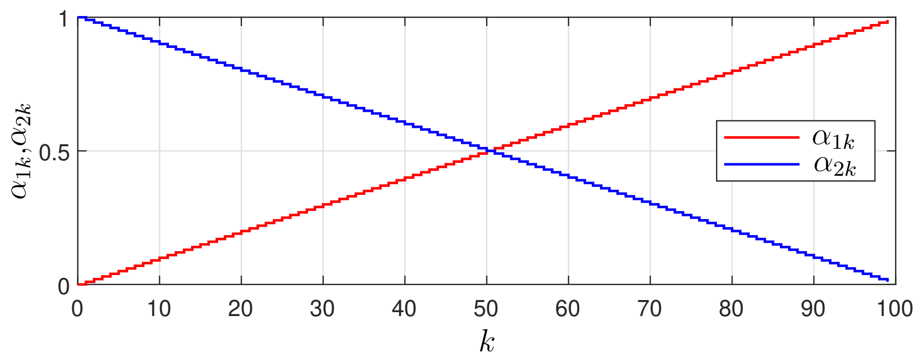

Figure 3.10: Time-varying parameters used during the simulation.

obtained by Gomes da Silva Jr. *et al.* (2007). Values marked in bold are the ones with the best results.

Considering the procedure $\mathcal{T}_3$ given in (3.48) with $z_k = \mathbf{0}$, different values of maximum admitted perturbation energy (δ^{-1}) are defined, resulting in values of γ, related to the minimization of the ℓ_2-gain. Table 3.2 presents the values of γ obtained for the set of tests. As the disturbance energy bound (δ^{-1}) grows, so does γ, such that the system is ISS. See that the ℓ_2 bounds obtained by Theorem 3.1 are bigger than the ones presented in (Gomes da Silva Jr. *et al.*, 2007) in cases where the admissible disturbance energy is lower, denoting that for these conditions, the method from (Gomes da Silva Jr. *et al.*, 2007) presents a better disturbance rejection. However, as the energy perturbation bound grows, Theorem 3.1 presents a better disturbance rejection. Values marked in bold are

Table 3.1: Maximal disturbance energy limit for different values of decay-rate performance.

$(1-\eta)$	Theorem 3.1 $\mu^{-1}=\delta^{-1}$	(Gomes da Silva Jr. *et al.*, 2007) $\mu^{-1}=\delta^{-1}$
1	**12.0064**	10.2737
0.99	**7.6854**	5.3997
0.975	**4.2769**	2.5087
0.95	**1.9518**	0.9449
0.925	**1.0304**	0.3356
0.9	**0.5549**	0.0741

the ones with the best results.

Table 3.2: Minimal ℓ_2-gain for different values of disturbance energy limit.

$\mu^{-1}=\delta^{-1}$	Theorem 3.1 γ	(Gomes da Silva Jr. *et al.*, 2007) γ
10	**221.611**	17094.7
8	**57.7056**	211.8103
6	**22.5822**	45.4023
4	**10.1838**	14.5536
2	**4.5572**	4.7053
1	2.8286	**2.2508**
0.5	2.1336	**1.2816**
0.1	1.4977	**0.4768**
0.01	1.2005	**0.1689**

3.4.4 Example 4

Consider the invariant continuous-time system presented in (Baiomy & Kikuuwe, 2020), discretized with sampling time $T_p = 0.01$ s, resulting in the discrete-time system (3.1) with matrices

$$A = \begin{bmatrix} 0 & -0.005 \\ 0.0101 & 1.0151 \end{bmatrix}, \; B = \begin{bmatrix} 0 \\ -0.0101 \end{bmatrix}.$$

The actuator dynamics is defined by $\Lambda = 10$ and $T_s = 1$. In this example, with no disturbance ($\omega_k = \mathbf{0}$), the objective is to evaluate the effects of magnitude and rate saturation levels on the size of the system's region of attraction through the optimization procedure $\mathcal{T}_1$ presented in (3.46). Fixing the magnitude saturation limit with $\rho_{\mathtt{M}} = 1$, different values for $\rho_{\mathtt{R}}$ were defined. Figure 3.11 shows the cut with $\bar{x} = \mathbf{0}$, and it is possible to see that the region of attraction gets smaller as the system's rate of change gets more constrained. The closed-loop corresponding to initial conditions belonging to the sets were simulated. As Figure 3.11 presents, when they start into the region of attraction, the system is asymptotically stable. Considering the most restricted case, i.e., $\rho_{\mathtt{R}} = 0.2$, an initial condition outside the corresponding region of attraction causes an unstable closed-loop behavior (dash-dotted magenta line). Note that even though the

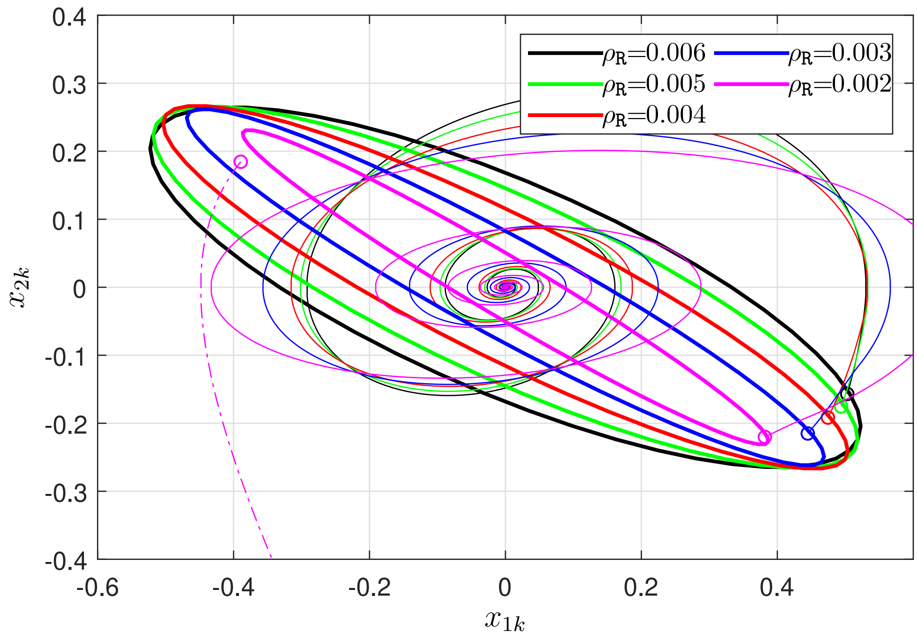

Figure 3.11: Cuts of the estimates of $\mathcal{R}_{\mathcal{A}}$ for different rate saturation constraints with corresponding state trajectory projections, for $\bar{x} = 0$.

stable trajectories leave the cuts of $\mathcal{R}_{\mathcal{E}} \subseteq \mathcal{R}_{\mathcal{A}}$, they do not leave the contractive set for all $k \geq 0$, as the presented behavior of $V(z_k)$ in Figure 3.12.

Hence, the same analysis is made fixing the rate saturation limit as $\rho_{\mathtt{R}} = 0.6$ and varying the values of $\rho_{\mathtt{M}}$. Figure 3.13 presents a cut at phase plane with $\bar{x} = \mathbf{0}$. Clearly, when more control energy is available, bigger is the region of attraction. The behavior of Lyapunov functions with initial conditions belonging to the ellipsoidal sets are shown in Figure 3.14, and notably, they are always less than 1 and monotonically decreasing.

An interesting analysis can be done comparing Figures 3.12 and 3.14. Note that by increasing the restriction of the actuator variation rate, the convergence speed towards the origin is modified, showing an abrupt change in the system's dynamics. Although the magnitude saturation constraint decreases the region of admissible initial states, its variation had a minor influence on the settling time of the function $V(z_k)$.

3.5 Final Considerations

In this chapter, results related to the synthesis of state feedback gains to LPV systems presenting magnitude and rate saturating were presented proposed. First, the problem

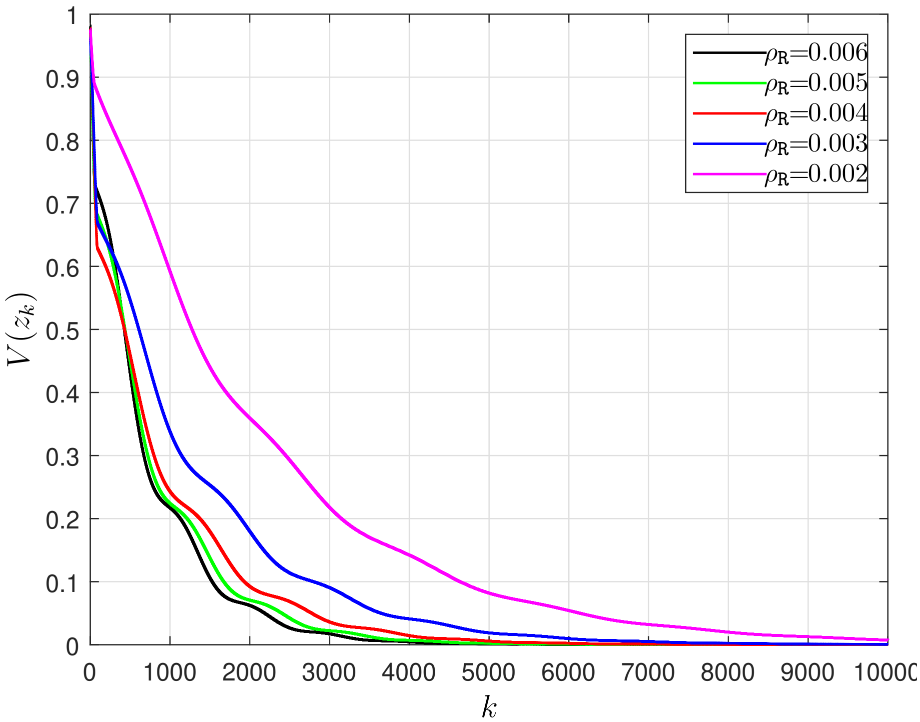

Figure 3.12: Time-behavior of the Lyapunov function for the trajectories with the initial state belonging to $\mathcal{E}(P)$ for different values of $\rho_{\mathtt{R}}$, illustrating that no trajectory leaves the corresponding region.

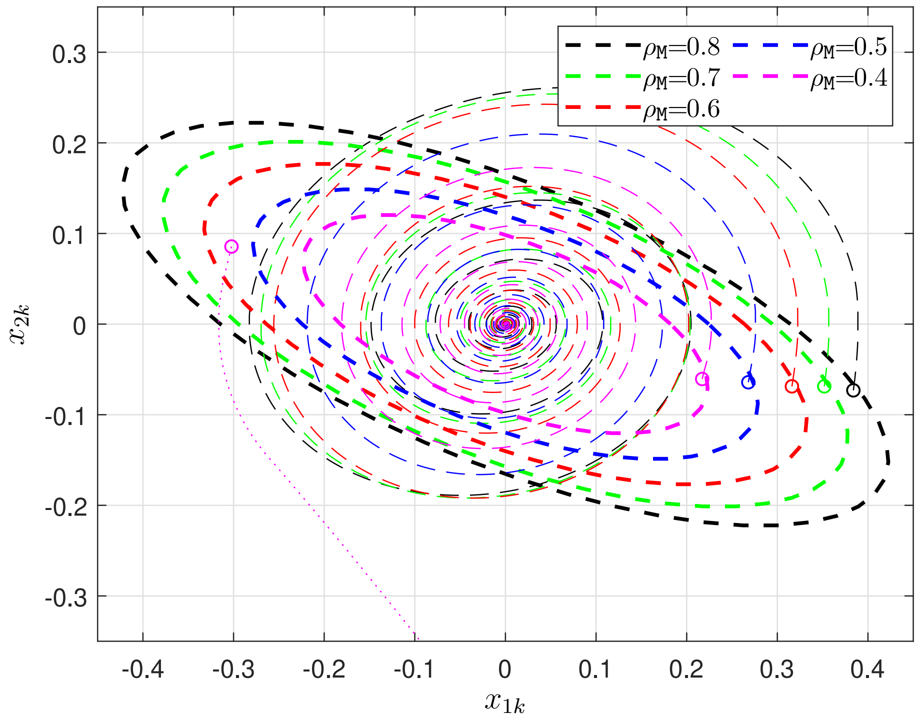

Figure 3.13: Cuts of the estimates of $\mathcal{R}_{\mathcal{A}}$ for different magnitude saturation constraints with corresponding state trajectory projections, for $\bar{x} = 0$.

to be investigated was defined, and some results from the literature that contribute to its solution were presented. Then, the stabilization conditions for systems with or without

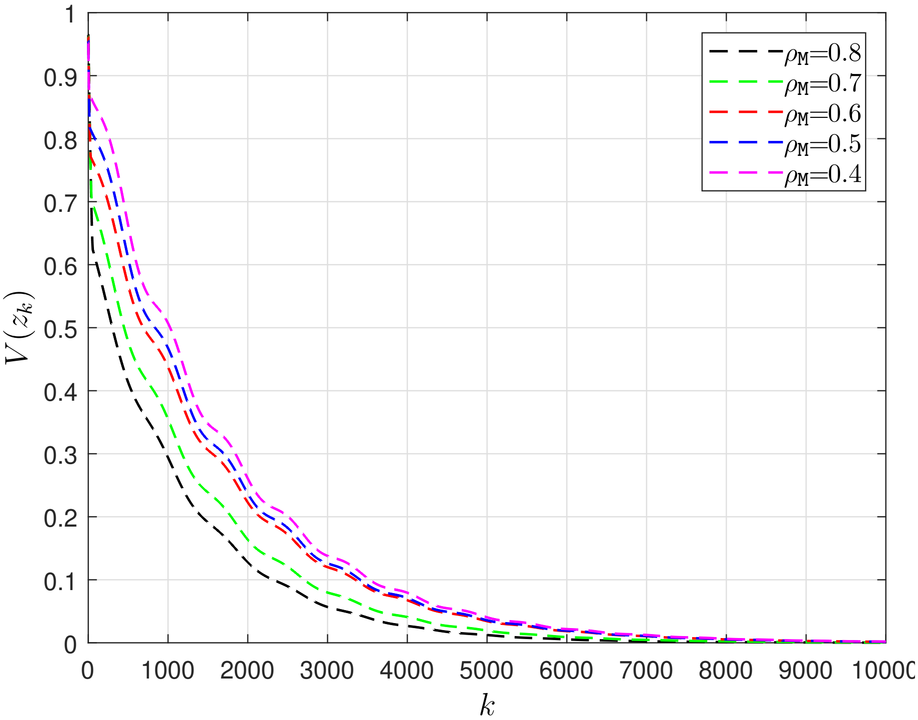

Figure 3.14: Time-behavior of the Lyapunov function for the trajectories with the initial state belonging to $\mathcal{E}(P)$ for different values of $\rho_{\mathtt{M}}$, illustrating that no trajectory leaves the corresponding region.

disturbance were presented. Then, stabilization conditions for systems with or without energy-limited disturbance were presented. From these, convex optimization procedures were proposed with the objectives of maximizing the estimate of the region of attraction, maximize the disturbance tolerance, and minimize the ℓ_2-gain. Finally, the efficiency of the proposed conditions was tested through numerical examples.

Chapter 4

Experimental control of a nonlinear system

In this chapter, the effectiveness of the new design conditions proposed is illustrated with a real-time experiment aiming to control the level of a second-order nonlinear process modeled as a *quasi*-LPV model. First, a brief description of the coupled tanks system is presented, followed by the system's physical modeling and dynamic equations. Finally, the experimental results are shown using the controller synthesis conditions proposed in this work.

4.1 System's Setup

The system used is available at the Signals and Systems Laboratory of CEFET-MG, *campus* Divinópolis and consists of four cylindrical tanks with a capacity of 200 liters, two reservoirs of 400 liters each, and two motor pumps with 1 HP of power each, model CAM-W6 from Dancor, activated by independent frequency inverters manufactured by WEG of model CFW09. Its hydraulic network supports different configurations, as valves interconnect the tanks. Figure 4.1 shows the tank system described. The levels of the tanks are measured with differential pressure sensors manufactured by Honeywell of the model 26PCBFA6D.

The controller is implemented with an open-source Python-based interface (Sousa *et al.*, 2018) and a Raspberry Pi 3 communicating with a programmable logic controller (PLC) of model Simatic S7-300 from Siemens. The PLC monitors the sensors' signals and sends the control signal to a frequency inverter manufactured by WEG of model CFW09 that varies the pump power. In addition, the plant has an interlocking safety system that limits the level height of the tanks to 0.7 meters so that an overflow does not occur.

Figure 4.1: Coupled tank system used in the experiments.

4.2 Physical Modeling

In the case of this experiment, the chosen configuration uses the two lower tanks. The pump acts by directing the water to tank T4, which is connected by a fixed-open valve to tank T3, where the level must be controlled. Then, the outflow of this tank goes to a reservoir of 400 liters capacity, where the fluid is recirculated. Moreover, a nonlinear solid designed in expanded polystyrene, based on a solid revolution of a Gaussian curve, is placed inside tank T3, as shown in Figure 4.2. Thus, the volume occupied by the fluid is not linear as a function of its height, causing significant changes in the dynamics of the system, allowing the system to be described in a *quasi*-LPV model. Figure 4.3 shows a simplified diagram of the configuration adopted.

The system model could be obtained through mass balance equations in each of the

Figure 4.2: Coupled tanks system used in the experiments.

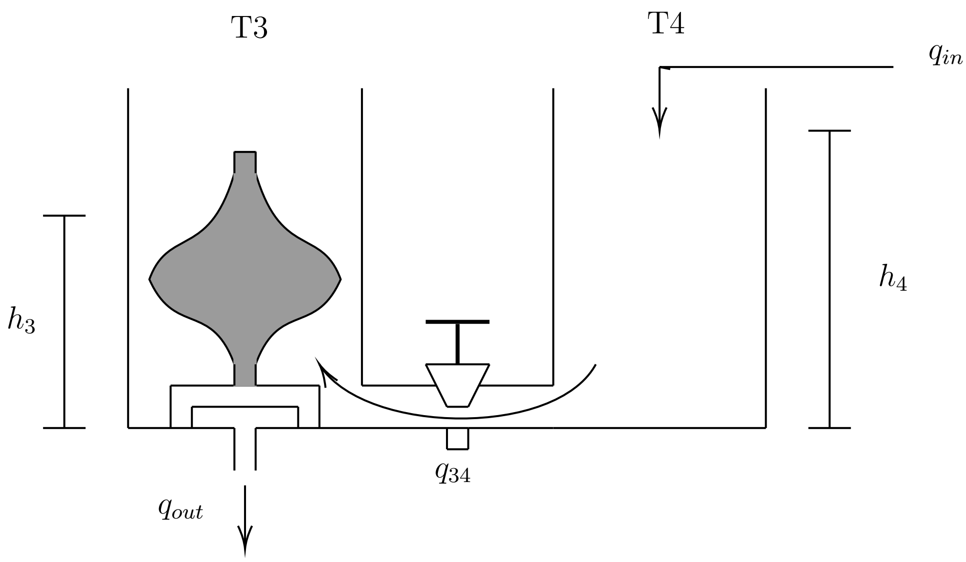

Figure 4.3: Schematic diagram of the tanks system (Figueiredo *et al.*, 2020).

tanks, such as

$$\dot{V}(t) = q_{in} - q_{out}.$$

where q_{in} is the input flow and q_{out} is the output flow. Through experimental data, the equation that describes the input flow as a function of the control signal $u(t)$ applied to the motor pump is modeled as

$$q_{in} = (18.9996\ u(t) + 265.2426) \times 10^{-4},$$

where the control signal is given by $0\% \leq u(t) \leq 100\%$. The flow between the tanks T3 and T4 depends on the difference of the measured levels of the respective tanks $(h_4(t) - h_3(t))$ and by experimental data, it follows that:

$$q_{34} = (37.3916(h_4(t) - h_3(t)) + 290.5831) \times 10^{-4},$$

where the levels $h_4(t)$ and $h_3(t)$ are directly measured in meters and verifies $0 \text{ m} \leq h_i(t) \leq 0.7 \text{ m}$, $i = 3{,}4$. Finally, the output flow equation was obtained empirically as

$$q_{out} = (8.7777 h_3(t) + 555.9995) \times 10^{-4}.$$

Due to the nonlinearity inside tank T3, its free area is given by

$$a(h_3(t)) = \frac{3r}{5}\left(2.7r - \frac{\cos(2.5\pi(h_3(t) - \upsilon))}{\sigma\sqrt{2\pi}} e^{-\frac{(h_3(t)-\upsilon)^2}{2\sigma^2}}\right),$$

where the tank radius is $r = 0.31$ m, $\upsilon = 0.4$, and $\sigma = 0.55$ refer to the Gaussian surface of the nonlinear solid. Since the area $a(h_3(t))$ varies according to the height h_3, the system can be described as a *quasi*-LPV model, where the varying parameters depend on the measured system's states. Then, using mass balance equations and following the steps from (Figueiredo *et al.*, 2020), assuming the level range $0.28 \text{ m} \leq h_3 \leq 0.48$ m, and discretizing the model with a zero-order holder and sampling time $T_p = 5.2632$ s (see (Lopes *et al.*, 2020) for details), the discrete-time model disregarding the disturbance is given by the following vertex matrices:

$$A_1 = \begin{bmatrix} 93.9626 & 5.9718 \\ 8.3235 & 89.6570 \end{bmatrix} \times 10^{-2},\ A_2 = \begin{bmatrix} 94.1012 & 5.8000 \\ 12.4222 & 84.5628 \end{bmatrix} \times 10^{-2},$$

$$B_1 = \begin{bmatrix} 3.1928 \\ 0.1412 \end{bmatrix} \times 10^{-4},\ B_2 = \begin{bmatrix} 3.1944 \\ 0.2128 \end{bmatrix} \times 10^{-4}.$$

The time-varying parameters are related to the measured states by

$$\alpha_{1k} = -5h_3 + 2.4,$$

and

$$\alpha_{2k} = 1 - \alpha_{1k}.$$

Because the process operates around $h_3^* = 0.38$ m, the limit of the symmetrical magnitude saturation of the actuator is $\pm\rho_{\mathtt{M}} = 15\%$. As a consequence of the limits on motor pump acceleration, the constrained rate on $q_{in}(t)$ is modeled here with $\rho_{\mathtt{R}} = 0.005$, $\Lambda = 10$, and $T_s = 5.2632$.

4.3 Experimental Results

Assuming the nominal operational condition, that is with $A = (A_1 + A_2)/2$ and $B = (B_1 + B_2)/2$, it is possible to use the methods proposed in (Gomes da Silva Jr. *et al.*, 2008) and (Bateman & Lin, 2002) to compare with this work's proposal. In order to match the conditions in (Bateman & Lin, 2002), it is assumed $\eta = 0$ and solved the procedure (3.46) with Corollary 3.1. The estimate of the region of attraction achieved by this proposal is 12.4% bigger than the one achieved by Gomes da Silva Jr. *et al.* (2008), and 3.5% bigger than the estimate from Bateman & Lin (2002). Thus the proposed method yields better estimates of the region of attraction. Moreover, the proposed method can handle the LPV case while the proposals in (Gomes da Silva Jr. *et al.*, 2008) and (Bateman & Lin, 2002) fail to handle such a case. Furthermore, the method in (Zhou, 2013) cannot be applied to LPV systems, even if it is adapted to controller design under actuator's rate saturation.

Considering the system without disturbance, the LPV controller design can be obtained by solving the convex optimization procedure (3.46) with Corollary 3.1 with $\eta = 0.0168$ that is obtained by increasing it from 0 until an estimate of the region of attraction compatible with the tank level range is obtained. For greater values of η, smaller are the estimates of the region of attraction. Thus, there is a trade-off between performance and operational range, which requires the designer's choice. Also, the optimization procedure (3.46) was modified to minimize $\texttt{trace}(Y) - 2\texttt{trace}(\tilde{H})$. The term $-2\texttt{trace}(\tilde{H})$ aims to counteract the effect of $\tilde{H}^{-1}$ recovering P_i. In this system, this addition allows to obtain an estimate of the region of attraction compatible with the physical limits of the tanks. Thus, solving the described optimization procedure, the following control gains are obtained:

$$\hat{K}_1 = \begin{bmatrix} -13.5166 & -7.4485 & 980.8274 \end{bmatrix} \times 10^{-3},$$

and

$$\hat{K}_2 = \begin{bmatrix} -13.8240 & -7.0629 & 980.8292 \end{bmatrix} \times 10^{-3}. \tag{4.1}$$

The resulting matrices of the polyquadratic Lyapunov function are

$$P_1 = \begin{bmatrix} 37.6235 & 19.3481 & 50.1352 \\ 19.3481 & 11.6306 & 27.0150 \\ 50.1352 & 27.0150 & 70.0079 \end{bmatrix},$$

and

$$P_2 = \begin{bmatrix} 38.2723 & 19.1468 & 50.6046 \\ 19.1468 & 11.1473 & 26.5086 \\ 50.6046 & 26.5086 & 70.1170 \end{bmatrix}.$$

Figure 4.4 shows the cut of the estimate $\mathcal{R}_\mathcal{E}$ at $\bar{x}_0 = 0$, thus in the process's phase-plane. The practical level trajectories obtained for two initial conditions at the border of the estimate of the region of attraction $\mathcal{R}_\mathcal{E}$: $z_{01} = \begin{bmatrix} -0.0969 & -0.1053 & 0.025 \end{bmatrix}^\top$ and

$z_{02} = \begin{bmatrix} 0.0959 & 0.1253 & -0.03428 \end{bmatrix}^\top$. It is possible to notice that the trajectories converge to the origin and do not leave the estimated region of attraction. For each of these initial

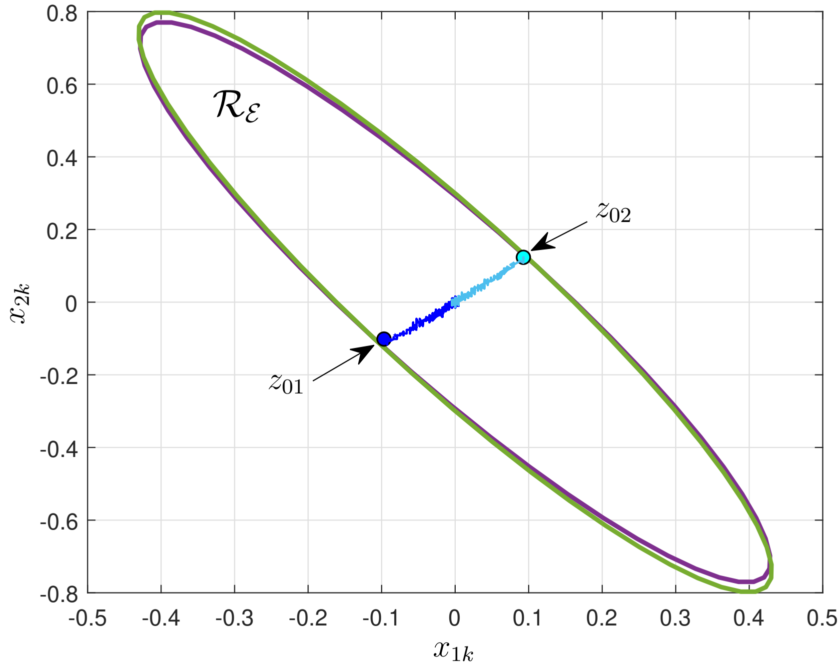

Figure 4.4: Cut of the estimated region of attraction (the intersection of green and purple ellipsoids) and projections of state trajectories resulting from the closed-loop experiment.

conditions, simulations and real-time experiments were performed in the closed-loop tank system. The simulations were executed by adding a random noise signal with magnitudes limited to ± 0.0046 m to the level measurements, reproducing the water agitation and electronic noise found in practical operational conditions. Figure 4.5 shows the simulated (red and magenta lines) and experimental data (cyan and blue lines) with the designed LPV controller. It is evident that the model well fits the real system behavior. In both experiments, the LPV controller acts to bring the level of T3 to its operational point, $h_3^* = 0.38$ m. Figure 4.6 shows the normalized decay rates of the state norm, computed as $\sqrt{\frac{\beta_2}{\beta_1}}\left(\sqrt{1-\eta}\right)^k$, with $\beta_1 = 0.8747$ and $\beta_2 = 117.3161$, (red line) and $\|z_k\|/\|z_0\|$ for both experiments (blue line for z_{01} and magenta dashed line for z_{02}). Note that the experimental data presents a faster response, which is expected since the η value yields a bound for all initial admissible conditions and all possible parameter sequences belonging to the unit simplex. The varying parameters during the experiment with z_{01} are shwon in Figure 4.7.

Magnitude and rate associated with this experiment are shown in Figure 4.8 for z_{01} (blue line) and z_{02} (cyan line), for the first 15 samples. The design conditions ensures the rate saturation function symmetrically constrained by $\rho_{\mathtt{R}} = 0.005$ (see $\mathtt{sat}_{\mathtt{R}}(\cdot)$ in the bottom plot). Consequently, the magnitude of u_k increases on a limited amount at the first samples, indicating the controller acting on its energy limits. Although it appears

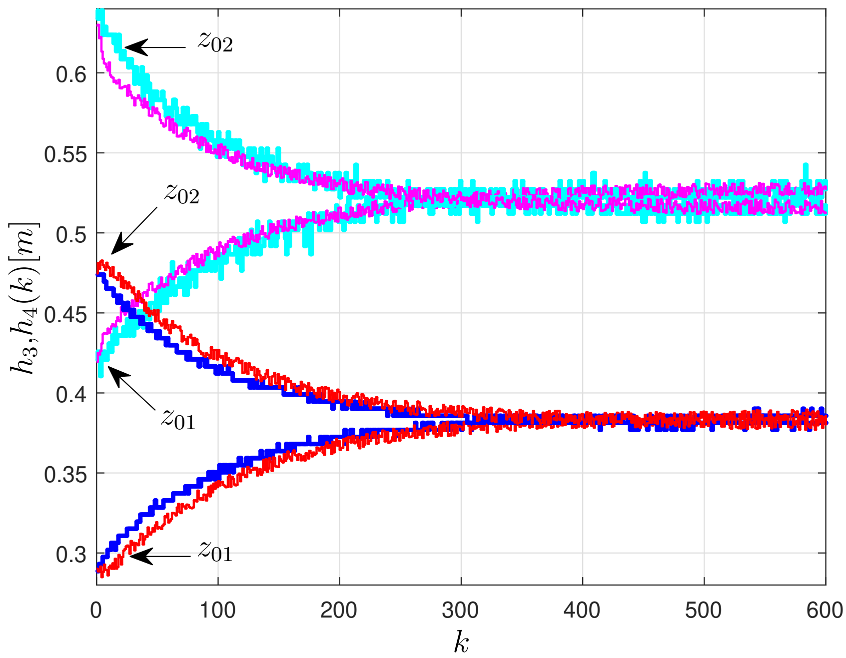

Figure 4.5: T4 and T3 levels from the experiment (cyan and blue lines), and from the numerical simulation (magenta and red lines).

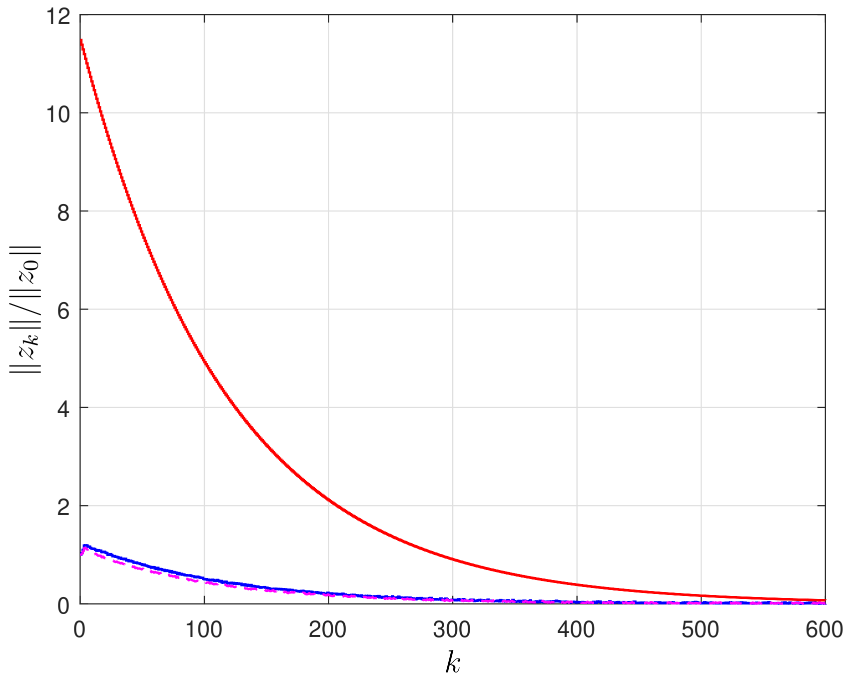

Figure 4.6: Red line represent the theoretical decay rate and blue and magenta dashed lines concern the experimental achievements for initial conditions z_{01} and z_{02}, respectively.

that the signal's rate of change is greater than $\rho_{\mathtt{R}} = 0.005$, this happens once the actuator has been modeled with a sampling time different from the plant discrete-time model. To facilitate understanding the graphics in this type of approach, it is recommended to implement it with synchronous sampling, i.e., T_s=1. The experimental data shows that the proposed approach can be implemented in practical systems, ensuring regional

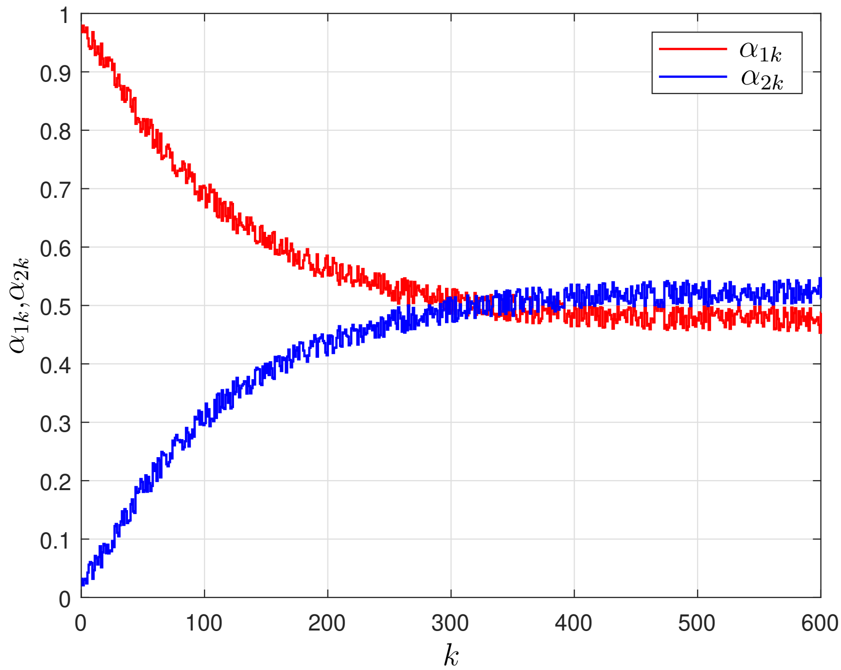

Figure 4.7: Time-varying parameters during the experiment with z_{01}.

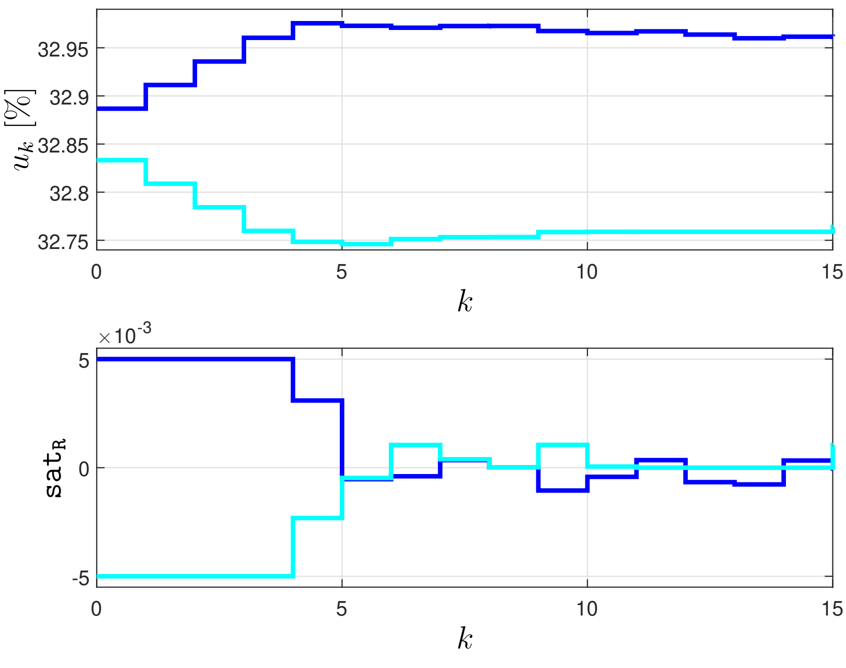

Figure 4.8: Control signal subject to rate saturation (top) and rate saturation reaching its bound (bottom) in the first samples of the experiment.

exponential convergence for initial conditions belonging to $\mathcal{R}_{\mathcal{E}}$.

4.4 Final Considerations

This chapter shows that the proposed approach on Chapter 3 can be implemented in practical LPV discrete-time systems under magnitude and rate saturation actuators, ensuring regional exponential convergence for initial conditions belonging to the estimated region of attraction. In this case, a nonlinear tanks system was modeled as a *quasi*-LPV system, where its dynamics varies as a function of its height.

Chapter 5

Conclusion

In this work, new conditions for the synthesis of parameter-dependent state feedback controllers that guarantee the asymptotic and input-to-state stability of LPV linear discrete-time systems with saturation in magnitude and rate of change for a set of initial conditions and limited energy disturbances were presented. Therefore, the main and specific goals proposed in Chapter 1 where achieved.

In Chapter 2, the main theoretical concepts and essential mathematical tools necessary for the development and understanding of this work were addressed.

In Chapter 3, conditions for local input-to-state stabilization in discrete-time LPV systems under magnitude and rate saturation were developed. This approach employs a parameter-dependent candidate Lyapunov function to reduce the conservatism jointly with generalized sector condition handling the saturation's nonlinearities. Moreover, the closed-loop exponential convergence performance specification can be ensured. Convex optimization procedures were proposed for different objectives, such as the maximization of the region of attraction, the maximization of the allowed disturbance energy, and the minimization of the ℓ_2-gain. Some numerical examples were presented to demonstrate the efficiency of the proposed technique and its behavior according to the variation of some system parameters. In the first example, it is shown how the use of a polyquadratic Lyapunov function yields to less conservative regions of attraction and that the initial states belonging to it converge to the origin without leaving it. In the second example, the input-to-state stability guaranteed by the parameter-dependent controller in the presence of energy-limited disturbances is demonstrated. In the third example, the trade-off between the maximum disturbance energy and the performance specification is presented and compared with a result from the literature. Likewise, it is done with the ℓ_2-gain and the disturbance energy limit. The last example of this chapter presents how saturation limits change the size of the attraction region in the context of magnitude and rate saturation.

In Chapter 4, the description and modeling of a nonlinear level control system described as a *quasi*-LPV system is presented, and the approach presented in the previous chapter is implemented as a practical experiment to demonstrate the proposal's efficiency. In this case, it is noted that even with the system reaching the actuator rate saturation limit, the LPV controller still guarantees stability for initial conditions belonging to the region of attraction.

Although the approaches developed here allow magnitude and rate saturation for initial conditions belonging to the region of attraction and still guarantee their asymptotic stability, it is difficult to find examples whose behavior presents both nonlinearities. Thus, this is an indication that the proposed conditions can still be relaxed in search of less conservative results.

5.1 Developed Works

During the development of the master's course and this thesis, some works were produced. The first paper, presented at a Brazilian national conference, was produced in order to introduce the control systems tools that would be used during the master's course. Thus, the following paper was presented:

L. A. L. OLIVEIRA, M. V. C. Barbosa, L. F. P. Silva, and V. J. S. Leite, "Estabilidade Entrada-Estado de Sistemas Discretos no tempo a Parâmetros Lineares Variantes e Sujeitos a Atuadores Saturantes," in XXIII Congresso Brasileiro de Automática, 2020.

So, the main theme of this thesis and research project resulted in two more papers, one presented at an international conference, and the other published in a scientific journal:

L. A. L. OLIVEIRA, M. V. C. Barbosa, L. F. P. Silva, and V. J. S. Leite, "Regional Polyquadratic Stabilization of Discrete-Time LPV Systems under Magnitude and Rate Saturating Actuators," in 2021 American Control Conference (ACC), 2021, pp. 4926-4931.

L. A. L. OLIVEIRA, M. V. C. Barbosa, L. F. P. Silva, and V. J. S. Leite, "Exponential Stabilization of LPV Systems Under Magnitude and Rate Saturating Actuators," in IEEE Control System Letters, vol. 6, pp. 1418-1423, 2022.

Currently, the following paper is under preparation to be submitted to a scientific journal:

L. A. L. OLIVEIRA, M. V. C. Barbosa, L. F. P. Silva, and V. J. S. Leite, ”ISS control for discrete-time LPV Systems Under Magnitude and Rate Saturating Actuators.” that includes part of the results presented in Chapter 3.

5.2 Future Works

Some topics can be investigated in order to extend the results obtained in this work:

1. to consider the use of Lyapunov functions dependent on homogeneous polynomial parameters in order to obtain less conservative estimates of the region of attraction, and extend the result to LPV systems polynomial on the states, using relaxations based on the sum of squares (SOS) (Note that the Lemma 2.3 used in this work was generalized in (Figueiredo *et al.*, 2021) to homogeneous polynomial parameter-dependent functions);
2. to consider the generalized sector condition for systems with magnitude and rate saturating actuators in the context of fuzzy Takagi-Sugeno systems;
3. to consider the presence of delay and elaborate synthesis conditions using Lyapunov-Krasovskii functions;
4. to investigate the design of controllers with an anti-windup loop to handle magnitude and rate saturation in discrete-time LPV systems;
5. to investigate the control signal written as a speed algorithm using Δu_k, without using nested saturations.

Appendix A

Tools

In this appendix, some mathematical tools used to achieve the conditions proposed in Chapter 3 are demonstrated.

A.1 Schur's complement

Schur's complement is a relationship between submatrices contained in a matrix. Let Q and R be symmetric matrices, then the condition

$$\begin{bmatrix} Q & S \\ S^T & R \end{bmatrix} \geq 0 \tag{A.1}$$

it's equivalent to

$$R \geq 0, \qquad Q - S^T R^{-1} S \geq 0.$$

Thus, the Schur's complement of the submatrix R corresponds to the following expression:

$$Q - S^T R^{-1} S \geq 0. \tag{A.2}$$

A.2 Proof of Lemma 2.3

Proof: The proof is reproduced from (Jungers & Castelan, 2011). Assume that $x_k \in \mathcal{L}_{\mathcal{V}}(c) \Leftrightarrow$ for all $\alpha \in \mathcal{P}$ and

$$V(x_k,\alpha_k) < c \Leftrightarrow x_k \in \bigcap_{\alpha_k \in \mathcal{P}} \mathcal{E}(P(\alpha_k),c).$$

Also,

$$\bigcap_{\alpha_k \in \mathcal{P}} \mathcal{E}(P(\alpha_k),c) \subset \bigcap_{i=1}^{N} \mathcal{E}(P_i,c).$$

To prove that

$$\bigcap_{i=1}^{N} \mathcal{E}(P_i,c) \subset \bigcap_{\alpha_k \in \mathcal{P}} \mathcal{E}(P(\alpha_k),c),$$

consider $x_k \in \bigcap_{i=1}^{N} \mathcal{E}(P_i,c)$, then for all $i = 1,\ldots,N$, it follows that $x_k^\top P_i x_k < c$. Applying the Schur's complement, the following inequality can be obtained:

$$\begin{bmatrix} c & x_k^\top \\ x_k & P_i^{-1} \end{bmatrix} > 0. \tag{A.3}$$

Thus, for all $\alpha \in \mathcal{P}$,

$$\begin{bmatrix} c & x_k^\top \\ x_k & P(\alpha_k)^{-1} \end{bmatrix} > 0, \tag{A.4}$$

which yields that $x_k \in \mathcal{E}(P(\alpha_k),c)$, for all $\alpha \in \mathcal{P}$, or $x_k \in \bigcap_{\alpha_k \in \mathcal{P}} \mathcal{E}(P(\alpha_k),c)$ ∎

References

Acosta, D. M., Yildiz, Y., & Klyde, D. H. 2014. Avoiding pilot-induced oscillations in energy-efficient aircraft designs. *In:* Samad, T., & Annaswamy, A. M. (eds), *The Impact of Control Technology*. IEEE CSS.

Alamo, T., Cepeda, A., Limon, D., & Camacho, E. F. 2006. Estimation of the domain of attraction for saturated discrete-time systems. *International Journal of Systems Science*, **37**(8), 575–583.

Baiomy, N., & Kikuuwe, R. 2020. An amplitude- and rate-saturated controller for linear plants. *Asian Journal of Control*, **22**(1), 77–91.

Bateman, A., & Lin, Z. 2002. An analysis and design method for discrete-time linear systems under nested saturation. *IEEE Transactions on Automatic Control*, **47**(8), 1305–1310.

Bateman, A., & Lin, Z. 2003. An analysis and design method for linear systems under nested saturation. *Systems & Control Letters*, **48**(1), 41–52.

Bender, F. A., & Gomes da Silva Jr., J. M. 2012. Output feedback controller design for systems with amplitude and rate control constraints. *Asian Journal of Control*, **14**(5), 1–5.

Berg, J. M., Hammett, K. D., Schwartz, C. A., & Banda, S. S. 1996. An analysis of the destabilizing effect of daisy chained rate-limited actuators. *IEEE Transactions on Control Systems Technology"*, **4**(2), 171–176.

Bertolin, A. L. J., Oliveira, R. C. L. F., De Oliveira, M. C., & Peres, P. L. D. 2018. LMI-based stability tests for LPV and switched discrete-time linear systems through redundant equations. *IFAC-PapersOnline*, **51**(26), 149–154.

Boyd, S., El Ghaoui, L., Feron, E., & Balakrishnan, V. 1994. *Linear matrix inequalities in system and control theory*. Philadelphia, PA: SIAM Studies in Applied Mathematics.

Briat, C. 2015. *Linear parameter-varying and time-delay systems — analysis, observation, filtering and control.* Advances in Delays and Dynamics, vol. 3. Berlin Heidelberg: Springer-Verlag.

Colmegna, P. H., Bianchi, F. D., & Sánchez-Peña, R. S. 2021. Automatic glucose control during meals and exercise in type 1 diabetes: Proof-of-concept in silico tests using a switched LPV approach. *IEEE Control Systems Letters*, **5**(5), 1489–1494.

Daafouz, J., & Bernussou, J. 2001. Parameter dependent Lyapunov functions for discrete time systems with time varying parameter uncertainties. *Systems & Control Letters*, **43**(5), 355–359.

De Caigny, J., Camino, J. F., Oliveira, R. C. L. F., Peres, P. L. D., & Swevers, J. 2009 (June). Gain-scheduled $\mathcal{H}_\infty$-control for discrete-time polytopic LPV systems using homogeneous polynomially parameter-dependent Lyapunov functions. *Pages 19–24 of: Proceedings of the 6th IFAC Symposium on Robust Control Design (ROCOND 2009).*

De Caigny, J., Camino, J. F., Oliveira, R. C. L. F., Peres, P. L. D., & Swevers, J. 2012. Gain-scheduled dynamic output feedback control for discrete-time LPV systems. *International Journal of Robust and Nonlinear Control*, **22**(5), 535–558.

De Souza, C., Castelan, E. B., & Leite, V. J. S. 2019 (December). Input-to-state stabilization of discrete-time LPV systems with bounded time-varying state delay and saturating actuators through a dynamic controler. *Pages 3782–3787 of: Proceedings of the 58th IEEE Conference on Decision and Control.*

de Souza, C., Leite, V. J. S., Silva, L. F. P., & Castelan, E. B. 2019. ISS robust stabilization of state-delayed discrete-time systems with bounded delay variation and saturating actuators. *IEEE Transactions on Automatic Control*, **64**(9), 3913–3919.

de Souza, C., Leite, V. J. S., Tarbouriech, S., & Castelan, E. B. 2021. Event-triggered policy for dynamic output stabilization of discrete-time LPV systems under input constraints. *Systems & control letters*, **153**, 104950.

Duda, H. 1997. Prediction of pilot-in-the-loop oscillations due to rate saturation. *Journal of Guidance, Control, and Dynamics*, **20**(3), 581–587.

Edwards, C., Marcos, A., & Balas, G. 2014. Special issue on linear parameter varying systems. *International Journal of Robust and Nonlinear Control*, **24**(14), 1925–1926.

Figueiredo, L. S. 2020. *Controle de sistemas LPV discretos no tempo sujeitos a atuadores ssaturantes.* M.Sc. Thesis, CEFET-MG – Centro Federal de Educação Tecnológica de Minas Gerais, Divinópolis, MG.

Figueiredo, L. S., Parreiras, T. A. R., Lacerda, M. J., & Leite, V. J. S. 2020. Design of LPV-PI-like controller with guaranteed performance for discrete-time systems under saturating actuators. *IFAC-PapersOnline*, 1–6.

Figueiredo, L. S., Lacerda, M. J., & Leite, V. J. S. 2021. Design of saturating state feedback control laws for discrete-time linear parameter varying systems through homogeneous polynomial parameter-dependent functions. *International Journal of Robust and Nonlinear Control*, **31**(14), 6585–6601.

Flores, G. P. 2019. *Síntese de controladores para seguimento de referências em sistemas LPV com saturação*. M.Sc. Thesis, Universidade Federal do Rio Grande do Sul, Porto Alegre, RS.

Forni, F., Galeani, S., & Zaccarian, L. 2012. Model recovery anti-windup for continuous-time rate and magnitude saturated linear plants. *Automatica*, **48**(8), 1502–1513.

Galeani, S., Onori, S., Teel, A. R., & Zaccarian, L. 2008. A magnitude and rate saturation model and its use in the solution of a static anti-windup problem. *Systems & Control Letters*, **57**(1), 1–9.

Geromel, J. C., Peres, P. L. D., & Bernussou, J. 1991. On a convex parameter space method for linear control design of uncertain systems. *SIAM Journal on Control and Optimization*, **29**(2), 381–402.

Gomes da Silva Jr., J. M., & Tarbouriech, S. 2005. Antiwindup design with guaranteed regions of stability: An LMI-based approach. *IEEE Transactions on Automatic Control*, **50**(1), 106–111.

Gomes da Silva Jr., J. M., Tarbouriech, S., & Garcia, G. 2003. Local stabilization of linear systems under amplitude and rate saturating actuators. *IEEE Transactions on Automatic Control*, **48**(5), 842–847.

Gomes da Silva Jr., J. M., Limón, D., Alamo, T., & Camacho, E. F. 2007. Output feedback for discrete-time systems with amplitude and rate constrained actuators. *Pages 401–423 of:* Tarbouriech, S., Garcia, G., & Glattfelder, A. H. (eds), *Advanced strategies in control systems with input and output constraints*. Lecture Notes in Control and Information Sciences. Springer.

Gomes da Silva Jr., J. M., Limón, D., Alamo, T., & Camacho, E. F. 2008. Dynamic output feedback for discrete-time systems under amplitude and rate actuator constraints. *IEEE Transactions on Automatic Control*, **53**(10), 2367–2372.

Hoffmann, C., & Werner, H. 2015. A survey of linear parameter-varying control applications validated by experiments or high-fidelity simulations. *IEEE Transactions on Control Systems Technology*, **23**(2), 416–433.

Hu, T., & Lin, Z. 2001. *Control systems with actuator saturation: Analysis and design.* Boston, MA: Birkhäuser.

Jungers, M., & Castelan, E. B. 2011. Gain-scheduled output control design for a class of discrete-time nonlinear systems with saturating actuators. *Systems & Control Letters*, **60**, 169–173.

Kapila, V., & Haddad, W. M. 1998. Fixed-structure controller design for systems with actuator amplitude and rate nonlinearities. *Pages 909–914 of: Proceedings of the 37th IEEE Conference on Decision & Control.*

Kapila, V., Pan, H., & de Queiroz, M. S. 1999. LMI-based control of linear systems with actuator amplitude and rate nonlinearities. *Pages 1413–1418 of: Proceedings of the 38th IEEE Conference on Decision & Control.*

Khalil, H. K. 2002. *Nonlinear Systems.* 3rd edn. Upper Saddle River, NJ: Prentice Hall.

Klyde, D. H., McRuer, D. T., & Myers, T. T. 1997. Pilot-induced oscillation analysis and prediction with actuator rate limiting. *Journal of Guidance, Control, and Dynamics*, **20**(1), 81–89.

Leite, V. J. S., & Peres, P. L. D. 2004. Robust control through piecewise lyapunov functions for discrete time-varying uncertain systems. *International Journal of Control*, **77**(3), 230–238.

Leith, D. J., & Leithead, W. E. 2000. Survey of gain-scheduling analysis and design. *International Journal of Control*, **73**(11), 1001–1025.

Lin, Z. 1997. Semi-global stabilization of linear systems with position and rate-limited actuators. *Systems & control letters*, **30**, 1–11.

Lopes, A. N. D., Leite, V. J. S., Silva, L. F. P., & Guelton, K. 2020. Anti-windup TS fuzzy PI-like control for discrete-time nonlinear systems with saturated actuators. *International Journal of Fuzzy Systems*, 1–16.

Molchanov, A. P., & Pyatnitskii, E. S. 1989. Criteria of asymptotic stability of differential and difference inclusions encountered in control theory. *Systems & Control Letters*, **13**(1), 59–64.

Montagner, V. F., Oliveira, R. C. L. F., & Peres, P. L. D. 2006 (July). Robust stability of linear time-varying polytopic systems through polynomially parameter-dependent Lyapunov functions. *In: Proceedings of the 5th IFAC Symposium on Robust Control Design (ROCOND 2006).*

Morato, M. M., Nguyen, M. Q., Sename, O., & Dugard, L. 2019. Design of a fast real-time LPV model predictive control system for semi-active suspension control of a full vehicle. *Journal of the Franklin Institute*, **356**(3), 1196 – 1224.

Olaru, S., & Niculescu, S.-I. 2008. Predictive control for linear systems with delayed input subject to constraints. *IFAC Proceedings Volumes*, **41**(2), 11208 – 11213.

Oliveira, R. C. L. F., & Peres, P. L. D. 2009. Time-varying discrete-time linear systems with bounded rates of variation: Stability analysis and control design. *Automatica*, **45**(11), 2620–2626.

Palmeira, A. H. K., Gomes da Silva Jr., J. M., Jr., Tarbouriech, S., & Ghiggi, I. M. F. 2016. Sampled-data control under magnitude and rate saturating actuators. *International Journal of Robust and Nnonlinear Control*, **26**(15), 3232–3252.

Palmeira, A. H. K., Gomes da Silva Jr., J. M., & Flores, J. V. 2018. Aperiodic sampled-data control for LPV systems under input saturation. *IFAC-PapersOnline*, **51**(26), 130–136.

Pan, H., & Kapila, V. 2001. LMI-based control of discrete-time systems with actuator amplitude and rate nonlinearities. *Pages 4140–4145 of: Proceedings of the 2001 American Control Conference.*

Quadros, M. M., Bessa, I. V., Leite, V. J. S., & Palhares, R. M. 2020. Fault tolerant control for linear parameter varying systems: an improved robust virtual actuator and sensor approach. *ISA Transactions*, **104**, 356–369.

Rugh, W. J., & Shamma, J. S. 2000. Research on gain scheduling. *Automatica*, **36**(10), 1401–1425.

Sato, M. 2015. Gain-scheduled state feedback controllers for discrete-time LPV systems using scheduling parameters affected by absolute and proportional uncertainties. *IFAC-PapersOnline*, **48**(26), 31–36.

Sename, O., Gaspar, P., & Bokor, J. (eds). 2013. *Robust control and linear parameter varying approaches: application to vehicle dynamics*. Lecture Notes in Control and Information Sciences, vol. 437. Berlin: Springer-Verlag.

Shamma, J. S., & Athans, M. 1990. Analysis of gain scheduled control for nonlinear plants. *IEEE Transactions on Automatic Control*, **35**(8), 898–907.

Shamma, J. S., & Athans, M. 1992. Gain scheduling: Potential hazards and possible remedies. *IEEE Control Systems Magazine*, **12**(3), 101–107.

Sontag, E. D. 1999. Stability and stabilization: discontinuities and the effect of disturbances. *Pages 551–598 of:* F. Clarke, R. J. Stern (ed), *Nonlinear Analysis, Differential Equations and Control*, vol. 528. Springer.

Sontag, E. D. 2008. Input to state stability: Basic concepts and results. *Pages 163–220 of:* Nistri, P., & Stefani, G. (eds), *Nonlinear and Optimal Control Theory*. Springer.

Sousa, A. C., Leite, V. J. S., & Rubio Scola, I. 2018. Affordable Control Platform with MPC Application. *Studies in Informatics and Control*, **27**(3), 265–274.

Tarbouriech, S., Prieur, C., & Gomes da Silva Jr., J. M. 2006. Stability analysis and stabilization of systems presenting nested saturations. *IEEE Transactions on Automatic Control*, **51**(8), 1364–1371.

Tarbouriech, S., Garcia, G., Gomes da Silva Jr., J. M., & Queinnec, I. 2011. *Stability and stabilization of linear systems with saturating actuators*. London, UK: Springer.

Tarbouriech, S., Queinnec, I., Biannic, J. M., & Prieur, C. 2016. Pilot-induced-oscillations alleviation through anti-windup based approach. *Pages 401–423 of:* Fasano, G., & Pintér, J. D. (eds), *Space Engineering*. Springer.

Tasoujian, S., Salavati, S., Franchek, M. A., & Grigoriadis, K. M. 2020. Robust delay-dependent LPV synthesis for blood pressure control with real-time bayesian parameter estimation. *IET Control Theory & Applications*, **14**(10), 1334–1345.

Tyan, F., & Bernstein, D. S. 1997. Dynamic output feedback compensation for linear systems with independent amplitude and rate saturations. *International Journal of Control*, **67**(1), 89–116.

Vafamand, N., Arefi, M. M., Khooban, M. H., Dragičević, T., & Blaabjerg, F. 2019. Nonlinear model predictive speed control of electric vehicles represented by linear parameter varying models with bias terms. *IEEE Journal of Emerging and Selected Topics in Power Electronics*, **7**(3), 2081–2089.

Wang, L. 2009. *Model predictive control system design and implementation using MATLAB®*. Springer.

Yang, D., Zong, G., & Karimi, H. R. 2020. $\mathcal{H}_\infty$ refined antidisturbance control of switched LPV systems with application to aero-engine. *IEEE Transactions on Industrial Electronics*, **67**(4), 3180–3190.

Zaccarian, L., & Teel, A. R. 2011. *Modern anti-windup synthesis: control augmentation for actuator saturation*. Princeton University Press.

Zhang, H., Li, P., Du, H., Wang, Y., & Nguyen, A.-T. 2020. Guest editorial: Emerging trends in LPV-based control of intelligent automotive systems. *IET Control Theory & Applications*, **14**(18), 2715–2716.

Zhou, B. 2013. Analysis and design of discrete-time linear systems with nested actuator saturations. *Systems & Control Letters*, **62**, 871 – 879.